NONLINEAR VISCOELASTIC BEHAVIORS OF MULTILAYERED (PULTRUDED) COMPOSITES AT VARIOUS TEMPERATURES AND STRESSES

A Thesis

by

MAITHRI MUDDASANI

Submitted to the Office of Graduate Studies of
Texas A&M University
in partial fulfillment of the requirements for the degree of

MASTER OF SCIENCE

August 2008

Major Subject: Mechanical Engineering

NONLINEAR VISCOELASTIC BEHAVIORS OF MULTILAYERED (PULTRUDED) COMPOSITES AT VARIOUS TEMPERATURES AND STRESSES

A Thesis

by

MAITHRI MUDDASANI

Submitted to the Office of Graduate Studies of
Texas A&M University
in partial fulfillment of the requirements for the degree of

MASTER OF SCIENCE

Approved by:

Chair of Committee,	Anastasia Muliana
Committee Members,	J. N. Reddy
	Eyad Masad
Head of Department,	Dennis O'Neal

August 2008

Major Subject: Mechanical Engineering

ABSTRACT

Nonlinear Viscoelastic Behaviors of Mulitlayered (Pultruded) Composites at Various Temperatures and Stresses. (August 2008)

Maithri Muddasani, B.E, Osmania University, India

Chair of Advisory Committee: Dr. Anastasia Muliana

This study presents experimental works and finite element (FE) analyses for understanding nonlinear thermo-viscoelastic behaviors of multilayered (pultruded) composites under tension. Uniaxial isothermal creep tests in tension are conducted on E-glass/Polyester pultruded composites of 0^o, 45^o and 90^o off-axis fiber orientations subject to combined temperatures and stresses. The temperatures range from 0°F to 125°F, and stress levels range from 20% to 60% of the ultimate tensile strength of the composite specimen. The creep responses seem to accelerate with temperature for higher temperatures (75^oF to 125^oF) and do not behave in any particular manner for lower temperatures (0^oF to 50^oF). Isochronous curves of time-dependent material responses show that the nonlinearity increases with time and also temperature for higher temperatures while there is no particular trend seen at lower temperatures. Also, the creep responses of the axial specimens show negligible nonlinearity when compared to that of the transverse and 45^o off-axis specimens. The Poisson's effect is studied and orthotropic material symmetry conditions are satisfied. A nonlinear viscoelastic constitutive model, based on convolution integral equation, is presented for orthotropic

materials. The nonlinear stress-temperature-dependent material parameters are coupled in the product form and are calibrated using the experimental data. Overall good predictions are shown but for a slight mismatch in the prediction of the responses at temperatures below 50^{o}F owing to the random behavior of the creep responses at lower temperatures. The numerical integration algorithm for the nonlinear viscoelastic model of orthotropic composite materials developed by Sawant and Muliana (2008) was used to integrate the constitutive material model to FE structural analyses. Sensitivity analysis is conducted to check for error in experiments by numerically simulating the testing procedure. A practical structural analysis is carried out on composite slabs using ABAQUS and our model is used to predict the responses of slabs under combined stress and temperature loading.

ACKNOWLEDGEMENTS

I would like to thank my committee chair, Dr. Anastasia Muliana, for her guidance throughout the course of this research, and my committee members, Dr. J. N. Reddy, and Dr. Eyad Masad, for their extended support in this research.

Thanks also go to my friends and colleagues and the department faculty and staff for making my time at Texas A&M University a great experience. Special thanks go to my friends, Sujeev and Pradeep, for their encouragement, guidance, and support.

Finally, thanks to my mother and father for their encouragement, patience, and love.

TABLE OF CONTENTS

CHAPTER Page

LIST OF FIGURES

FIGURE Page

FIGURE Page

LIST OF TABLES

CHAPTER I

INTRODUCTION

Multilayered (pultruded) composites consist of different types of reinforcement layers embedded in a polymeric matrix system. They are manufactured through pultrusion, which is a low cost manufacturing technique to construct long prismatic structural components. They usually have a thick cross-section, while being lightweight. Figure 1.1 (a) shows the pultrusion process where different forms of reinforcement layers are stacked and pulled through heated steel forming die while the resin system is injected to bind the reinforcements, thus giving rise to long prismatic structural components with constant cross-section as shown in figure 1.1 (b). The presence of soft polymeric matrix in these composites leads to time-dependent behaviors. In addition, the relatively low fiber volume fraction (less than 50%) and the presence of voids in the matrix intensify the nonlinear viscoelastic responses of these materials. The responses of pultruded composites are also dependent on temperatures, moisture, and applied loads. Pultruded composites are mainly used in civil structures where they can be exposed to extreme environmental conditions such as temperature changes from below 0°F in winters to above 100°F in summers. Hence, understanding the effect of temperatures and stresses on the viscoelastic responses of these composites becomes essential.

This thesis follows the style of Composites Science and Technology.

a)

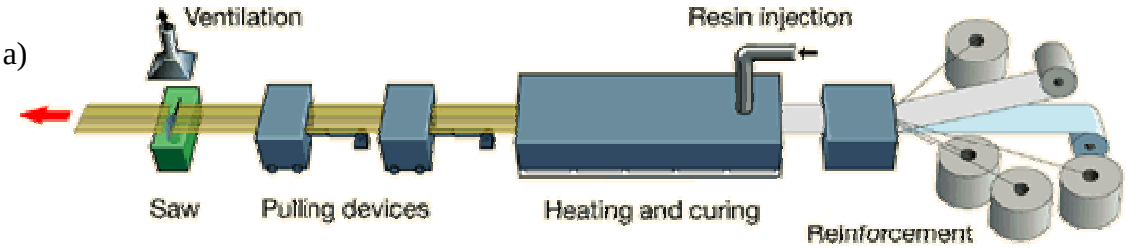

b)

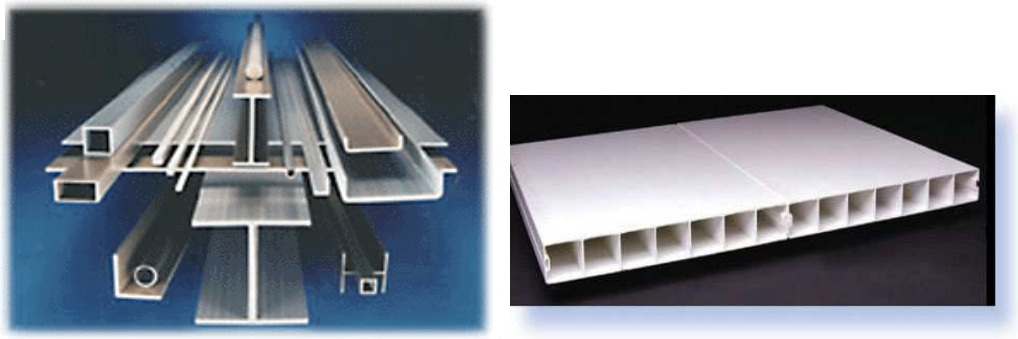

Figure 1.1 a) Pultrusion process b) Pultruded composites with thick cross-section

This study presents uniaxial tensile creep tests and finite element modeling on investigating the effects of temperature and stress on the viscoelastic behaviors of the pultruded composites. The creep tests are performed under combined temperatures, ranging from 0°F to 150°F, and stresses, ranging from 20% to 60% of the specimen's ultimate tensile strength. Multilayered (pultruded) composites that consist of alternate layers of E-glass unidirectional and randomly oriented fibers embedded in polyester resin are presently studied.

This chapter presents a literature review of experimental, analytical and numerical studies on nonlinear thermo-viscoelastic behaviors of fiber-reinforced polymer (FRP) composites including pultruded systems. The objectives and outlines of the present study are also described.

1.1 STATE-OF-THE-ART KNOWLEDGE IN NONLINEAR THERMO-VISCOELASTIC BEHAVIORS OF COMPOSITE MATERIALS AND STRUCTURES

1.1.1 Nonlinear thermo- viscoelastic experimental studies on FRP composites

Experimental studies have been extensively conducted on various unidirectional thin section FRP laminates to characterize the nonlinear thermo-viscoelastic behaviors. Lou and Schapery [16] studied the nonlinear time-dependent behaviors of various off-axis angles by testing unidirectional glass/epoxy eight-ply laminates at angles of 0^o, 30^o, 45^o, 60^o and 90^o. One hour creep tests were performed at 73^oC followed by two hour recovery period. Ten such cycles of creep-recovery were conducted on each specimen. It was found that each of the specimens exhibited an appreciable amount of nonlinear viscoelastic behavior with the exception of those loaded along the fibers. The Schapery's nonlinear single integral constitutive equation [29] was used to characterize the viscoelastic behavior and it was seen that the four nonlinear parameters in the constitutive equation, which in general are functions of multi-stress states, can be modeled as a function of single octahedral shear stress in the epoxy matrix. Mohan and Adams [18] investigated the effect of temperature and moisture content on nonlinear

viscoelastic responses by performing uniaxial creep followed by recovery tests for neat epoxy resin, graphite/epoxy and glass/epoxy materials under tensile and compressive loadings. The tests were conducted at various temperatures and relative humidity. The Schapery's single integral constitutive equation was applied for the creep-recovery behaviors and it was shown that temperature and moisture content affected the nonlinear viscoelastic parameters in the Schapery equation.

Katouzian et al. [12] found that the nonlinear viscoelastic responses for both polymers and $[45_4]_s$ laminated systems were more pronounced by increasing the temperature, where as $[90_4]_s$ laminates exhibited linear viscoelastic responses. They conducted 10 hour creep tests at various temperatures of 23 ^{o}C, 100 ^{o}C and 140 ^{o}C and several stress levels on neat epoxy resin (thermoset), PEEK polymer (thermoplastic), carbon/PEEK and carbon/epoxy composites and used the Schapery integral model to characterize the nonlinear parameters. Sternstein et al. [34] performed three point bending stress relaxation tests for 10,000 seconds followed by recovery tests for 30,000 seconds on polysulphone neat resin and T300/polysulphone laminates. It was found that the viscoelastic behaviors of neat resins that depend on the magnitude of stress and temperature were less pronounced than that of the laminated composites. This can be explained by the existence of void and fiber-matrix shearing that may accelerate the relaxation in composite systems.

Violette and Schapery [39] studied the effects of time and temperature on the compressive strength of unidirectional composites. Unidirectional carbon/epoxy composite specimens were subjected to various temperatures of 24 ^{o}C, 50 ^{o}C, and 60 ^{o}C

and constant compression loading rates. Two nonlinear viscoelastic constitutive models were used to characterize the elastic and viscoelastic material properties. The predictions for the failure strength indicated that the failure followed a power law in time. A finite element model, based on a nonlinear quasi-elastic constitutive equation and a locally discrete representation of the fibers and matrix, has successfully predicted the compressive strength of a notched unidirectional composite material over a range of time and temperature.

1.1.2 Analytical and numerical studies on thermo-viscoelastic behaviors of FRP laminated composites

Analytical and numerical models have been developed to predict linear and nonlinear thermo-viscoelastic behaviors of FRP laminated composites. Orthotropic or anisotropic modeling approaches have been made extensively to analyze the material behavior. Schapery [30] derived the effective anisotropic viscoelastic modulus and thermal expansion coefficient of laminated composites having unidirectional fiber reinforcements and used correspondence principle to relate the effective viscoelastic moduli constituent properties. Tuttle et al. [38] and Pasricha et al. [23] analyzed laminated plates subjected to a repeated number of creep-recovery intervals at different temperatures, using combined classical laminated theory (CLT) with nonlinear viscoelastic/viscoplastic constitutive models. The model predicted creep responses of different laminates with various stacking sequences. The ability of the model to predict long term responses was considered for cyclic thermo-mechanical model. Reasonable

agreements were obtained between measured and predicted strains for all laminates for the six month testing period. Yi et al. [41-43] used a strain-based Schapery integral relation and developed a FE integration procedure to analyze nonlinear viscoelastic response in laminated composites subjected to mechanical and hygrothermal loadings. The FE methods have been used to analyze interlaminar stress, bending and twisting of viscoelastic laminated composites. Muliana and Haj-Ali [21] derived a viscoelastic multi-scale model to analyze time–stress–temperature behaviors of graphite/epoxy laminated composite materials and structures. The experimental creep data of Hiel et al. [10] was used to verify their multi-scale model. The effect of temperatures on creep responses was carried through the time-shift factor. Integrated multi-scale and FE models were used to analyze long-term responses of FRP lap-joint and notched plate composite structures. Dillard and Brinson [4] developed a hereditary based numerical procedure for two dimensional analysis of orthotropic laminated composites based on first-order forward time-stepping solution in conjunction with classical lamination theory where the stress was assumed to be a function of current strain and strain rate. Roy and Reddy [27] developed a numerical integration method for the Schapery nonlinear viscoelastic model coupled with moisture sorption used for 2D FE modeling of adhesively bonded joints. The nonlinear viscoelastic parameters depended on stress and temperature. A coupled nonlinear Fickean diffusion model was also used where its diffusion coefficient was a function of temperature, dilatational strain and stress, and moisture concentration. Bottoni et al. [3] presented a finite element model for the analysis of linear viscoelastic behavior for orthotropic thin-walled beams subject to long-

term loading. It is based on the assumption that the cross-sections remain undistorted in their own planes after deformation is introduced. Maxwell model was used to describe linear viscoelastic constitutive behavior and different viscoelastic laws are adopted for normal and shear moduli variation with time. Linear viscoelastic analyses of prismatic beams with general cross-sections are performed. Exponential algorithm is used for time integration. Accurate results are obtained for the linear viscoelastic case with the implemented procedure. Numerical examples for cases of a GFRP pultruded channel beam under torsion and a tubular beam with cross-section composed of two different materials are considered. Evolution with time of stresses, strains and displacements are obtained. Convergence features of the method have been investigated and it is shown that accurate solutions can be obtained even with very coarse meshes. The time integration algorithm has shown very accurate results by adopting very few integration instants. Sawant & Muliana [28] formulated a numerical algorithm for nonlinear thermo-mechanical viscoelastic analyses of orthotropic composite materials and structures that follow thermo-rheologically complex behaviors. The algorithm was verified for nonlinear stress-dependent viscoelastic behaviors of glass/epoxy-laminated composites under general stress–temperature loading conditions and the predictions were shown to be successful. It can also be easily integrated with general displacement based FE framework for performing structural analyses. The following study uses this algorithm to integrate the constitutive material model with FE to perform practical structural analysis.

Other numerical simulations such as Artificial Neural Networks (ANNs) etc. have been used to develop viscoelastic constitutive models. M.S. Al-Haik et al. [1] developed

an alternative model based on an artificial neural network (ANN) to predict the stress relaxation of the unidirectional polymer matrix composites at high temperatures. The model was validated with 9000 experimental data sets obtained from isothermal stress relaxation tests. Haj-Ali et al. [8] have also used ANNs to develop nonlinear and multi-axial constitutive models for FRP composites. This model was integrated with displacement-based FE software for the nonlinear analysis of composite structures and trained with experimental data obtained from off-axis tension/compression and pure shear (Arcan) tests.

Several studies have been made on the Poisson's effect in viscoelastic materials. Lakes and Wineman [15] have discussed that Poisson's ratio in viscoelastic solids, which in general is a time-dependent quantity, has a different time-dependence depending on the test modality chosen. They developed interrelations between Poisson's ratio in creep and relaxation and it is seen that the difference is minor for a moderate degree of viscoelasticity. Correspondence principles were developed for Poisson's ratio in the time domain and frequency domain. It was found that the viscoelastic Poisson's ratio need not increase with time, or be monotonic with time as shown for selected material systems and in materials with designed microstructure. Hilton (2001) examined the consequences of and the constraints imposed by an assumption of time-independent PRs and under what conditions constant viscoelastic PRs could exist. They proved that time-independent viscoelastic Poisson ratios (PR) can only exist under separation of variable solutions which severely limits the class of applicable problems to quasi-static ones with incompressible homogeneous materials and non-moving boundaries under

separable stress or displacement boundary conditions without any thermal expansions. Equal time variations for material properties in all directions were shown to be another simultaneous requirement for achieving time-independent PRs instead of the incompressibility condition. It was concluded that viscoelastic materials are best characterized in terms of relaxation or creep functions, moduli or compliances rather than combinations of the latter with Poisson's ratios. The assumption of constant PRs was shown to be unjustified in problems involving thermal and chemical expansions, such as curing and manufacture of viscoelastic composites. Their review indicated that experimental results widely confirm the time dependent nature of viscoelastic PRs unless the above extremely limiting conditions are imposed.

1.1.3 Viscoelastic behaviors of pultruded multilayered FRP composite systems

While majority of the current work has been focused on characterizing the nonlinear thermo-viscoelastic responses of FRP laminated composites, there are a limited number of studies conducted on the viscoelastic behaviors of multilayered (pultruded) composites. Spence [33] studied the time-dependant behaviors of pultruded composites by conducting creep compression test on a unidirectional pultruded glass/epoxy rod for duration of 840 hours. The test was carried out at room temperature under load of 30% of the specimen's ultimate strength. The axial strain was measured as 0.04% and thus no appreciable time-dependent behavior was found in the specimen for the duration of the test. Bank and Mosallam [2] studied nonlinear responses of pultruded frames by conducting long-term creep tests for about 10,000 hours and short-term failure tests on

E-glass/vinylester thick-section frame structures with continuous filament mat (CFM) and unidirectional (roving) layers at 25% of the ultimate strength. The frame exhibited nonlinear behavior at high load levels, and while increasing the load up to ultimate failure at 25 kips, progressive damage occurred. Mottram [19] conducted short-term as well as 24 h creep tests on an assembled pultruded beam under three point bending. The assembled beam had two pultruded E-glass/polyester I-sections sandwiched between plate elements, bonded with epoxy adhesive. The short-term tests reported a 7% reduction in the stiffness of the beam assembly from the original elements and this was attributed to the flexibility of adhesive bonding. The tension and shear creep data taken from the longer creep tests were fitted with Findley's power-law model and combined with the Timoshenko beam theory to predict the mid-span deflection in the composite systems for time durations of one week, one year and ten years. The deflections were found to be 25%, 60% and 100% respectively of the specimen's initital deflection.

McClure and Mohammadi [17] used Findley's power law and Boltzmann superposition principle to predict the long-term behaviors of thick-section composites. For their study, they performed long-term creep (2500 hour) tests on E-glass/polyester pultruded angle sections under a load of 45% of the specimen's ultimate strength. Scott and Zureick [31] found that the Findley model was valid only if the material undergoes primary creep deformation, in which strain rate decreases with time. They performed long-term creep tests under compression on pultruded E-glass/vinylester specimens, cut from the flanges and web of an I-shaped pultruded beam, for duration of 6000–12,000 hours under three load levels of 20%, 40%, and 60% of the average ultimate stress

(compressive) and used Findley's power law to model the overall time dependent behavior.

Shao and Shanmugam [32] investigated the time-dependent creep behavior of pultruded composite sheet piling. Two panels were tested under equally spaced three point bending at a span to depth ratio of 48; one was subject to a constant load of 50% of maximum load and the other to 25% of the same. The tensile creep, shear creep, and deflection creep were recorded over 1 year. The time-dependent tensile and shear moduli were obtained using the simplified Findley's model, and the deflection creeps were predicted based on both Findley's model and Timoshenko's equation. It was found that the time exponents in Findley's model for tensile, shear and deflection creep were of close value and could therefore be averaged to provide a viscoelastic material constant for the composite sheet piling. With the averaged viscoelastic parameters, Timoshenko's equation resembled the Findley's power law model for the prediction of deflection creep and agreed well with experimental results up to 1 year. It was estimated that, over 30 years, the viscoelastic tensile and shear moduli will be reduced to 68 and 36% of their respective initial values and the creep deflection will reach 50% of its static deflection.

Choi and Yuan [5] conducted an experimental investigation into the time-dependent deformation of pultruded glass fiber reinforced polymer (GFRP) composite columns under an axial-compressive loading at the environmental controlling room with a constant temperature and relative humidity. Tests were conducted for about 2,500 h on two types of cross-sectional columns: closed-cross section such as square tube (box) and opened-cross section such as wide flange. Both types of columns were 1,200 mm in

length, and had cross-sectional dimensions of 102 mm×102 mm and with a 6.4 mm thickness. A total of eight GFRP composite columns were tested at four different stress levels; 20, 30, 40, and 50% of the average ultimate compressive strength from the short-term column tests. They found that the Findley's power law model can be successfully used to predict time-dependent deformation of GFRP composite columns, and the time-dependent compressive elastic modulus would be decreased by 30% of initial value over a 50-year period.

Haj-Ali and Muliana [9] and Muliana and Haj-Ali [20] performed short-term creep tests of 1 hour on E-glass/vinylester thick-section multilayered systems reinforced with roving and CFM. Several uniaxial, transverse and off-axis specimens and notched plates were tested at different stresses and room temperatures. The off-axis specimens showed pronounced nonlinear viscoelastic behaviors under high load levels, while the uniaxial and transverse specimens showed mild nonlinear viscoelastic responses. Muliana et al. [22] have shown that high temperatures and stresses accelerate the nonlinear deformations of thick-section multilayered composites by performing isothermal uniaxial thirty minute creep tests in tension and compression on axial, transverse, and 45^{o} off-axis specimens made of E-glass/polyester and E-glass/Vinylester at temperatures from 75^{o}F to 150^{o}F and stress levels ratio from 0.2 to 0.6 of the ultimate strength. The creep responses showed thermo-rheologically complex behaviors. The long-term creep responses were constructed by creating master curves for each off-axis specimens at the reference temperature (75°F).

1.2 RESEARCH OBJECTIVE

Currently there are limited studies on nonlinear thermo-viscoelastic behaviors of pultruded composites. The pultruded composites exhibit different responses under tension and compression. The differences in their responses are due to the presence of significant amount of voids in the pultruded system. The voids in the matrix are further enlarged during tension increasing the defects in the polymer, while compression loads tend to close the voids. Compressive strength of the pultruded systems can be twice as much as the tensile strength. Thus the nonlinear responses might further be enhanced under tension.

This study presents experimental and numerical works for understanding thermo-viscoelastic behaviors of pultruded composites under tension. Chapter II presents uniaxial isothermal creep tests in tension on pultruded composites of 0^o, 45^o and 90^o off-axis fiber orientations at different temperatures and stress levels. The temperatures range from 0^oF to 150^oF and load ratios vary from 0.2 to 0.6 of the ultimate tensile strength of the composite measured at room temperature. The upper limits of stress and temperature were chosen in order to avoid material failure as this study does not deal with damage. Isochronous curves of time-dependent material responses are plotted, which portray the nonlinear elastic and time-dependent behaviors of the material. It is seen that the nonlinearity increases with increase in temperature for higher temperatures while there is hardly any temperature effect on nonlinearity seen at lower temperatures (0^oF to 50^oF). Also, the axial specimens show negligible nonlinearity when compared to the transverse and 45 off-axis specimens. The Poisson's effect is also examined by measuring the ratio

of strains in the transverse direction to the ones in the axial direction during the creep tests. The major Poisson's ratio, obtained from the axial specimens, remains almost constant with time, stress and temperature. The minor Poisson's ratio, measured using the transverse specimens, is also almost constant with time but shows appreciable stress-temperature-dependent behavior.

Chapter III describes a nonlinear viscoelastic constitutive model for orthotropic materials. The Schapery [29] nonlinear single integral constitutive model is modified to include the effects of stress and temperature on time-dependent material responses. This constitutive model is applied independently for each component in the compliance matrix. The material symmetry conditions are imposed to the compliances, which give nine independent time integral equations. The stress and temperature dependent nonlinear material parameters are incorporated into the equation and are coupled in the product form, which follows the characterization method of Muliana et al. [22] on multilayered FRP composites. The material parameters in the integral model are characterized using the uniaxial creep tests for several off-axis specimens and are presented as a function of effective stress and temperature. This viscoelastic model is used to simulate the creep behaviors. Predictions of the model are shown to be successful.

Chapter IV deals with FE analysis of the nonlinear viscoelastic responses of the studied pultruded composites. The numerical integration algorithm for the nonlinear viscoelastic model of orthotropic composite materials developed by Sawant and Muliana [28] was used to integrate the constitutive material model to FE structural analyses.

Sensitivity analysis is conducted to check for error in experiments by numerically simulating the testing procedure in ABAQUS and finding the effects of several testing error parameters such as material imperfection (error margins in the fiber angle), misalignment of testing instruments, end-clamping conditions and manual error on the results obtained. It is found that the effect of end clamping conditions on the recorded strain data is very negligible, of a maximum of 0.05%, whereas the effect of material imperfection was quite significant ranging from 6% to 15%. A practical structural analysis is carried out on composite slabs using ABAQUS and the responses of the slabs are predicted under 150°F temperature and 2ksi uniform load for about 4200 sec.

CHAPTER II

NONLINEAR THERMO-VISCOELASTIC BEHAVIORS OF MULTILAYERED (PULTRUDED) COMPOSITE SYSTEMS

This chapter presents uniaxial tensile creep tests on several off-axis multi-layered specimens at different isothermal temperatures and stresses. The multilayered composite consists of repeating layers of unidirectional fiber (roving) and continuous filament mat (CFM) reinforcements. The system is made of E-glass fiber and polyester resin matrix. Isothermal creep-recovery tests are performed at temperatures ranging from 0°F to 125°F, and stresses, ranging from 20% to 60% of the specimen's ultimate strength. The upper limits of temperature and stress level were chosen in order to avoid specimen failure. The creep responses of the material are investigated and their dependence on time and temperature with varying stress levels is studied. The nonlinear behaviors are also evaluated using isochronous plots.

2.1 CREEP TESTS ON OFF-AXIS MULTI-LAYERED SYSTEMS

The studied multilayered composite system is manufactured by Creative Pultrusion Inc. The composite system comprises of two roving and three CFM layers of E-glass fiber and polyester resin as shown in the figure 2.1.

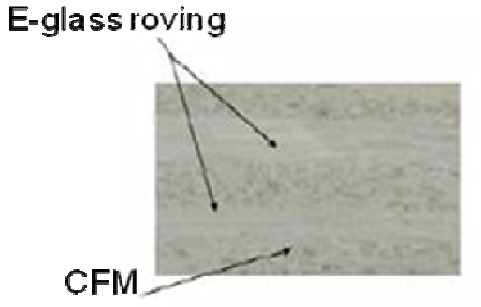

Figure 2.1 E-glass polyester multi-layered composite

Fiber volume fraction (FVF), effective elastic modulus, and ultimate tensile strength for the E-glass/polyester system are taken from the study by Muliana et al. [22] as given in Table (2.1).

Table 2.1 Effective tensile material properties for E-glass/polyester system with FVF 34% measured at T=75°F (Muliana et al., 2006)

Off-axis angle (θ)	0°	45°	90°
Young Modulus ksi	1902	1359	1273
(GPa)	(13)	(9)	(9)
σ_t^{ult} ksi	32	12	9
(MPa)	(221)	(83)	(62)

The creep tension tests are carried out according to the ASTM D3039 standard procedure. The MTS-810 test frame with 22 kips capacity is used to conduct creep-recovery tests. An environmental chamber placed around the test frame, shown in figure

2.2, is used to control the testing temperatures. A liquid nitrogen cylinder is used to cool the chamber for testing at cold temperatures. The specimen is held by gripping to the jaws in order for testing. The strains are recorded using an on-board data acquisition system.

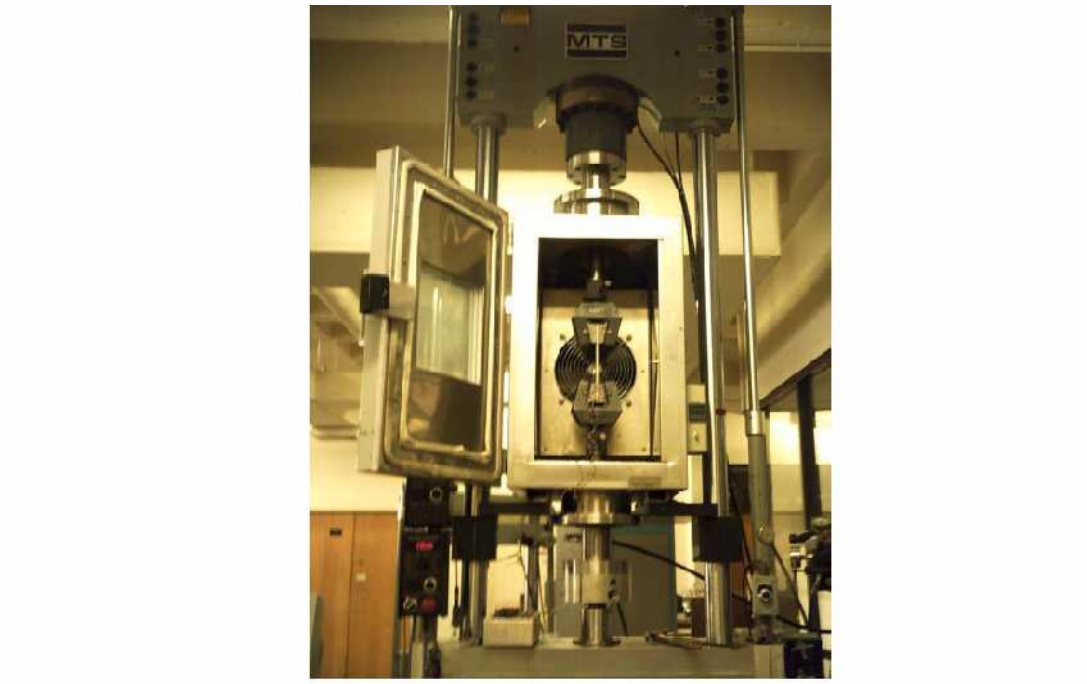

Figure 2.2 MTS-810 test frame with environment chamber

CEA series gauges, manufactured by Vishay Micro-Measurements, are used to measure the strains. The general temperature range for such type of gauge is -100 to +350F (-75 to +175°C), which is adequate for the temperature range considered in this experimental study. M-bond 200 adhesives were used to bond the strain gages to the specimen.

Axial, transverse, and 45^{o} off-axis coupons are cut from the thick unidirectional E-glass/polyester composite plates such that the orientation of the roving layers is controlled. The dimensions of the coupons are 9.5 x 1.25 x 0.25 inches.

Uniaxial tension tests are carried out under isothermal conditions at various stress levels ranging from 0.2 to 0.6 load ratios of the specimen's ultimate strength and temperatures ranging from 0^{o}F to 125^{o}F. Muliana et al. [22] performed similar tests on E-glass/polyester coupons under tension and found that immediate failure occurred in axial and 45 off-axis specimens at 150^{o}F for load ratios of 0.2 and 0.6 respectively. Hence, the upper limits of 125^{o}F and 0.6 load ratio are chosen to avoid failure in the E-glass/polyester tensile specimens as this study does not deal with it.

The coupons are prepared accordingly for creep tests. A strain gauge is attached at the center on each side of the specimen in the longitudinal direction in order to measure axial strains. Another gauge is mounted on one of the sides in the transverse direction for measuring transverse strains. The specimens are soaked in the environmental chamber at the tested temperature for at least 30 minutes prior to each creep test. To measure the equilibrium of temperature in the tested specimens, a dummy coupon is placed in the environmental chamber and the temperature distribution inside the specimen is monitored using a thermocouple. Muliana et al. [22] found the averaged time required for the axial and 45^{o} off-axis specimens to achieve achieve steady state at the temperature of 150^{o}F from the reference condition (75^{o}F) to be about 1000 seconds.

Therefore it is not practical to conduct temperature recovery tests for these short-term creep tests. The recovery tests are conducted by removing only the stresses.

The specimen is gripped along 2 inches at both edges. The uniaxial tension tests are conducted isothermally for thirty minute creep followed by ten minute recovery. Axial strains are monitored using the two longitudinal strain gauges attached to the specimen on either sides and transverse strain is recorded from the transverse strain gauge mounted on one side. During testing, there was a temperature fluctuation of about $\pm 1^{o}$F and load variation of about ±1% of the applied loads. Error estimates of recorded strain measurements in off-axis creep tests due to the misalignment of the material symmetry are performed and are given in detail in chapter four. It is found that the maximum error from the strain was about 1% in the center of the coupon, where the strain was measured. Haj-Ali and Kilic [7] found in their study that the added shear stress in tension due to misalignment of the material can be reduced by using longer coupons (12") and also relatively larger section areas (0.625 in^{2}). The effect of grip pressure on the strains is also investigated in detail in chapter IV. It is found that a change of 2 ksi in grip pressure accounts for 0.5% change in the strains hence making its impact negligible.

A single coupon is used for multiple creep tests under combined load ratios of 0.2, 0.4, and 0.6 of the specimen's ultimate tensile strength, and temperatures 0^{o}F, 25^{o}F, 50^{o}F, 75^{o}F, 100^{o}F, and 125^{o}F. It was established by Yeow et al. [40] that the same specimen can be used for multiple creep tests without significantly altering the mechanical properties. The coupons subjected to multiple creep tests are given at least

24 hours recovery duration between the consecutive tests. Muliana et al. [22] have also investigated the repeatability of off-axis coupons at temperatures of 75^{o}F-150^{o}F and found that the maximum compliance variability with respect to the average compliances from 4-5 repeated tests was 6.6%.

Each off-axis angle is tested starting with the lowest temperature and stress level (0^{o}F and 0.2 ratio of ultimate strength respectively) and ending with the highest temperature (125^{o}F) and stress level (0.6 load ratio), except for the 45^{o} off-axis angle. In case of the 45^{o} off-axis coupons, the tests are only conducted at lower temperatures of 0^{o}F to 50^{o}F and the data from Muliana et al. [22], available for temperatures 75^{o}F-150^{o}F at load ratios 0.2 and 0.4 and for 75^{o}F- 125^{o}F at load ratio 0.6, is taken in order to investigate the responses at higher temperatures. Table (2.2) lists an array of off-axis creep tensile tests. Creep tests at the low temperatures of 0^{o}F to 50^{o}F were repeated for the 45^{o} off-axis specimens in order to understand the peculiar behavior of creep responses at these temperatures. The creep responses were not much affected by the change in temperatures at these low temperatures nor did they follow any particular trend. Also, the value of the responses remained very close to one another at these low temperatures. Repeated tests were carried out using the same coupons as for the previous tests allowing a recovery period of 24 hours between repeated tests. Maximum recorded strain difference from two different coupons in the repeated tests is 3%. Experimental tests repeated twice are marked in Table (2.2). The transverse specimens that were tested next also showed a similar peculiar trend in creep responses at temperatures below

ambient temperatures and the responses were very close to each other at 0^{o}F, 25^{o}F and 50^{o}F. Hence the axial coupons were tested only at 0^{o}F and 50^{o}F, avoiding testing at 25^{o}F as there was not much difference in the responses at these temperatures.

Table 2.2 Creep tests with different off-axis E-glass/polyester coupons subjected to various fractions of their ultimate tensile strength and temperatures

0˚	**45˚**	**90˚**
T0-02-0	T45-02-0*	T90-02-0
T0-02-050	T45-02-025*	T90-02-025
T0-02-075	T45-02-050*	T90-02-050
T0-02-100		T90-02-075
T0-02-125		T90-02-100
		T90-02-125
T0-04-0	T45-04-0*	T90-04-0
T0-04-050	T45-04-025*	T90-04-025
T0-04-075	T45-04-050*	T90-04-050
T0-04-100		T90-04-075
T0-04-125		T90-04-100
		T90-04-125
T0-06-0	T45-06-0*	T90-06-0
T0-06-050	T45-06-025*	T90-06-025
T0-06-075	T45-06-050*	T90-06-050
T0-06-100		T90-06-075
T0-06-125		T90-06-100
		T90-06-125

Tx-y-z – Tension–off-axis angle–loading ratio–temperature
*Experimental tests were repeated twice

2.2 NONLINEAR VISCOELASTIC RESPONSES AT VARIOUS TEMPERATURES AND STRESSES

2.2.1 Creep responses at various temperatures and stresses

The time-dependent responses for the axial, transverse and 45^{o} off-axis coupons at different temperatures and stresses are presented here. Average strains from two axial gages are reported for all the responses. Figure 2.3 (a-c) shows the axial creep responses of axial, transverse and 45^{o} off-axis specimens at the reference temperature of 75^{o}F with increasing load ratios from 0.2 to 0.6. The reference temperature of 75^{o}F i.e., room temperature is chosen where all the properties of the material are independent on temperatures. The figure shows increase in creep responses as load level increased. The axial specimen shows negligible creep and creep behavior increases from axial to transverse to 45 off-axis specimens as seen in the figure.

Figures 2.4-2.6 (a-c) shows the creep responses of all the three off-axis coupons at the load levels of 0.2, 0.4 and 0.6 load ratio with increasing temperature from 0^{o}F to 125^{o}F. It can be seen that the creep behavior increases with increase in temperature from 75^{o}F onwards for each offaxis angle at all the load ratios. But at the lower temperatures below 50^{o}F the creep responses do not systematically increase or decrease with increase in temperature but rather follow a random order. Also, the creep responses are very close to one another at these low temperatures. Consider the 45 off-axis specimen (Fig. 2.6 (a-c)), for load ratio 0.2 the responses at lower temperatures seem to increase uniformly

with temperature. But for load ratios 0.4 and 0.6 this trend no longer persists and the responses at 25^{o}F and 50^{o}F almost overlap with each other. In order to check for this peculiar behavior the tests at lower temperatures were repeated two to three times for the 45 off-axis coupons but similar behavior was observed every time. Similar behavior is seen in the axial and transverse specimens also (Figs. 2.4-2.5 (a-c)). Also, the axial specimens show negligible creep behavior as compared to the other two off-axis angles. The 45^{o} off-axis specimens show very high creep behavior and temperature dependence is also magnified for higher temperatures. Tables 2.3-2.5 give the percentage changes in the axial creep responses for all the off-axis specimens at different temperatures from the reference temperature of 75^{o}F. It can be seen that the effect of temperature is very significant for the 45^{o} off-axis specimens compared to the transverse or axial specimens where the effect is almost negligible.

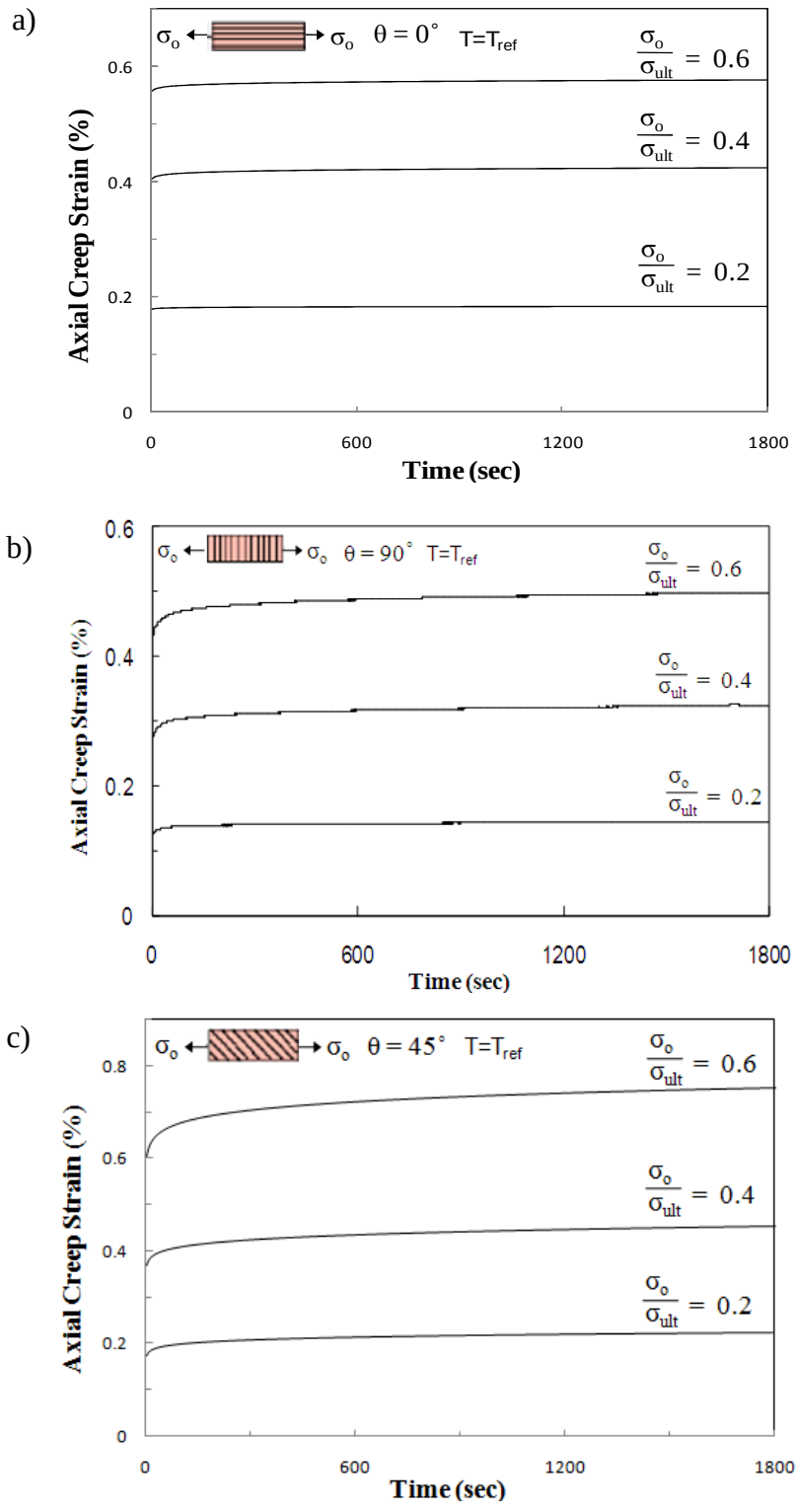

Fig 2.3 Creep responses at $T=T_{ref}$ of a) axial b) transverse and c) 45 off-axis specimens for different load ratios (creep behavior increases from (a) to (c))

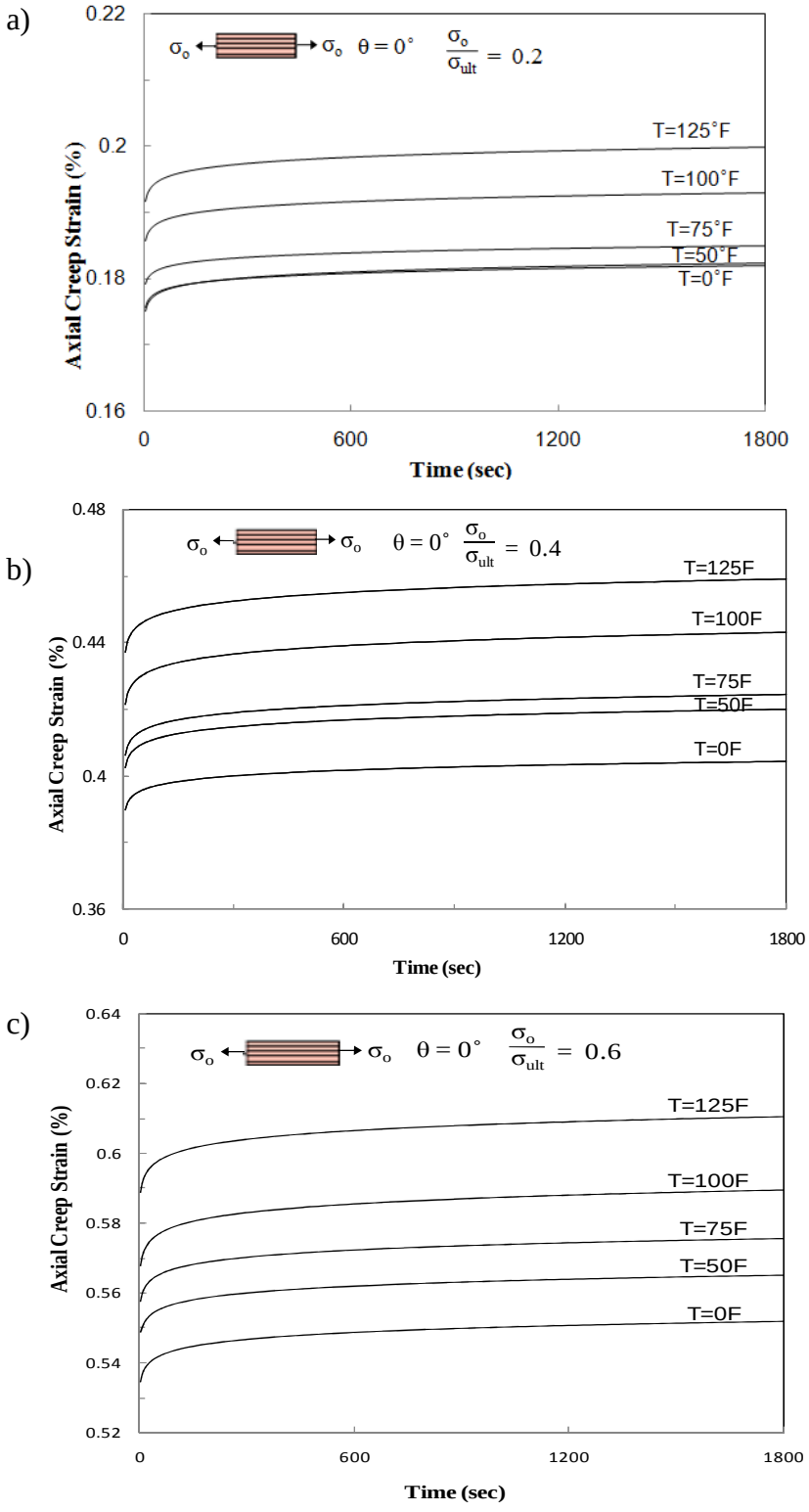

Fig 2.4 Creep responses of axial specimens at different temperatures for load ratio a) 0.2 b) 0.4 and c) 0.6 (negligible creep and temperature dependence are seen)

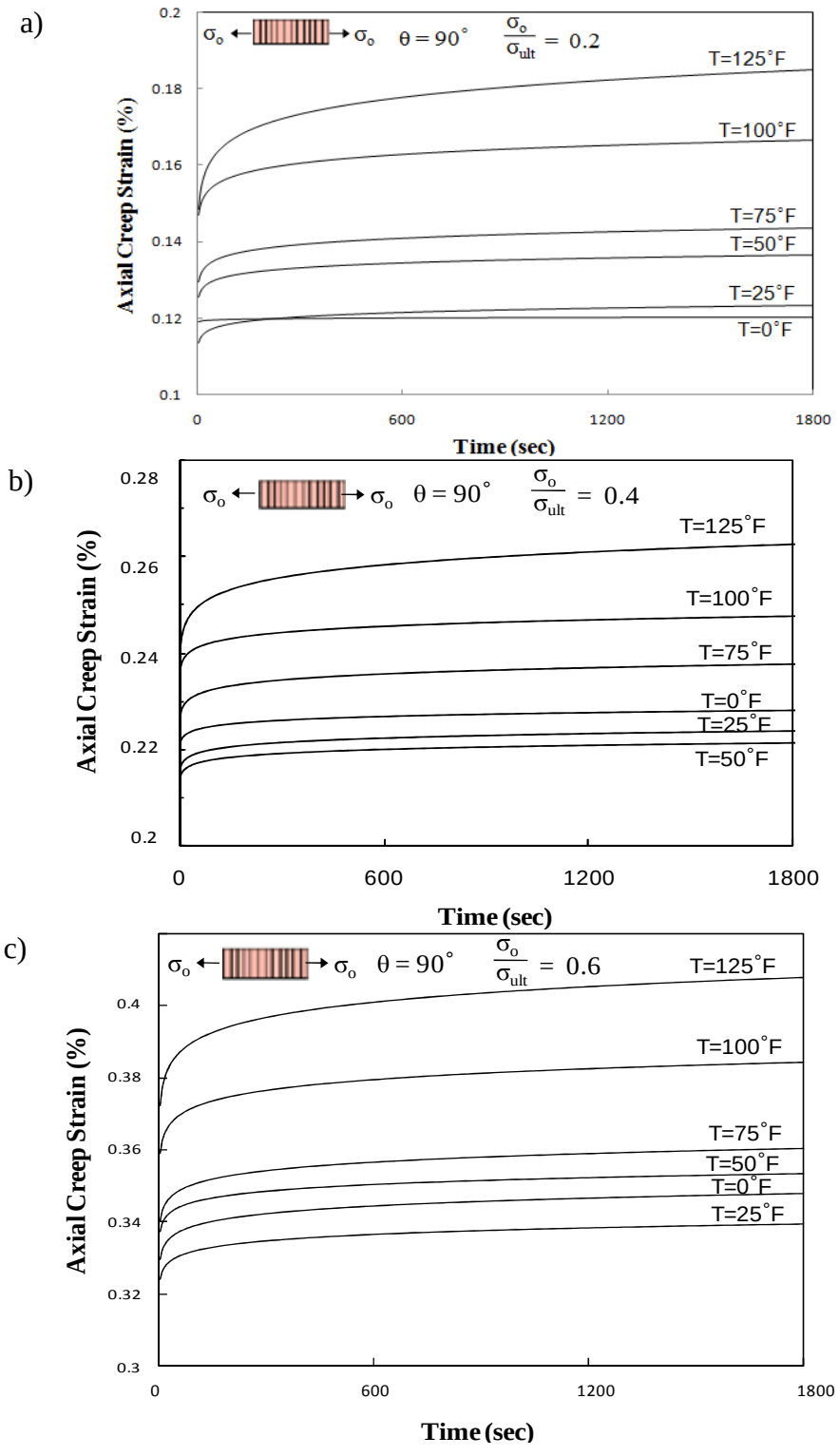

Fig 2.5 Creep responses of transverse specimens at different temperatures for load ratios a) 0.2 b) 0.4 and c) 0.6 (influence of temperature on creep behavior)

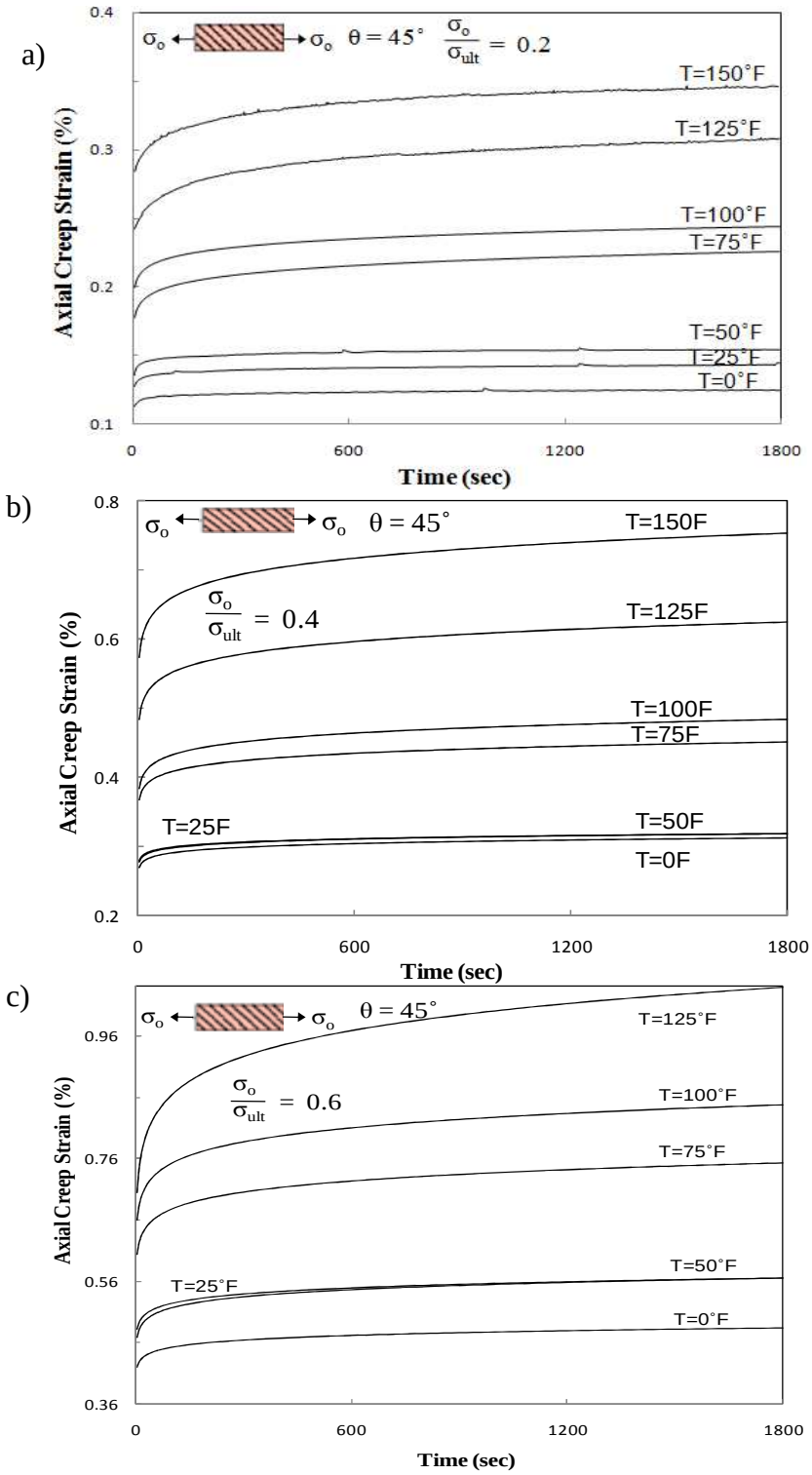

Fig 2.6 Creep responses of 45 off-axis specimens at different temperatures for load ratios a) 0.2 b) 0.4 and c) 0.6 (clearly show accelerated creep behaviors and their temperature influence)

Table 2.3 Percentage changes in axial creep strain at various temperatures from $T_{ref} = 75^0F$ for axial specimens

Temperature(^{0}F)		0	50	75	100	125
Load ratio 0.2	t = 0 s t = 1800s	2.0 1.6	2.2 1.5	0 0	3.6 4.3	7.0 8.0
Load ratio 0.4	t = 0s t = 1800s	4.0 4.7	0.9 1.1	0 0	3.8 4.3	7.6 8.1
Load ratio 0.6	t = 0s t = 1800s	4.1 4.2	1.6 1.9	0 0	1.8 2.4	5.6 6.0

Table 2.4 Percentage changes in axial creep strain at various temperatures from $T_{ref} = 75^0F$ for transverse specimens

Temperature(^{0}F)		0	25	50	75	100	125
Load ratio 0.2	t = 0 s t = 1800s	7.9 16.1	12.3 14.1	3.2 4.8	0 0	13.5 16.1	14.8 28.8
Load ratio 0.4	t = 0s t = 1800s	7 10.9	14.4 15.7	16.5 18.7	0 0	12.6 11.7	18.2 28.6
Load ratio 0.6	t = 0s t = 1800s	6.6 7.1	10.2 11.7	1.8 4.0	0 0	11.5 13.1	20.0 26.1

Table 2.5 Percentage changes in axial creep strain at various temperatures from $T_{ref} = 75^0F$ for 45^0 off-axis specimens

Temperature(^{0}F)		0	25	50	75	100	125
Load ratio 0.2	t = 0 s t = 1800s	36.6 44.8	28.3 36.2	23.8 31.5	0 0	12.0 8.0	24.2 36.7
Load ratio 0.4	t = 0s t = 1800s	23.9 29.4	26.8 31.1	24.2 29.7	0 0	4.5 6.9	31.6 38.2
Load ratio 0.6	t = 0s t = 1800s	30.4 35.7	20.1 24.9	22.5 24.8	0 0	9.1 12.6	16.6 38.0

2.2.2 Nonlinear viscoelastic behavior

Knauss et al. [13,14] studied the nonlinearly thermo-mechanical creep behavior of (bisphenol A) polycarbonate under pure shear loading as well as combined two-dimensional shear with superposed tensile and compressive stress. For pure shear case, shear creep tests were conducted in the nonlinearly viscoelastic range on an Arcan specimen geometry at different temperatures (0 to 140◦C) and under different stress levels. Isochronous plots were created from the creep data and it was seen that nonlinearly viscoelastic behavior starts to take effect near 1% strain at the temperatures considered. It was also seen that time-temperature trade-off as practiced for 'time-temperature shifting' at small strains does not apply in the nonlinear domain. For the second type of loading, creep responses of the Arcan were measured at 80◦C in the nonlinearly viscoelastic regime and the influence of the dilatational deformation component on the nonlinearly viscoelastic creep behavior was studied. It was seen that the creep behavior under shear and normal stress or deformation imposition differ significantly and that the normal strain has a disproportionately large effect on creep response in shear.

In order to understand the nonlinearity in the time-dependent material responses of the off-axis pultruded specimens, isochronous plots from the creep tests are constructed. At each selected time 't', the plot of stress versus corresponding strain can be referred to as an isochrone or isochronous response, which in this case is a creep isochrone (Rajagopal and Wineman [24]). Figures 2.7-2.9 (a-d) shows the isochronous responses for all the off-axis specimens at times 0 sec, 50 sec, 400 sec and 1800 sec with increase

in temperature from 0^{o}F to 125^{o}F. The responses show nonlinearity with respect to time, temperature, and stress. The instantaneous elastic responses (0 sec) show less amount of nonlinearity in the stress-strain relations, while at the later time (1800 sec) significant nonlinear relations are shown. Hence the change in nonlinearity with respect to time can be noted. Also, at low temperatures of 0^{o}F, 25^{o}F, and 50^{o}F the responses are less sensitive to temperature changes, whereas from 75^{o}F onwards the nonlinearity is seen to be increasing with stress and temperature. Here again, there is no particular trend in the nonlinear responses with increase or decrease in temperatures at these low temperatures.

The nonlinear responses are accelerated in the transverse and 45˚ off-axis specimens compared to the axial specimens. The responses for axial specimens show very little change in nonlinearity with time or temperature as noted from figure 2.7 (a-d). This can be attributed to the hardening behavior of the axial specimens as seen in the responses from the quasi-static loading discussed in detail in chapter III (figure on page 52). However it shows significant stress-dependent responses. The 45˚ off-axis specimens show the highest amount of nonlinearity among all the three as seen from the figure 2.9(a-d). Also, we can clearly see the significant increase in nonlinearity with increase in time from 0 sec to 1800 sec and with increase in temperature from 75^{o}F to 125^{o}F for the 45˚ off-axis angle, while the change in temperatures below 50^{o}F does not show any particular impact on the nonlinearity. The transverse specimens also show increase in nonlinearity as time increased and as temperature increased from 75^{o}F to 125^{o}F as seen from figure 2.8 (a-d) but the effect is less significant compared to the 45˚ off-axis angle.

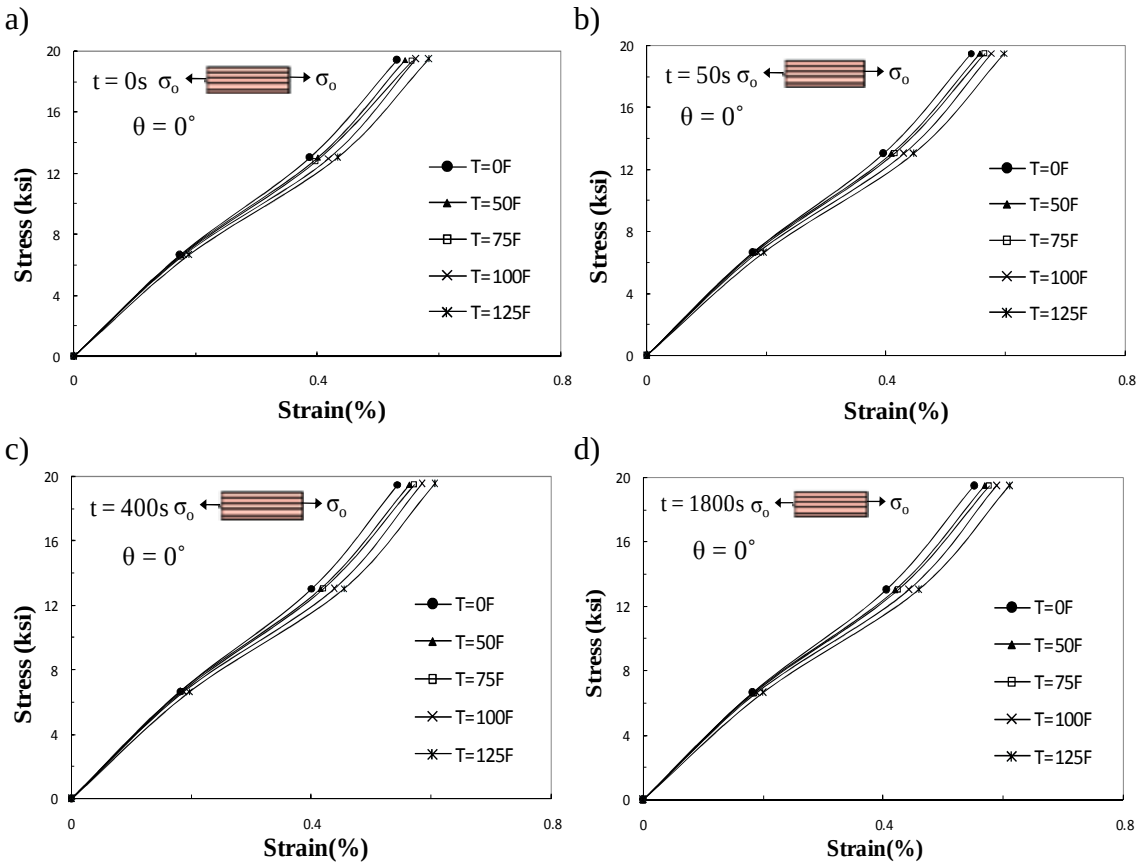

Fig 2.7 Isochronous plots of the axial specimens for different temperatures at (a-d) 0s, 50s, 400s and 1800s (showing less change in nonlinearity due to time and temperature)

If we observe the isochronous plots from 0s to 1800s for each off-axis angle, at each time the nonlinearity increases with temperature for higher temperatures of 75^{o}F to 100^{o}F. The increase in nonlinearity with temperature seems to be accelerated with time. This means that the increase of nonlinearity with temperature may be a function of time. In order to investigate this effect more clearly the distances of the isochrones at different temperatures from the reference temperature are studied with increase in time. These distances are taken at the highest stress level where significant changes are noted.

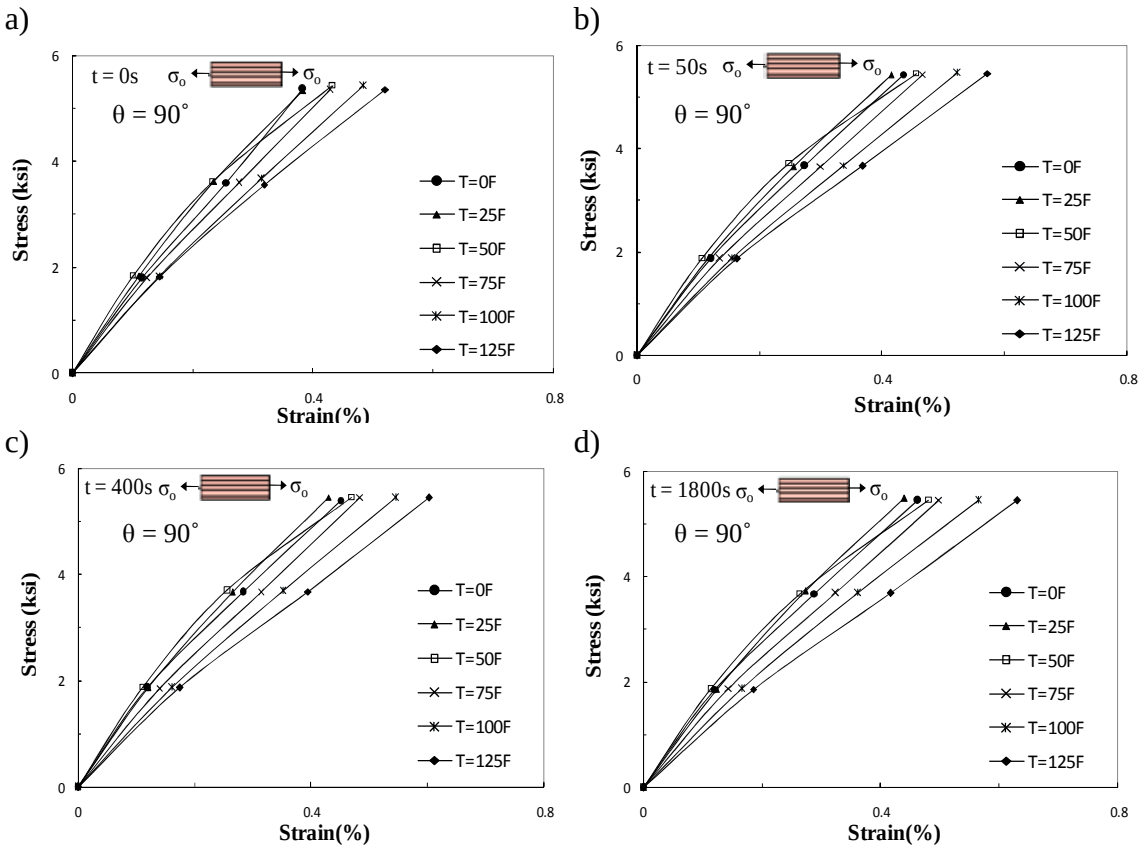

Fig 2.8 Isochronous plots of the transverse specimens for different temperatures at (a-d) 0s, 50s, 400s and 1800s (showing increase in nonlinearity with time and temperature)

Figure 2.10 shows isochronous plots of the transverse specimens at 100^{o}F at different times from 0 seconds to 1800 seconds with respect to those at the reference temperature of 75^{o}F. Again, the increase in nonlinearity with time and temperature can be noted. The distance 'δ' between curves at the two temperatures at highest stress level of 0.6 ratio is measured at different times. The figure shows the distance δ between the isochrones at t=1800s. Distances are measured at each time in such a manner. The distances are measured with respect to the reference temperature because at that temperature linear

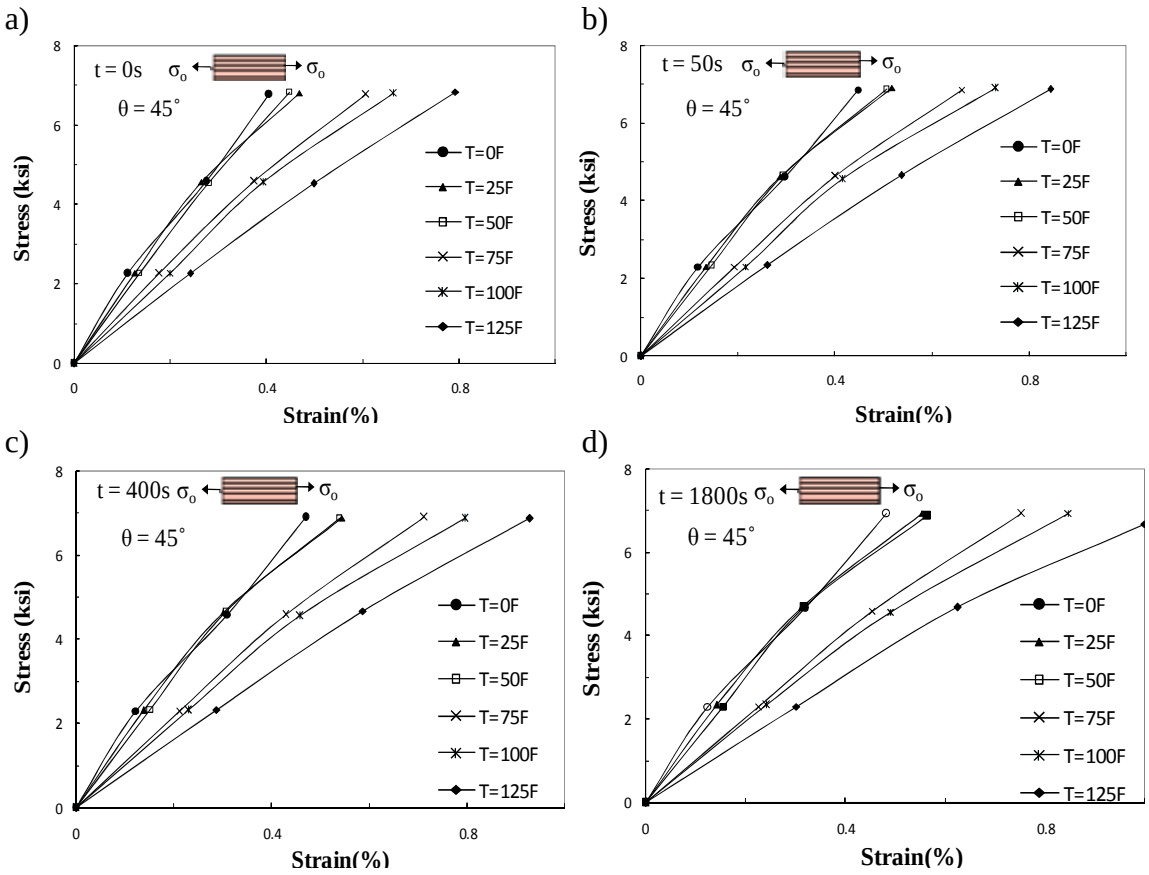

Fig 2.9 Isochronous plots of the 45˚ off-axis specimens for different temperatures at (a-d) 0s, 50s, 400s and 1800s (showing significant increase in nonlinearity with time and temperature)

behavior is assumed and the responses are considered to be temperature-independent. In similar manner, the offset distances of isochrones at each temperature are measured from the reference temperature at the highest stress level and these distances are plotted with respect to time for each off-axis angle as shown in figure 2.11(a-c).

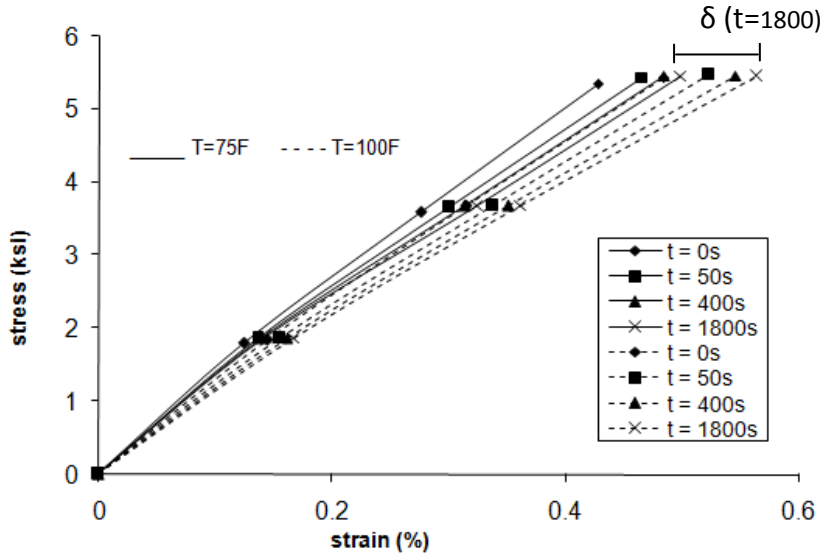

Fig 2.10 Isochronous plots of transverse specimens at T_{ref} and 100˚F showing distance measured between the two curves at different times

Figure 2.11 shows that the offset distances are generally constant with time for all the temperatures except 125 ^{o}F, though the distances at t=0s (instantaneous elastic responses) are slightly different than the distances after that time onwards, for all the off-axis specimens. From figure 2.11 (a), it can be seen that the offset distances for axial specimens remain almost constant with time for all the temperatures. In case of the transverse and 45 ^{o} off-axis specimens the distances remain almost constant with time for all the temperatures except 125 ^{o}F (see Fig 2.11 b and c) where the distances increase with time. Hence it can be concluded that the increase in temperature is independent of time (t > 0s) for all the temperatures except for at 125 ^{o}F in the off-axis specimens.

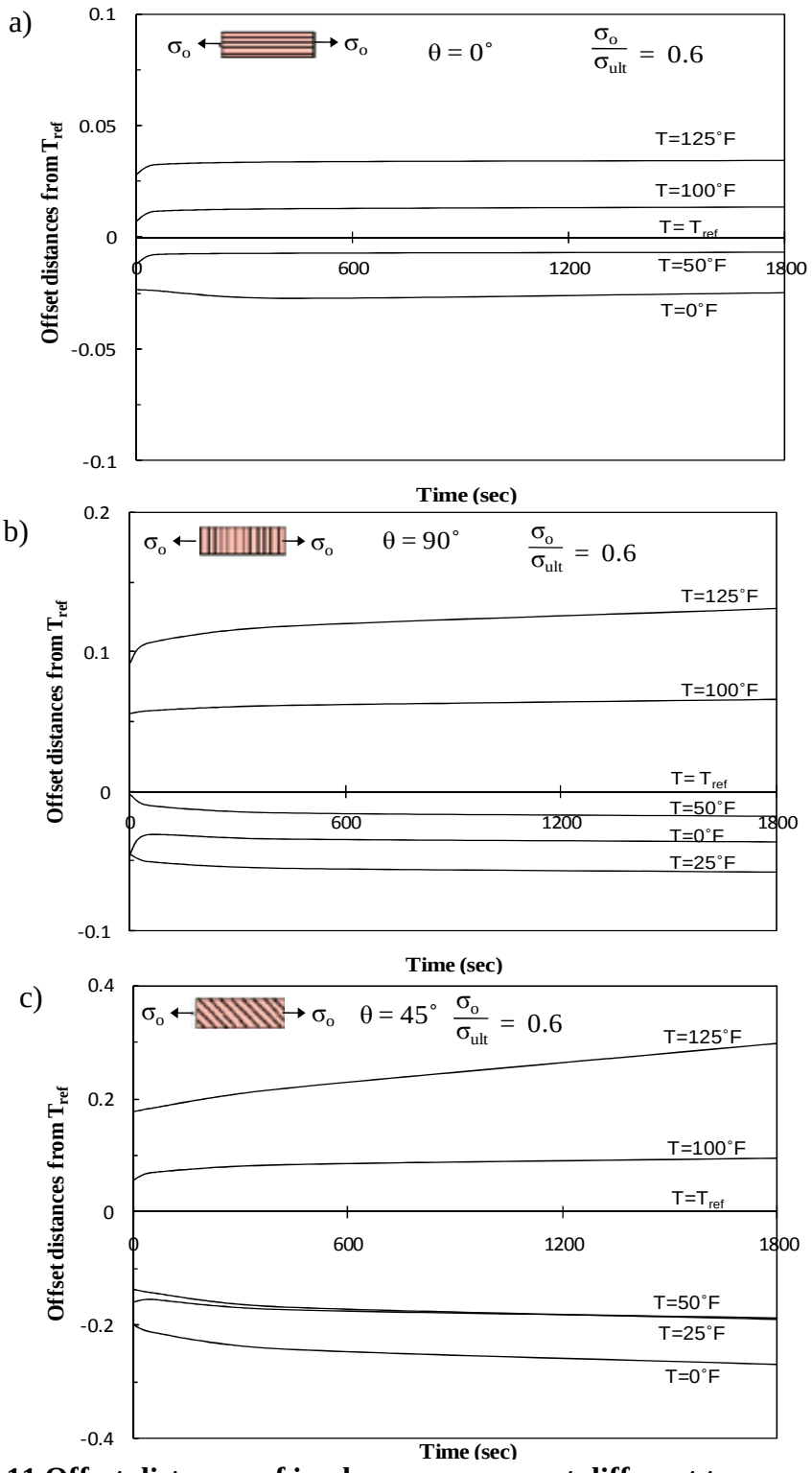

Figure 2.11 Offset distances of isochronous curves at different temperatures from the reference temperature 75˚F with increasing time

The time-dependent moduli from the creep tests on the off-axis specimens are reported at different temperatures (figure 2.11 (a-c)). The moduli are measured from the isochronous plots at early stress-strain responses, which are assumed stress independent. It is seen that the change in modulus with temperatures at different times is relatively uniform as incurred from the plots below. Also, the moduli at lower temperatures are stiffer than the ones at ambient and elevated temperatures. The decrease in the moduli with increase in temperature is more pronounced in the 45^{o} off-axis and transverse specimens compared to the axial specimens (Fig. 2.12).

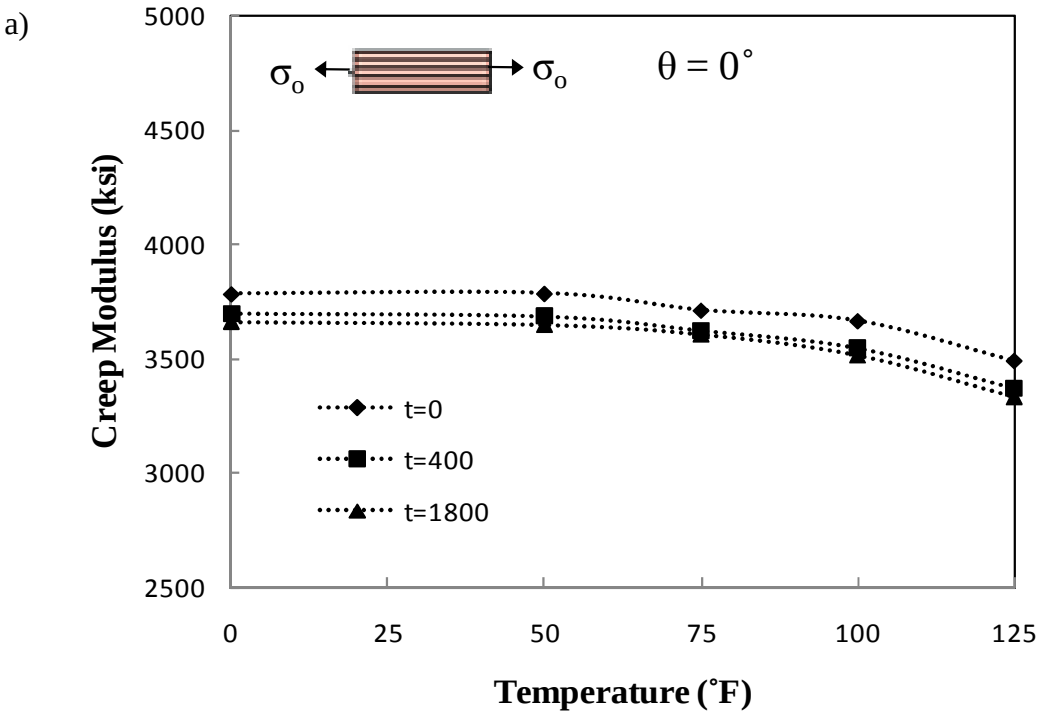

Fig 2.12 Creep modulus vs. temperature for a) axial b) transverse and c) 45^{o} off-axis specimens at different times showing uniform behavior

b)

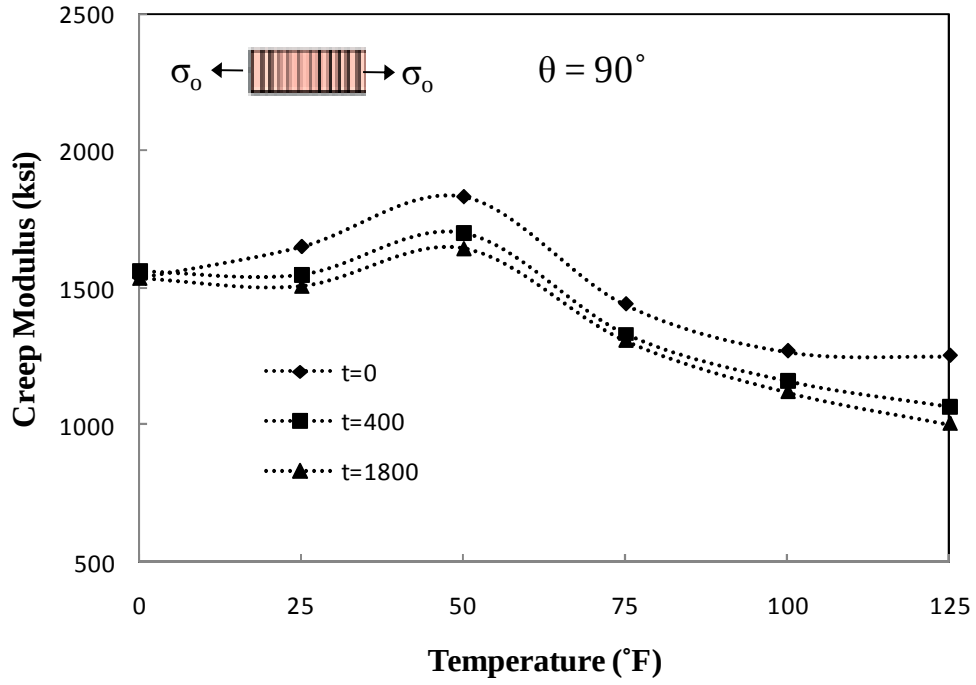

c)

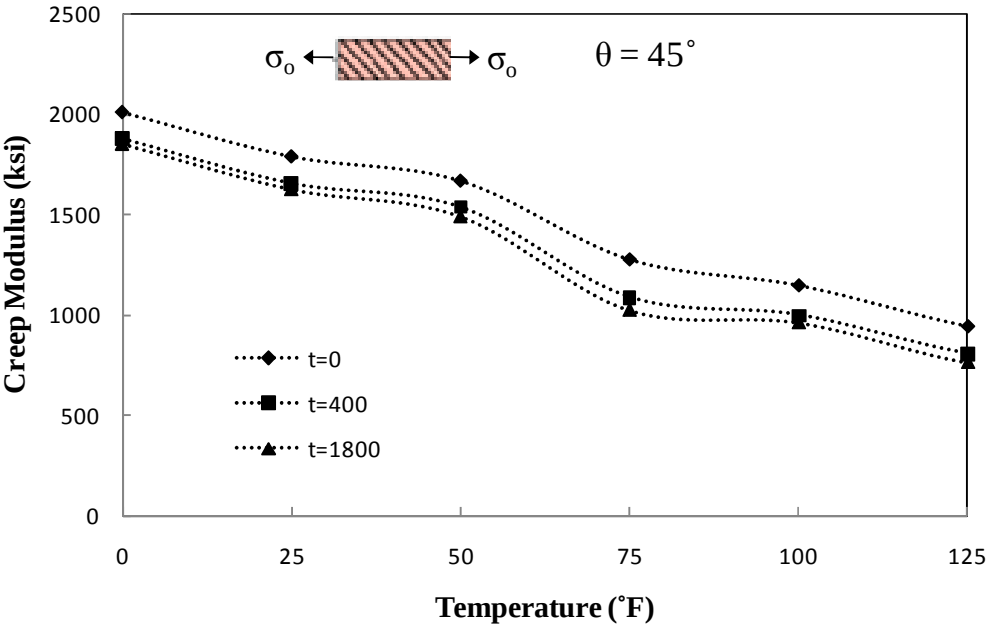

Fig 2.12 Continued

2.3 POISSON'S EFFECT

This study examines the material symmetry and Poisson's effect on creep tests for off-axis systems. The Poisson's effect is studied by measuring the ratio of strains in the transverse direction to the ones in the axial direction during the creep tests. The major and minor Poisson's ratios remain almost constant with time for all the cases and the major Poisson's ratio is mostly stress-temperature-independent.

The major Poisson's ratio υ_{12} is obtained from the axial specimens, where loading is along the fibers, using the transverse strain data obtained from the strain gauge in the transverse direction. Figure 2.13 (a-c) shows υ_{12} at various temperatures for load ratio 0.2, 0.4 and 0.6. It is seen that the value slightly increases with temperature for each of the load ratios with a change of about 2-9%. Hence the effect of temperature on υ_{12} can be considered negligible. For the transverse specimens (figure 2.14) the minor Poisson's ratio i.e., υ_{21} decreases with increase in temperature for the load ratios 0.2 and 0.6 by an amount of 8-16% and 10-30% respectively. It does not show any particular trend at load ratio 0.4 but changes by a maximum amount of 30-40%. This trend has not yet been accounted for. Thus, the effect of temperature on υ_{12} is negligible but it significantly affects $\upsilon_{21.}$

Effect of stress on major Poisson's ratio $\upsilon_{12,}$ is shown in figure 2.15 (a-b) where the value decreases by a negligible amount of about 3-6% with increase in stress. Figure 2.16 (a-b) shows the effect of stress on Poisson's ratio υ_{21} for the reference temperature and T=125F. It is seen that the value decreases by about 30-40% with increase in load ratio from 0.2 to 0.6 for both the temperatures. Thus υ_{21} is affected by stress where as υ_{12} is not much affected.

Tables 2.6 and 2.7 present the Poisson's ratios υ_{12} and υ_{21} respectively at time t=0s for various stresses and temperatures. It again shows that υ_{12} remains almost constant with stress and temperature, with a slight change of 6-7%, whereas υ_{21} decreases by about 10-30% with increase in temperature, and 20-40% with increase in stress level. The slight changes in υ_{12} can be caused due to material imperfections or variability in experimental creep tests and thus the major Poisson's ratio υ_{12} is treated as a constant for the material.

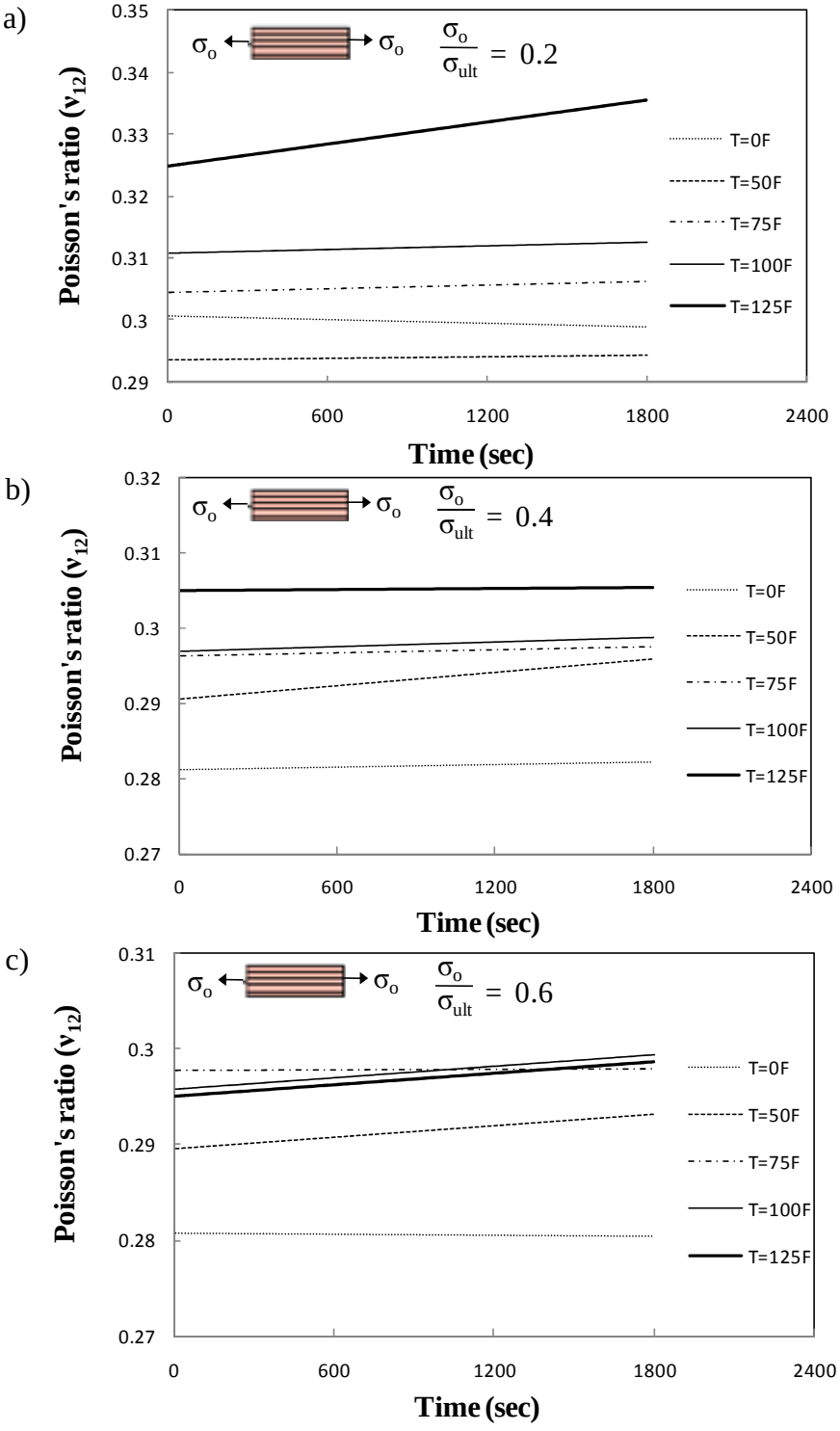

Fig 2.13 Major Poisson's ratio (ν_{12}) variation with time at different temperatures for load ratio a) 0.2 b) 0.4 and c) 0.6

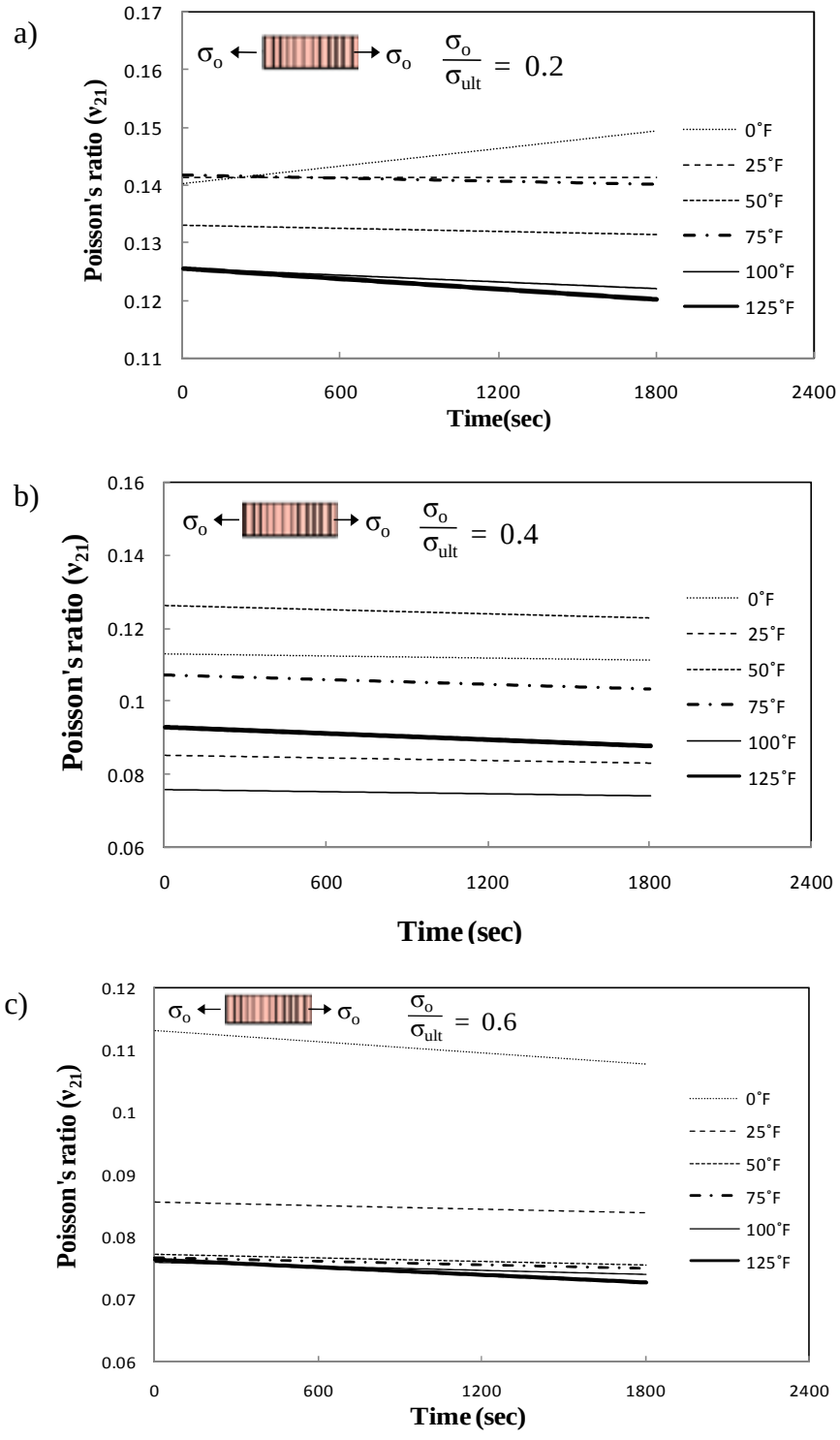

Fig 2.14 Minor Poisson's ratio (ν_{21}) variation with time at different temperatures for load ratio a) 0.2 b) 0.4 and c) 0.6

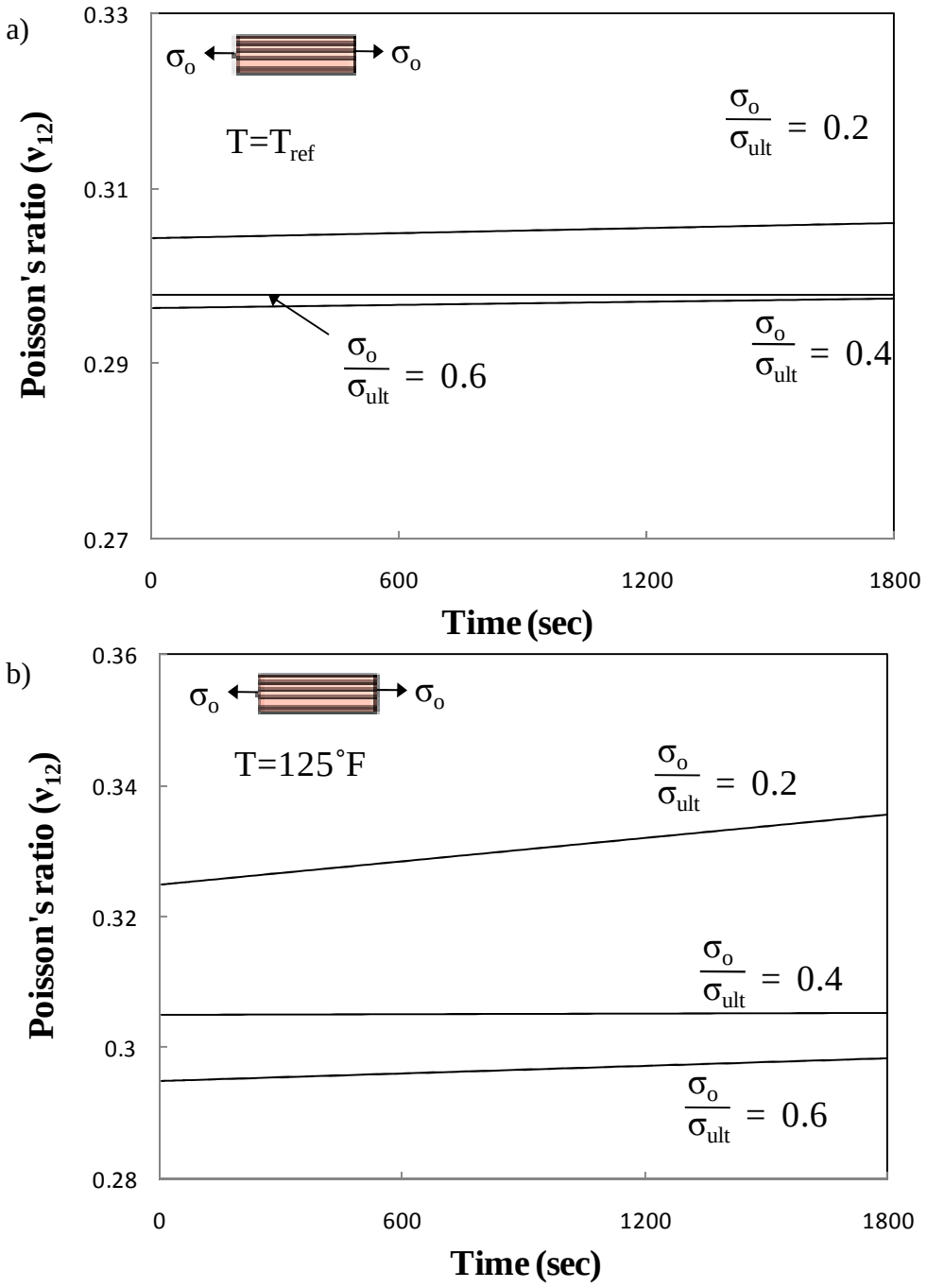

Fig 2.15 Major Poisson's ratio (ν_{12}) variation with time at different load ratios for a) $T=T_{ref}$ b) $T=125^{o}F$

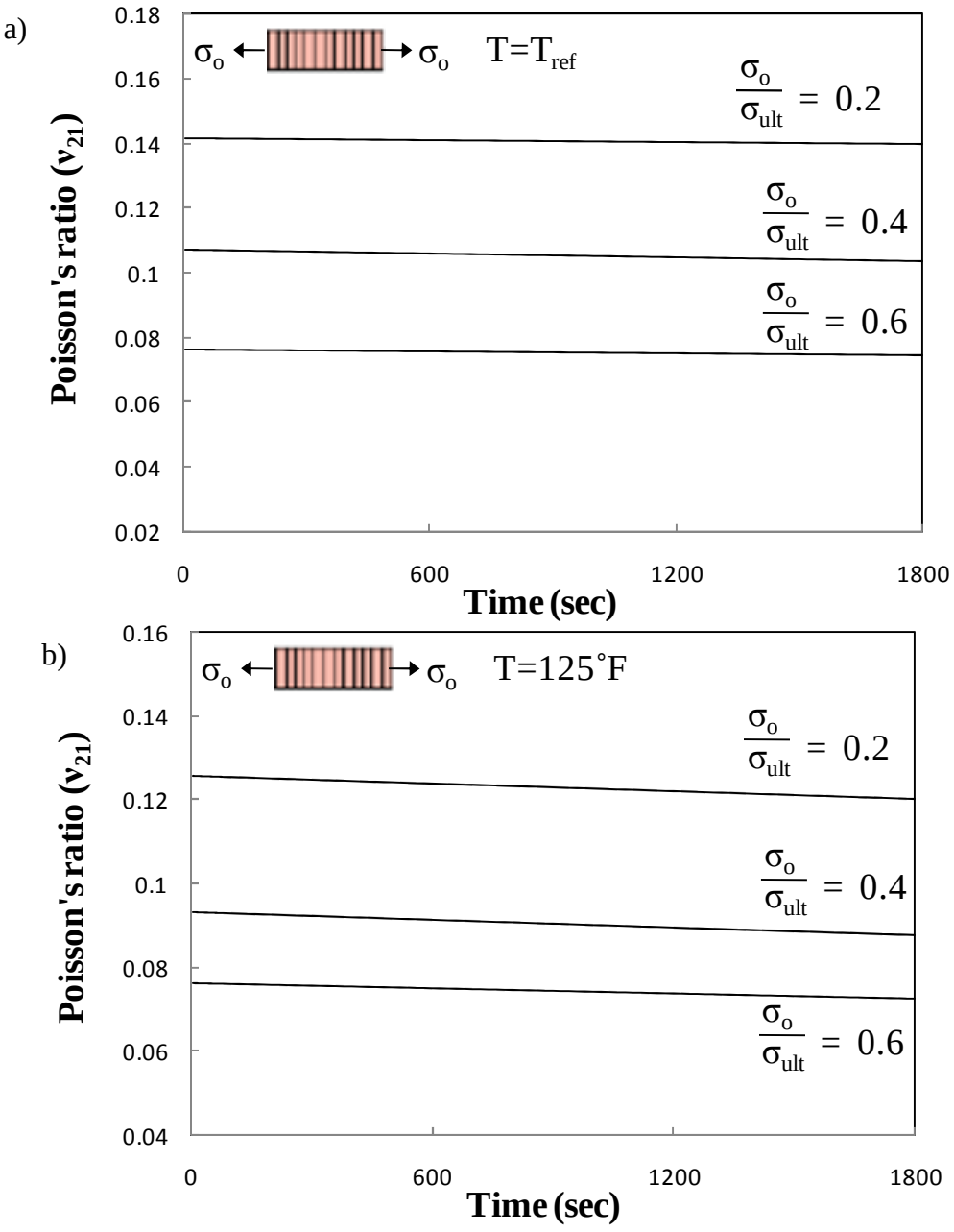

Fig 2.16 Minor Poisson's ratio (ν_{21}) variation with time at different load ratios for a) $T=T_{ref}$ b) $T=125^{o}F$

Table 2.6 Major Poisson's Ratio, $v_{12,}$ at t=0s for various stresses and temperatures

Temperature(^{0}F)	Poisson's Ratio v_{12}		
	Load Ratio 0.2	Load Ratio 0.4	Load Ratio 0.6
0	0.30	0.28	0.28
50	0.29	0.29	0.29
75	0.30	0.30	0.30
100	0.31	0.30	0.30
125	0.32	0.30	0.30

Table 2.7 Minor Poisson's Ratio, $v_{21,}$ at t=0s for various stresses and temperatures

Temperature(^{0}F)	Poisson's Ratio v_{21}		
	Load Ratio 0.2	Load Ratio 0.4	Load Ratio 0.6
0	0.14	0.11	0.11
25	0.14	0.09	0.09
50	0.13	0.13	0.08
75	0.14	0.11	0.08
100	0.13	0.08	0.08
125	0.13	0.09	0.08

Tables 2.8 examines the material symmetry condition of orthotropic materials i.e., $\nu_{12}/E_{11} = \nu_{21}/E_{22}$, at different temperatures and stresses. It is seen that the condition of material symmetry is closely satisfied for all the cases with a slight error of 6-11% for some of the cases which can be accounted for by the material imperfections and experimental test variability. Thus a condition of orthotropic material symmetry can be successfully imposed on the composite.

Table 2.8 Orthotropic symmetry condition check ($\nu_{12}/E_{11} = \nu_{21}/E_{22}$) for various stresses and temperatures at t=0 sec

Temperature(^{0}F)	ν/E (x10^{-2} 1/ksi)					
	Load Ratio 0.2		Load Ratio 0.4		Load Ratio 0.6	
	ν_{12}/E_{11}	ν_{21}/E_{22}	ν_{12}/E_{11}	ν_{21}/E_{22}	ν_{12}/E_{11}	ν_{21}/E_{22}
0	0.81	0.86	0.88	0.8	0.76	0.79
50	0.78	0.88	0.88	0.81	0.8	0.8
75	0.83	0.95	0.90	0.82	0.84	0.81
100	0.85	0.98	0.94	0. 85	0.84	0.87
125	0.94	0.99	0.1	0.87	0.87	0.89

CHAPTER III

CHARACTERIZATION OF NONLINEAR THERMO-VISCOELASTIC MATERIAL PARAMETERS

This chapter presents characterization of nonlinear thermo-viscoelastic properties of the multilayered (pultruded) composite system. A thermo-viscoelastic constitutive model of orthotropic materials having stress and temperature dependent material properties is considered for the multi-layered composite specimens. The stress and temperature dependent nonlinear material parameters in the integral model are coupled in the product form, which follows the characterization method of Muliana et al [22] on multilayered FRP composites. The material parameters are characterized using the experimental data from the uniaxial isothermal creep tests at various off-axis angles and are expressed as a function of effective stress and temperature. The model is used to simulate the creep behaviors. Overall good predictions are shown.

3.1 NONLINEAR THERMO-VISCOELASTIC MODEL

A stress-temperature dependent nonlinear viscoelastic behavior for a multilayered system is presented in this section. A general linear viscoelastic constitutive equation for anisotropic materials under uncoupled thermo-mechanical loading can be written in the following form:

$$\varepsilon_{ij}(t) = \int_0^t \mathrm{D}_{ijkl}\,(t-\tau)\frac{d\sigma_{kl}(\tau)}{d\tau}\,\mathrm{d}\tau + \int_0^t \alpha_{ij}\frac{dT(\tau)}{d\tau}\,d\tau \qquad (3.1)$$

or

$$\sigma_{ij}(t) = \int_0^t C_{ijkl}\,(t-\tau)\,\frac{d\varepsilon_{kl}(\tau)}{d\tau}\,\mathrm{d}\tau + \int_0^t \beta_{ij}\,(t-\tau)\,\frac{dT(\tau)}{d\tau}\,d\tau \qquad (3.2)$$

Where the component of time dependent compliance and modulus tensors are $D_{ijkl}(t)$ and $C_{ijkl}(t)$, respectively; $\boldsymbol{\alpha}$ and $\boldsymbol{\beta}$ are second order tensors defining coefficient of thermal expansion and thermo elastic moduli, respectively. In general, the material compliance or moduli can be functions of time, stress, strain, temperature and other field variables. The time, stress and temperature dependent compliance is expressed as:

$$D_{ijkl}(t,\boldsymbol{\sigma},T) = D_{ijkl}(0,\boldsymbol{\sigma},T) + \Delta D_{ijk}(t,\boldsymbol{\sigma},T) \qquad (3.3)$$

Where $\mathbf{D}(0, \boldsymbol{\sigma}, T)$ is the compliance at time 0, which is often considered as the time independent (instantaneous elastic) compliance, and $\Delta\mathbf{D}(t, \boldsymbol{\sigma}, T)$ is the transient compliance. Substituting Eq. (3.3) into (3.1) gives

$$\varepsilon_{ij}(t) = \int_0^t [\mathrm{D}_{ijkl}\,(0,\boldsymbol{\sigma},T) + \Delta\mathrm{D}_{ijkl}(t-\tau,\boldsymbol{\sigma},T)]\,\frac{d\sigma_{kl}(\tau)}{d\tau}\,\mathrm{d}\tau + \int_0^t \alpha_{ij}\,\frac{dT(\tau)}{d\tau}\,d\tau \qquad (3.4)$$

$$= \mathrm{D}_{ijkl}(0,\boldsymbol{\sigma},T)\sigma_{kl}(t) + \int_0^t \Delta\mathrm{D}_{ijkl}\,(t-\tau,\boldsymbol{\sigma},T)]\,\frac{d\sigma_{kl}(\tau)}{d\tau}\,\mathrm{d}\tau + \int_0^t \alpha_{ij}\,\frac{dT(\tau)}{d\tau}\,d\tau \qquad (3.5)$$

Schapery [29] developed a nonlinear viscoelastic constitutive model based on a single integral equation with four nonlinear stress dependent material parameters. Lou and Schapery [16] have extended the Schapery nonlinear single integral form to characterize time-stress dependent behaviors of orthotropic materials. Sawant and

Muliana [28] adopted the extension of Schapery nonlinear single integral equation to orthotropic materials and further extended it to represent the stress-temperature dependent behaviors of a non-aging material. In this study, a nonlinear viscoelastic constitutive model based on single integral equation with two nonlinear material parameters is chosen to represent the stress-temperature dependent behavior of multilayered composites. Under isothermal conditions, the total stress-temperature dependent mechanical strain for a nonlinear orthotropic viscoelastic material is expressed as:

$$\varepsilon_{ij}(t) = \mathrm{g}(\bar{\sigma}^{\mathrm{t}}, \mathrm{T})\mathrm{D}^{0}_{ijkl}\sigma_{kl}(t) + \mathrm{f}(\bar{\sigma}^{\mathrm{t}}, \mathrm{T}) \int_{0}^{t} \Delta \mathrm{D}_{ijkl}\,(t-\tau, \sigma, T)\, \frac{d\sigma_{kl}(\tau)}{d\tau}\, \mathrm{d}\tau \qquad (3.6)$$

Here $D^{0}_{ijkl}(t)$ and $\Delta D^{t}_{ijkl}(t)$ are components of the instantaneous elastic and transient compliances. The nonlinear stress-temperature dependences are carried through the parameters g and f. The parameter g is the nonlinear instantaneous elastic compliance that measures the increase or decrease in stiffness as a function of stress and temperature. The parameter f accounts for the effect of nonlinearity in the transient compliance. The parameter T denotes the current temperature. The superscript denotes a dependent time variable. The reason for choosing the two nonlinear parameters as opposed to the four nonlinear parameters in the Schapery model is that we only have data from creep responses for material characterization. In order to characterize four nonlinear parameters, additional data from recovery responses is needed. It is noted that the transient creep parameter f combines the effect of the Schapery's nonlinear

parameters g1, g2, in case of the transient part of the creep response which is explained in detail later in this section.

Material characterization is performed using data from the uniaxial creep tests for axial, transverse and 45 off-axis specimens. When a constant stress σ_{ij}^{o} is applied at t = 0, the equation (3.6) reduces to:

$$\varepsilon_{ij}(t) = \mathrm{g}(\bar{\sigma}^{\mathrm{t}}, \mathrm{T})\mathrm{D}_{ijkl}^{0}\sigma_{kl}^{0} + \mathrm{f}(\bar{\sigma}^{\mathrm{t}}, \mathrm{T})\Delta\mathrm{D}_{ijkl}(t)\sigma_{kl}^{0} \tag{3.7}$$

The stress-temperature effects on the overall time-dependent responses are coupled in product forms following the characterization methods of Muliana et al. [22] on multilayered FRP composites, thus giving,

$$\varepsilon_{ij}(t) = \mathrm{g}(\bar{\sigma}^{\mathrm{t}})\mathrm{g}(\mathrm{T})\mathrm{D}_{ijkl}^{0}\sigma_{kl}^{0} + \mathrm{f}(\bar{\sigma})\mathrm{f}(\mathrm{T})\Delta\mathrm{D}_{ijkl}(t)\sigma_{kl}^{0} \tag{3.8}$$

The transient compliance can be modeled using the Power law or Prony series exponential functions given in Eq. (3.9) and (3.10) respectively. Other empirical functions can also be used to represent creep responses.

$$\Delta\mathrm{D}_{ijkl}^{t} = \mathrm{C}_{ijkl}(t)^{n_{ijkl}} \quad \text{or} \tag{3.9}$$

$$\Delta\mathrm{D}_{ijkl}^{t} = \sum_{n=1}^{\mathrm{N}_{ijkl}} \mathrm{D}_{ijkl(n)}\left(1 - \exp\left[-\lambda_{ijkl(n)}\, t\right]\right) \tag{3.10}$$

The parameters **C** and **n** in the power law model are assumed stress-temperature-independent and measured at the reference condition (i.e., room temperature). Findley et al. [6] used power law function for transient compliance in the Boltzmann convolution integral equation, which is widely used to represent linear viscoelastic behaviors and has been extended to model nonlinear viscoelastic responses, and incorporated the temperature and stress dependent material parameters in the power law coefficients. **N** in Eq. (3.10) is the number of terms for each component in the transient compliance tensor, $\mathbf{D}_{(n)}$ is the n^{th} coefficient of the Prony series for each component in the transient compliance tensor, and $\boldsymbol{\lambda}_{(n)}$ is the n^{th} reciprocal of retardation time that corresponds to $\mathbf{D}_{(n)}$. Both $\mathbf{D}_{(n)}$ and $\boldsymbol{\lambda}_{n}$ are also stress-temperature independent. Using the power law model for the transient compliance, the mechanical strain in Eq. (3.8) is expressed by:

$$\varepsilon_{ij}(t) = g(\bar{\sigma}^{t})g(T)D^{0}_{ijkl}\sigma^{0}_{kl} + f(\bar{\sigma})f(T)C_{ijkl}(t)^{n_{ijkl}}\sigma^{0}_{kl} \tag{3.11}$$

The material characterization is performed by fitting linear and nonlinear responses to Eq. (3.11). The responses at the reference conditions of 75^{o}F temperature and 0.2 load ratio are assumed to be linear. Consider figure 3.1 showing the force-displacement curve during quasi-static loading on uniaxial, transverse, and 45^{o} off-axis E-glass/polyester specimens under tension at a temperature of 75^{o}F. The specimen dimensions were 9.5x1.25x0.25 in. Each curve ends where the specimen has failed implying its ultimate tensile strength (see Table 2.1). It can be inferred from the figure that responses are

almost linear below 20% of the ultimate tensile strength for each off-axis angle. Thus, this study assumes that stresses below 20% of the ultimate tensile strength are linear. All the nonlinear parameters are assumed to be unity at this reference condition. Also, it can be observed from the figure that the hardening in the axial specimens whereas the transverse and 45^{o} off-axis tend to soften. This may be due to the fact that the fibers take most of the loading in case of the axial specimens but the matrix also is the load-bearing element in case of the other two.

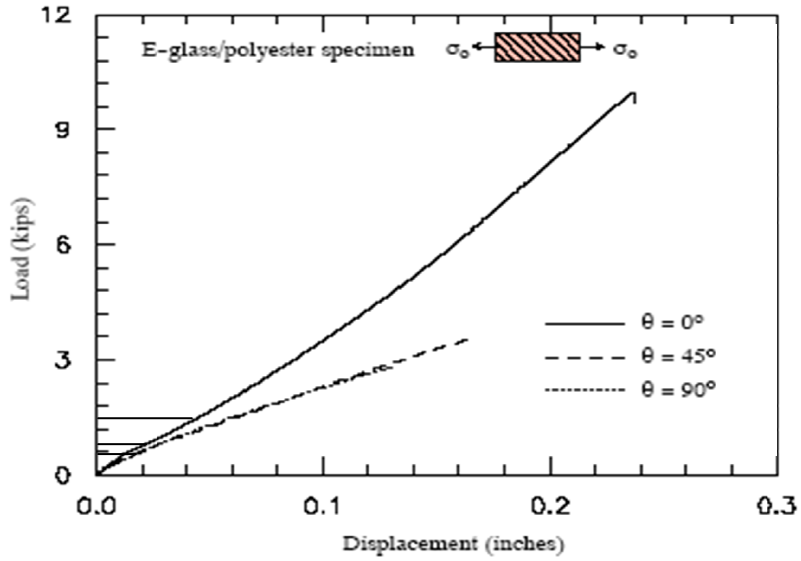

Figure 3.1 Force-displacement curves on off-axis specimens under quasi-static loading shows linear responses at load less than 0.2 times failure load

3.2 MATERIAL CHARACTERIZATION

The material parameters in the integral model are characterized using the experimental data from the uniaxial isothermal creep tests. The time-stress-temperature-dependent material parameters in Eq. (3.11) are determined for each off-axis specimen using creep-recovery data under isothermal conditions. The nonlinear material parameters are then modeled as a function of mean effective stress and temperature.

Linear viscoelastic behavior is characterized by characterizing each component in $\mathbf{D}^{o}$ and $\Delta\mathbf{D}(t)$ from each off-axis angle. For an average state of plane stress in a unidirectional fiber composite, only four principle creep compliances, D_{1111}, D_{2222}, D_{1122}, and D_{1212} are needed to completely characterize the linear viscoelastic behavior. D_{1111} is obtained from the loading along the fibers from the axial specimen data and D_{2222} from loading perpendicular to the fibers, i.e., the transverse specimen data. D_{1122} is obtained using the transverse strain from the axial specimens. Now, D_{1212} can be obtained after applying transformation given in Eq. 3.12, where D_{θ} is the compliance from tests on coupons with any fiber off-axis angle θ (figure 3.2). In our case the data from 45^{o} off-axis specimens is used and D_{1212} is computed.

$$D_{\theta} = l^4 D_{1111} + 2l^2m^2 D_{1122} + m^4 D_{2222} + l^2m^2 D_{1212} \tag{3.12}$$

Where,

$l = \cos\theta$, $m = -\sin\theta$ and $\theta = 45^{o}$

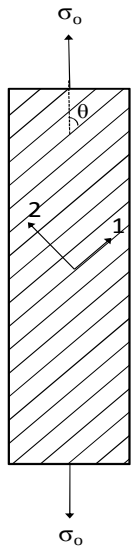

Figure 3.2 Uniaxial creep loading on off-axis coupons having fiber orientation θ with respect to global co-ordinates

The composite system follows transversely isotropic material so that rest of the complinces can be obtained as: $D_{1122} = D_{2211} = D_{1133} = D_{3311}$ and $D_{2233} = D_{3322}$. There is no available data to obtain the value of D_{2233} and it is assumed to be equal to 0.8 D_{1122} as that is generally the case when looked into literature (Swanson [35]). Also, $D_{3333} = D_{2222}$ and $D_{1313} = D_{1212}$. Due to lack of shear testing data available for D_{2323}, it is taken as independent of time and the value is assumed to be $2(D_{1122} - D_{1122})$ considering the property of transversely isotropic materials (Jones [26]).

The process of material characterization can be described in the following steps:

1. The linear material parameters $\mathbf{D}^{o}$, **C**, and **n** are calibrated from a linear creep response at the reference condition (σ_0/σ_{ult} = 0.2, T = 75˚F and g^{σ}, g^{T}, f^{σ}, and f^{T}=1) where the creep strain can be rewritten as,

$$\varepsilon_{ij}(t) = \mathrm{D}^{0}_{ijkl}\sigma^{0}_{kl} + \Delta\mathrm{D}_{ijkl}(\mathrm{t})\sigma^{0}_{kl} \tag{3.13}$$

The components of intitial compliance $\mathbf{D}^{o}$ are computed using instantaneous elastic strain $\boldsymbol{\varepsilon}_{c}^{o}$ for each off-axis angle. The parameters **C** and **n** are determined for each angle by fitting the transient compliance using power law:

$$\Delta\mathrm{D}_{ijkl}(\mathrm{t}) = \mathrm{C}_{ijkl}(t)^{n_{ijkl}} \tag{3.14}$$

2. Stress-dependent material parameters are then characterized using creep responses from several stress levels at the reference temperature (75^{o}F) as shown in Eq. (3.15). Here the temperature-dependent parameters, g^{T} and f^{T}, are both equal to one.

$$\varepsilon_{ij}(t) = [\mathrm{g}^{\sigma}\mathrm{D}^{0}_{ijkl} + \mathrm{f}^{\sigma}\mathrm{C}_{ijkl}(t)^{n_{ijkl}}]\sigma^{0}_{kl} \tag{3.15}$$

where the parameter g^{σ} is a function of effective stress, and is obtained from the instantaneous elastic responses for each off-axis angle. f^{σ} is obtained by the fitting the transient responses. In case of axial fibers the effective stress ($\overline{\sigma}$) is the same as the applied stress as it is along the principle fiber direction i.e., $\overline{\sigma} = \sigma_{11} = \sigma_0$ and the stress dependent parameter is given as:

$$g(\overline{\sigma}) = \frac{\varepsilon_{11}^{0}}{\sigma_{11} D_{1111}^{0}} \tag{3.16}$$

For the transverse specimens the loading is perpendicular to the fiber direction and $\overline{\sigma} = \sigma_{22} = \sigma_0$, so g^{σ} can be obtained as,

$$g(\overline{\sigma}) = \frac{\varepsilon_{22}^{0}}{\sigma_{22} D_{2222}^{0}} \tag{3.17}$$

For the 45^{o} off-axis specimens, g^{σ} is a function of the effective stress. The applied creep stress σ_0 is transformed from global co-ordinate system to material co-ordinate system to obtain the principle stresses.

$$\begin{bmatrix} \sigma_{11} \\ \sigma_{22} \\ \sigma_{12} \end{bmatrix} = [T] \begin{bmatrix} \sigma_{xx} \\ \sigma_{yy} \\ \sigma_{xy} \end{bmatrix} = [T] \begin{bmatrix} \sigma_0 \\ 0 \\ 0 \end{bmatrix}$$

Where, (3.18)

$$[T] = \begin{bmatrix} \cos^2\theta & \sin^2\theta & 2\sin\theta\cos\theta \\ \sin^2\theta & \cos^2\theta & -2\sin\theta\cos\theta \\ -\sin\theta\cos\theta & \sin\theta\cos\theta & \cos^2\theta - \sin^2\theta \end{bmatrix}$$

And for $\theta = 45^{o}$ we have,

$$\sigma_{11} = \sigma_0 \cos^2\theta = \frac{\sigma_0}{2}$$

$$\sigma_{22} = \sigma_0 \sin^2\theta = \frac{\sigma_0}{2} \tag{3.19}$$

$$\sigma_{11} = -\sigma_0 \sin\theta \cos\theta = -\frac{\sigma_0}{2}$$

The effective stress can now be computed as given in Eq. (3.18)

$$\overline{\sigma} = \sqrt{\frac{3}{2} S_{ij} S_{ij}} \quad (3.20)$$

Where S_{ij} is the deviatoric stress tensor and can be computed as,

$$S_{ij} = \sigma_{ij} - \frac{1}{3}\sigma_{kk}\,\delta_{ij} \quad (3.20)$$

For the 45-offaxis specimens, g^{σ} as a function of the effective stress, can be obtained as:

$$g(\overline{\sigma}) = \frac{\varepsilon_{xx}^{0}}{\sigma_{xx} D_{\theta}^{0}} \quad (3.21)$$

The stress-dependent material parameters are then expressed as an average function of effective stress ($\overline{\sigma}$) for any angle in general.

3. Similarly, the temperature dependent responses are characterized using the creep responses at several temperatures at the reference stress level. These stress-independent responses have g^{σ} and f^{σ} equal to one and the equation for creep strain is written as follows:

$$\varepsilon_{ij}(t) = [g^{T} D_{ijkl}^{0} + f^{T} C_{ijkl}(t)^{n_{ijkl}}]\sigma_{kl}^{0} \quad (3.22)$$

The temperature-dependent nonlinear parameters are modeled as a function of temperature (T) for each off-axis angle and an average temperature dependent function is obtained in general.

Aforementioned characterization methods are followed. The linear viscoelastic parameters in the nonlinear viscoelastic model are calibrated from stress and temperature independent creep responses performed under a low magnitude of applied stress (0.2 of

ultimate failure load) and at the reference temperature (75 ^{o}F). The creep compliances of axial, transverse and 45 off-axis specimens from this lowest load level (0.2) at temperature 75°F are then used to calibrate $\mathbf{D}^{o}$, **C**, and **n** by matching the overall responses with the experimental data. The calibrated linear parameters are given in table 3.1. The higher values of the components of **C** and **n** imply that time-dependent behaviors are more pronounced for the off-axis specimens. The nonlinear viscoelastic parameters g^{σ}, g^{T}, f^{σ}, and f^{T} are held equal to one during this calibration stage.

Table 3.1 Linear viscoelastic parameters for axial, transverse and 45^{o} off-axis coupons used for calibration of nonlinear parameters

$\mathbf{D}^{0}$ x 10^{-4} 1/ksi (1/MPa)		**C** x 10^{-5} 1/ksi (1/MPa)	**n**
Axial (D_{1111})	7.55 (52.05)	3.18 (21.93)	0.245
Transverse (D_{2222})	6.87 (47.36)	1.56 (10.76)	0.21
45^{o} off-axis	2.69 (18.55)	0.21 (1.44)	0.195

The responses from the higher load levels at the reference temperature are then used to calibrate the stress-dependent material parameters. For this purpose the temperature dependent parameters are held equal to one. Figure 3.3 shows creep compliances of transverse specimens under uniaxial tension at 75^{o}F for stress levels 0.2-0.6.

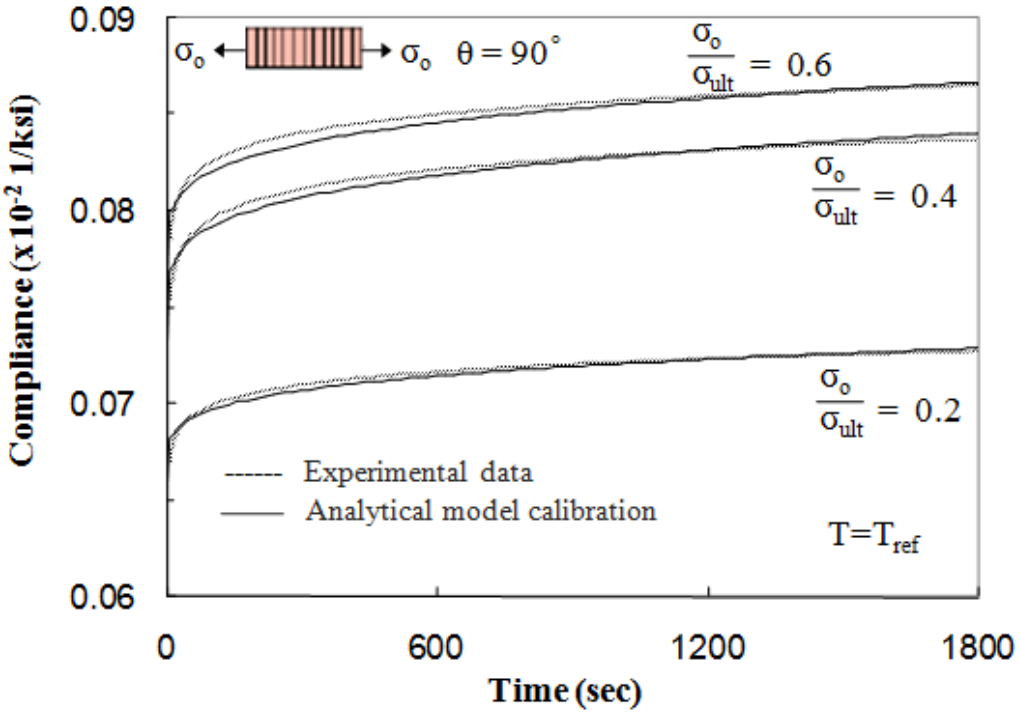

Figure 3.3 Creep compliances for transverse specimens at T=75°F (experimental data used for stress-dependent parameter calibrations)

For characterizing the temperature dependent material parameters, the response at the lowest load level and different temperatures are used. Thus the temperature-dependent parameters are characterized using the creep compliances at the lowest load level (0.2) and several temperatures (0-125°F), as illustrated in figures 2.4-2.6 (a). At these temperatures and the lowest load level (0.2), the stress dependent nonlinear parameters are held equal to one. Figure 3.4 shows creep compliances of transverse specimens under uniaxial tension at load ratio 0.2 for temperatures of 0^{o}F to 125^{o}F. Similar calibration procedure is also performed to characterize material parameters for the axial and 45^{o} off-axis specimens.

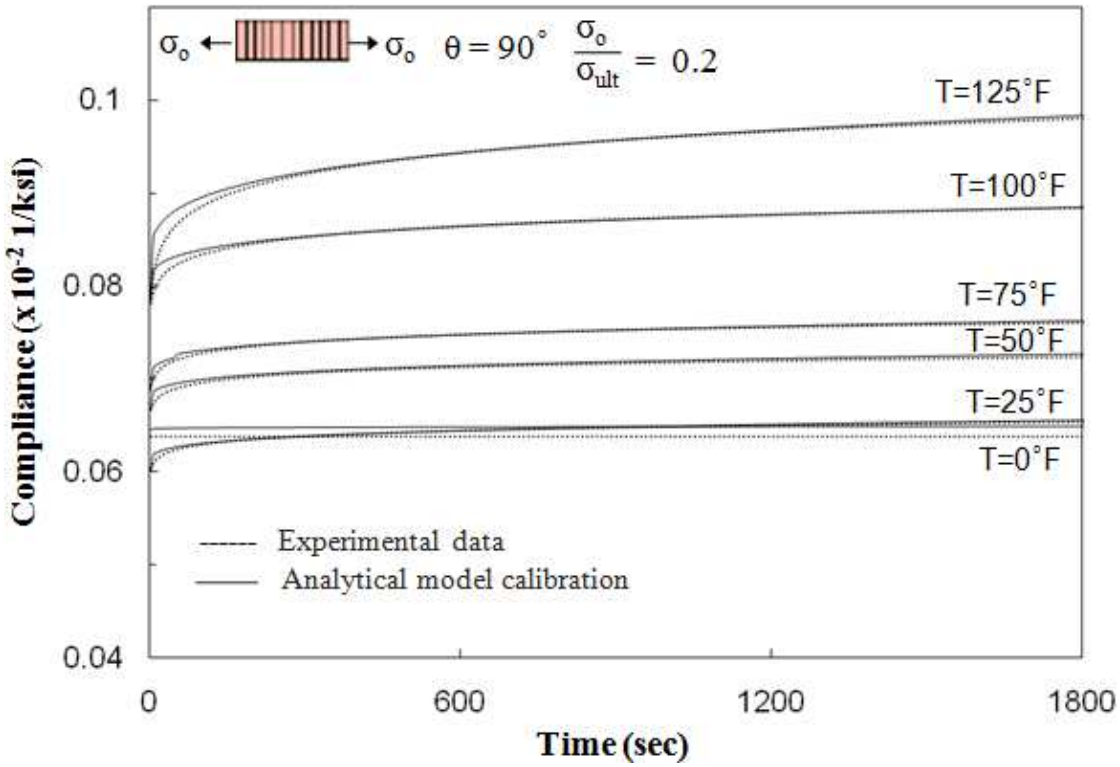

Figure 3.4 Creep compliances for transverse specimens at load ratio 0.2 (experimental data used for temperature-dependent parameter calibrations)

Figures 3.5-3.7 (a-b) present the calibrated nonlinear material parameters as a function of effective stress and temperature, for the axial, transverse and 45^{o} off-axis specimens under uniaxial tension. At the stresses lower than 20% of the ultimate strength, all nonlinear stress-dependent parameters in Eq. (3.11) are set to be one as illustrated in figure 3.1. The stress-dependent parameters are calibrated from the creep responses for stress levels 40% and 60% of the ultimate strength at room temperature. The temperature dependent parameters are calibrated from creep test of 0.2 load ratio at

0^{o}F, 25^{o}F, 50^{o}F, 100^{o}F and 125^{o}F. Polynomial functions are used to fit the calibrated stress and temperature parameters (Table 3.2 and 3.3). The accuracy of these polynomial functions is within these calibrated stresses and temperatures; beyond these calibrated limits, the polynomial function may not represent the actual material behaviors. The temperature dependent parameters monotonically increase beyond 75^{o}F but follow a random variation at low temperatures of 0^{o}F to 50^{o}F (Figs. 3.5-3.7 a). This reemphasizes the random behavior of creep responses at lower temperatures as seen earlier in section 2.2. All the parameters show a general increasing trend excepting the stress-dependent parameter for axial specimens (Fig. 3.5 b). The parameter increases until 0.4 load ratio and then sharply decreases for 0.6 load ratio. This can be related to the hardening behavior of the axial specimens in figure 3.1 due to which the compliance goes down and these responses are characterized based on compliances. This may also be due to specimen failure beginning to occur at this high load level. Muliana et al. [22] have found in their experimental study that the axial specimens have failed even at load ratio 0.2 for elevated temperatures beyond 125^{o}F. Figure 3.8 presents the averaged nonlinear parameters as a function of the effective stress and temperature for any general off-axis angle. Polynomial functions are again used to fit the parameters (Tables 3.2 and 3.3) and the curves smoothly and monotonically increase with stress and temperature.

a)

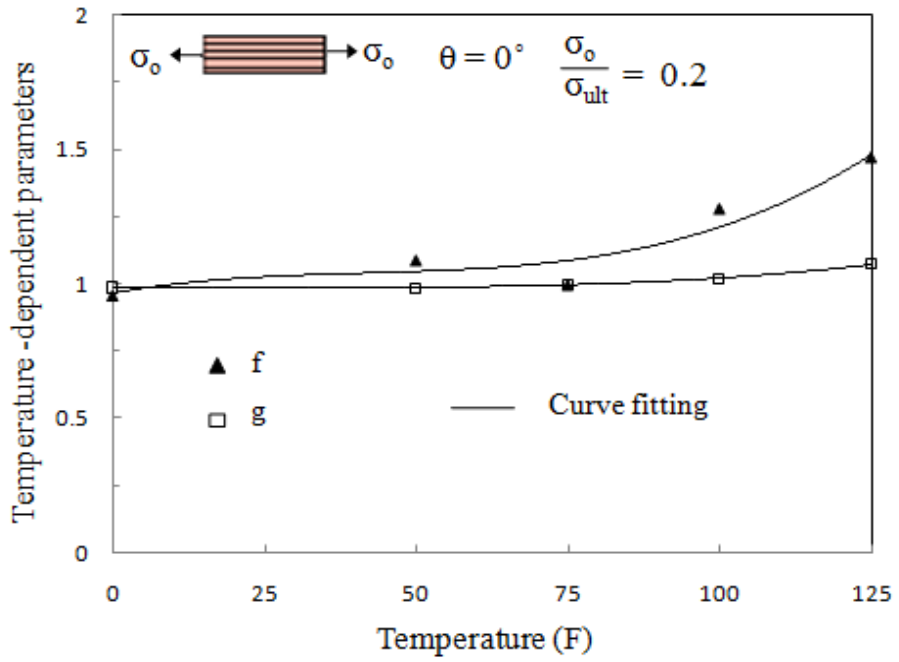

b)

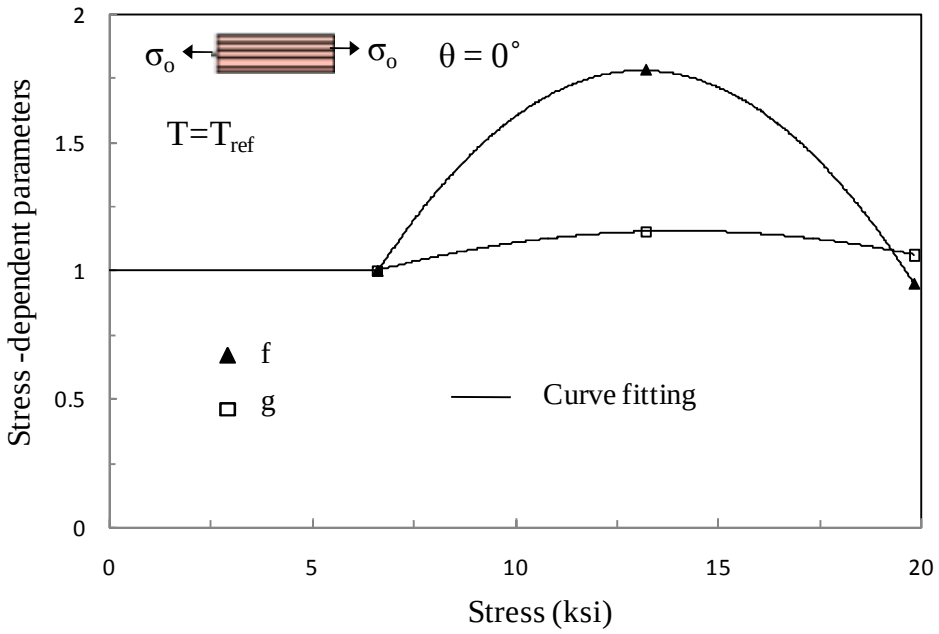

Figure 3.5 Nonlinear parameters for axial specimens under uniaxial creep a) Temperature dependent b) Stress-dependent

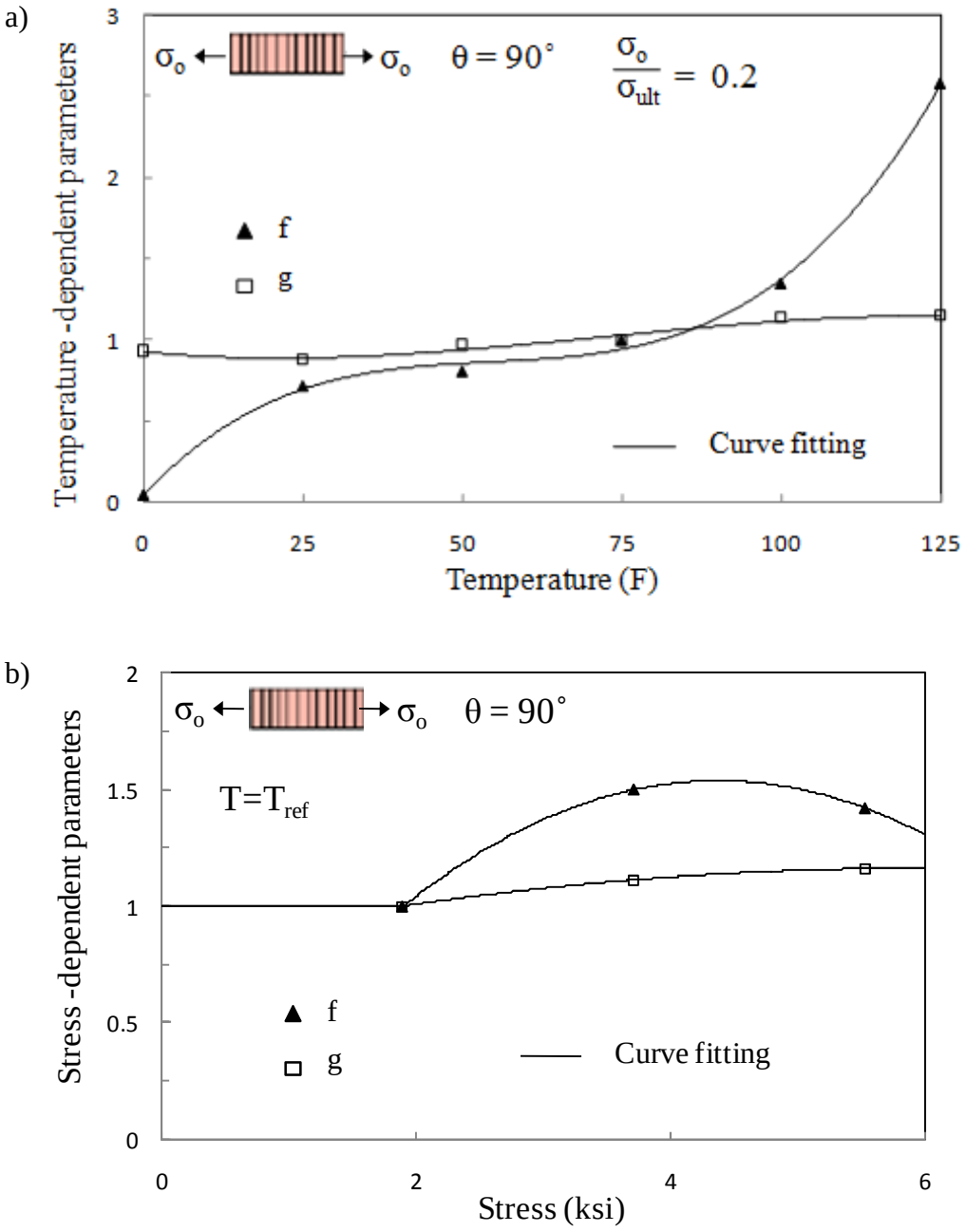

Figure 3.6 Nonlinear parameters for transverse specimens under uniaxial creep a) Temperature dependent b) Stress-dependent

a)

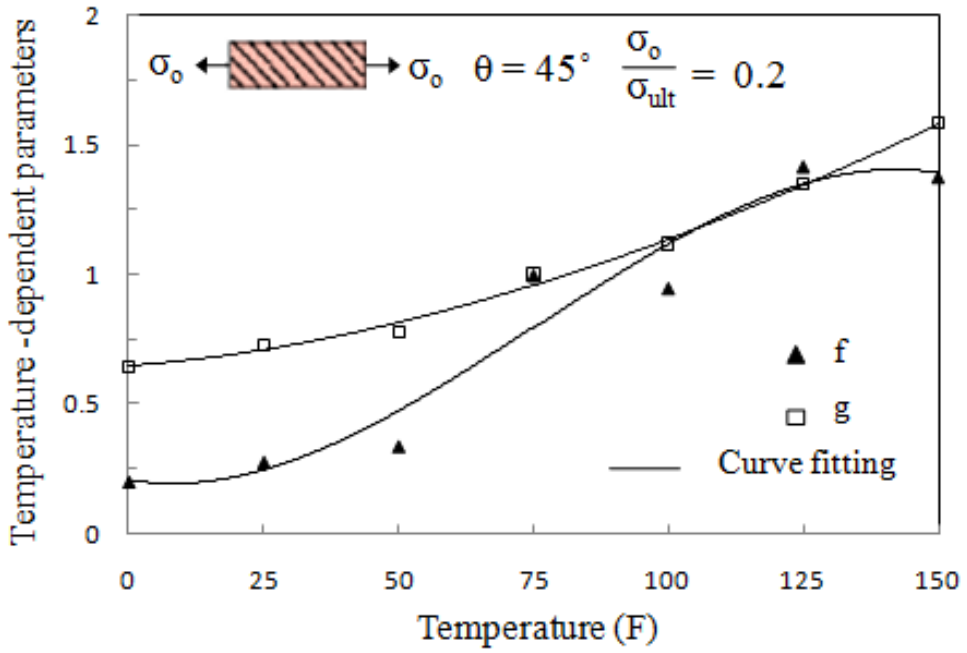

b)

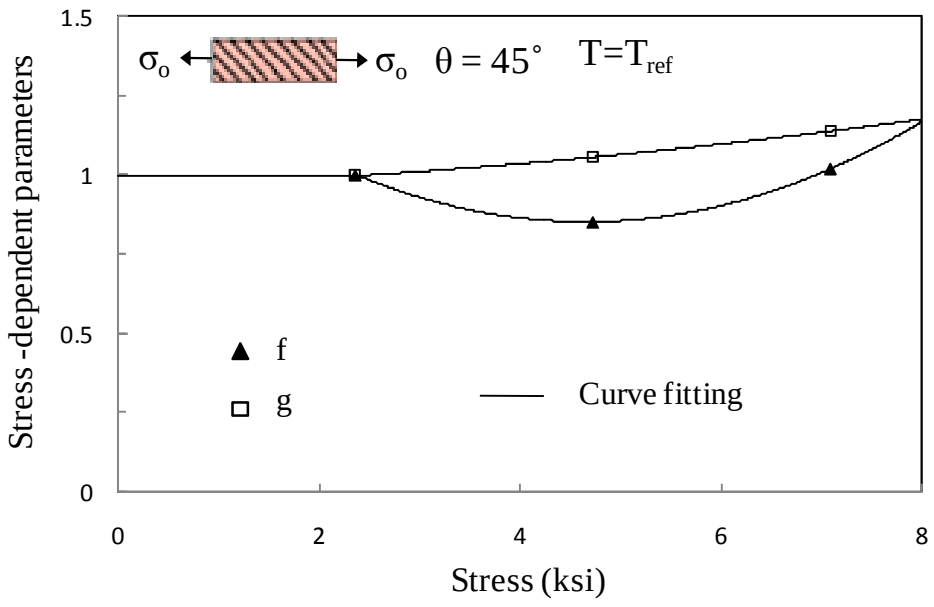

Figure 3.7 Nonlinear parameters for 45 off-axis specimens under uniaxial creep a) Temperature dependent b) Stress-dependent

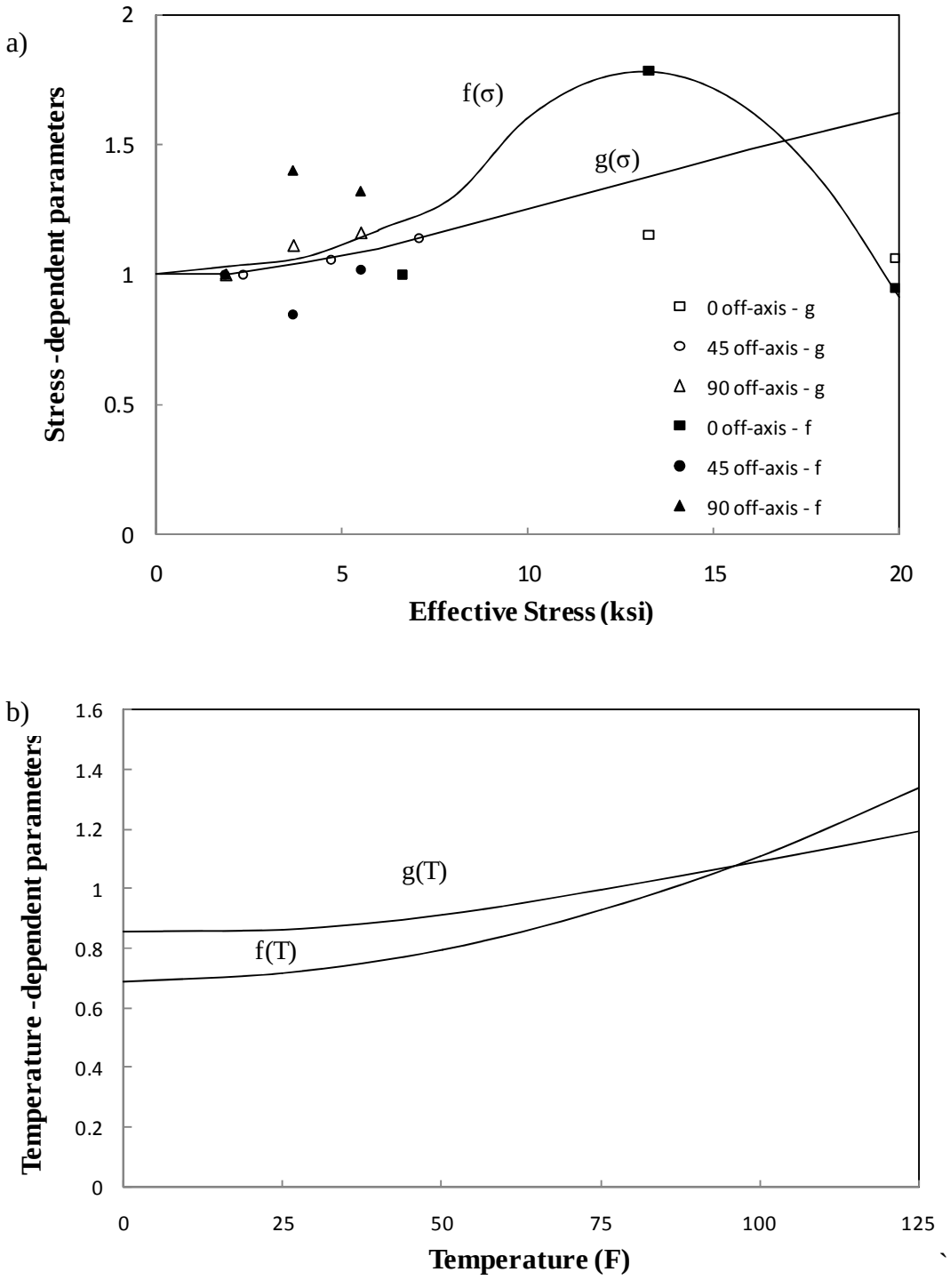

Figure 3.8 Averaged Nonlinear parameters as a function of a) Effective stress b) Temperature

Table 3.2 Stress-dependent nonlinear parameters

Off-axis Angle	Nonlinear parameter	Effective stress dependency
0	$g(\sigma)$	$-2.753 \times 10^{-3}(\sigma)^2 + 7.748 \times 10^{-2}(\sigma) + 0.6079$
	$f(\sigma)$	$-1.839 \times 10^{-2}(\sigma)^2 + 0.4829(\sigma) - 1.390E+00$
45	$g(\sigma)$	$2.038 \times 10^{-3}(\sigma)^2 + 0.0104(\sigma) + 0.9641$
	$f(\sigma)$	$4.833 \times 10^{-2}(\sigma)^2 - 0.3528(\sigma) + 1.493E+00$
90	$g(\sigma)$	$-9.659 \times 10^{-3}(\sigma)^2 + 0.1158(\sigma) + 0.816$
	$f(\sigma)$	$-8.756E-02x2 + 0.7645(\sigma) - 0.1306$
Average	$g(\sigma)$	$0.035(\sigma) + 0.903$
	$f(\sigma)$	$0.013 (\sigma)^2 - 0.009(\sigma) + 0.911$

Table 3.3 Temperature-dependent nonlinear parameters

Off-axis Angle	Nonlinear parameter	Temperature dependency
0	$g(T)$	$8.315 \times 10^{-8}(T)^3 - 5.4 \times 10^{-6} (T)^2 + 4.923 \times 10^{-5}(T) + 0.9896$
	$f(T)$	$6.702 \times 10^{-7}(T)^3 - 8.326 \times 10^{-5} (T)^2 + 4.121 \times 10^{-3} (T) + 0.9644$
45	$g(T)$	$-5 \times 10^{-8} (T)^3 + 4 \times 10^{-5} (T)^2 + 0.001(T) + 0.648$
	$f(T)$	$-7.378 \times 10^{-7} (T)^3 + 1.819 \times 10^{-4} (T)^2 - 1.758 \times 10^{-3}(T) + 0.1988$
90	$g(T)$	$-5.117 \times 10^{-7} (T)^3 + 1.103 \times 10^{-4} (T)^2 - 4.014 \times 10^{-3} (T) + 0.9308$
	$f(T)$	$4 \times 10^{-6} (T)^3 + 0.041(T) + 0.053$
Average	$g(T)$	$2 \times 10^{-5} (T)^2 + 0.848$
	$f(T)$	$4 \times 10^{-5} (T)^2 + 0.0002(T) + 0.6875$

3.3 PREDICTION OF NONLINEAR THERMO-VISCOELASTIC BEHAVIORS

Predictions of the overall nonlinear time-stress-temperature dependent responses of the axial, transverse and 45^{o} off-axis coupon tests at load ratios 0.4 and 0.6 that were not used in the calibration process are presented in Figures 3.9 to 3.11 (a-b). Overall good predictions are shown. There was a mismatch of about 6-10% in the prediction of the responses at 0^{o}F and 125^{o}F for all the off-axis angles. The mismatch in the 125^{o}F was mostly in the transient part than in the initial part. Here it would be apt to refer back to figure 2.11 and recall the discussion that the effect of temperature on nonlinearity may be a function of time for 125^{o}F. In this case, the transient creep parameter *f*, which is used here is only a function of stress and temperature. An additional time function may have to be incorporated into the temperature-stress-dependent parameters for depicting the nonlinearity at higher temperatures. Thus, the mismatch in the prediction of temperatures beyond 125^{o}F may be accounted for by this drawback of the model. The mismatch at lower temperatures may be accounted for by referring back to the discussion in section 2.2.1. The creep responses of all the off-axis specimens at lower temperatures did not follow any particular trend for different load ratios. When the nonlinear parameters were characterized for the temperatures 0^{o}F to 50^{o}F at the reference stress level of 0.2 load ratio there is no guarantee that this will rightfully predict the responses at higher stress levels due to the random trend in the responses at these temperatures. This can be a reason for the mismatch in the predictions at lower temperatures for the off-axis specimens. For all elevated temperatures in general, the

model predicted the time-stress-temperature dependent behaviors almost accurately with a maximum error of about 2 to 3%. This reaffirms the assumption that the stress and temperature effects on the time-dependent behaviors of multi-layered composites can be coupled in the product form as validated by Muliana et al. [22].

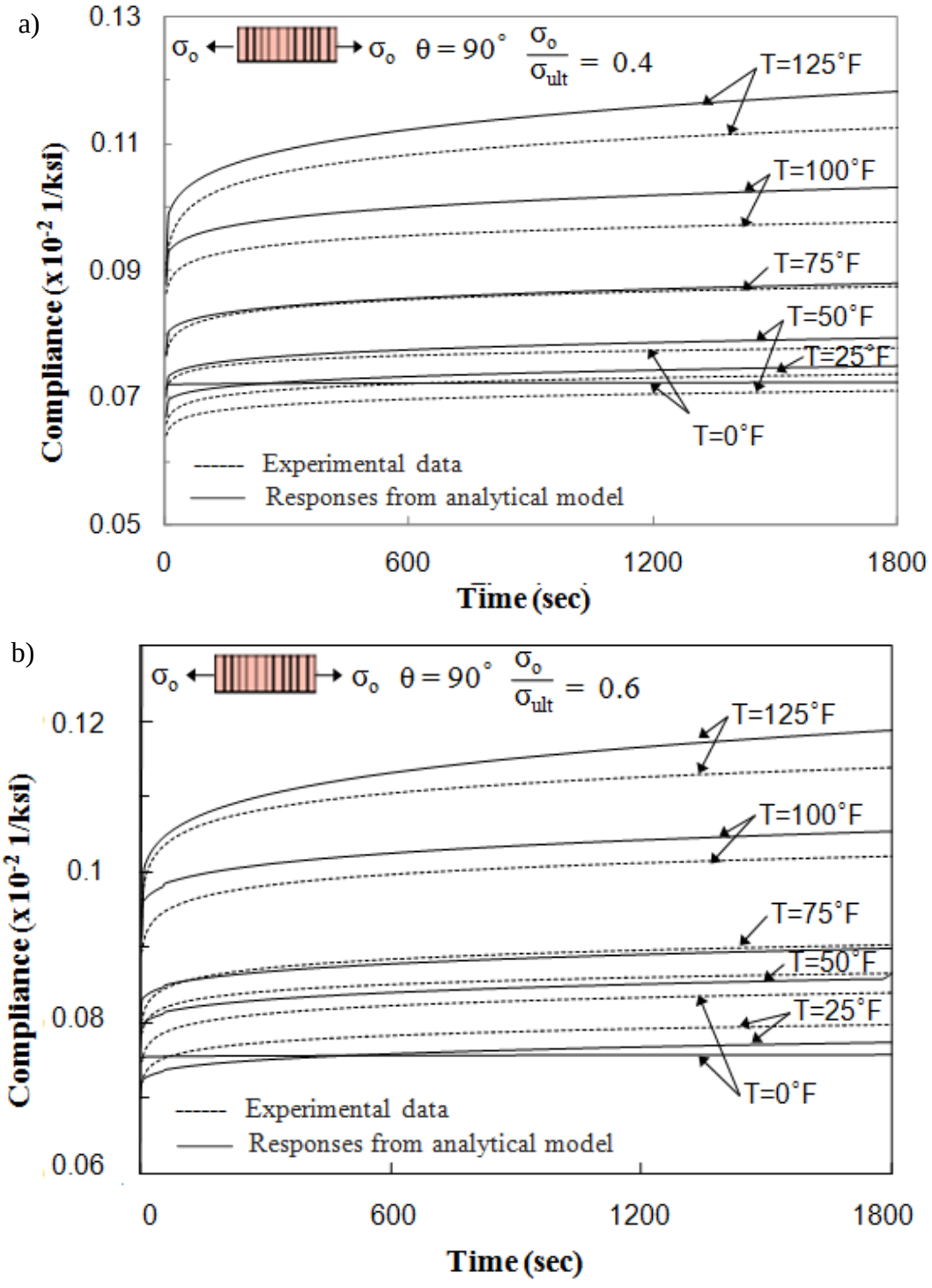

Figure 3.9 Prediction of the model for transverse specimens for load ratio a) 0.4 and b) 0.6

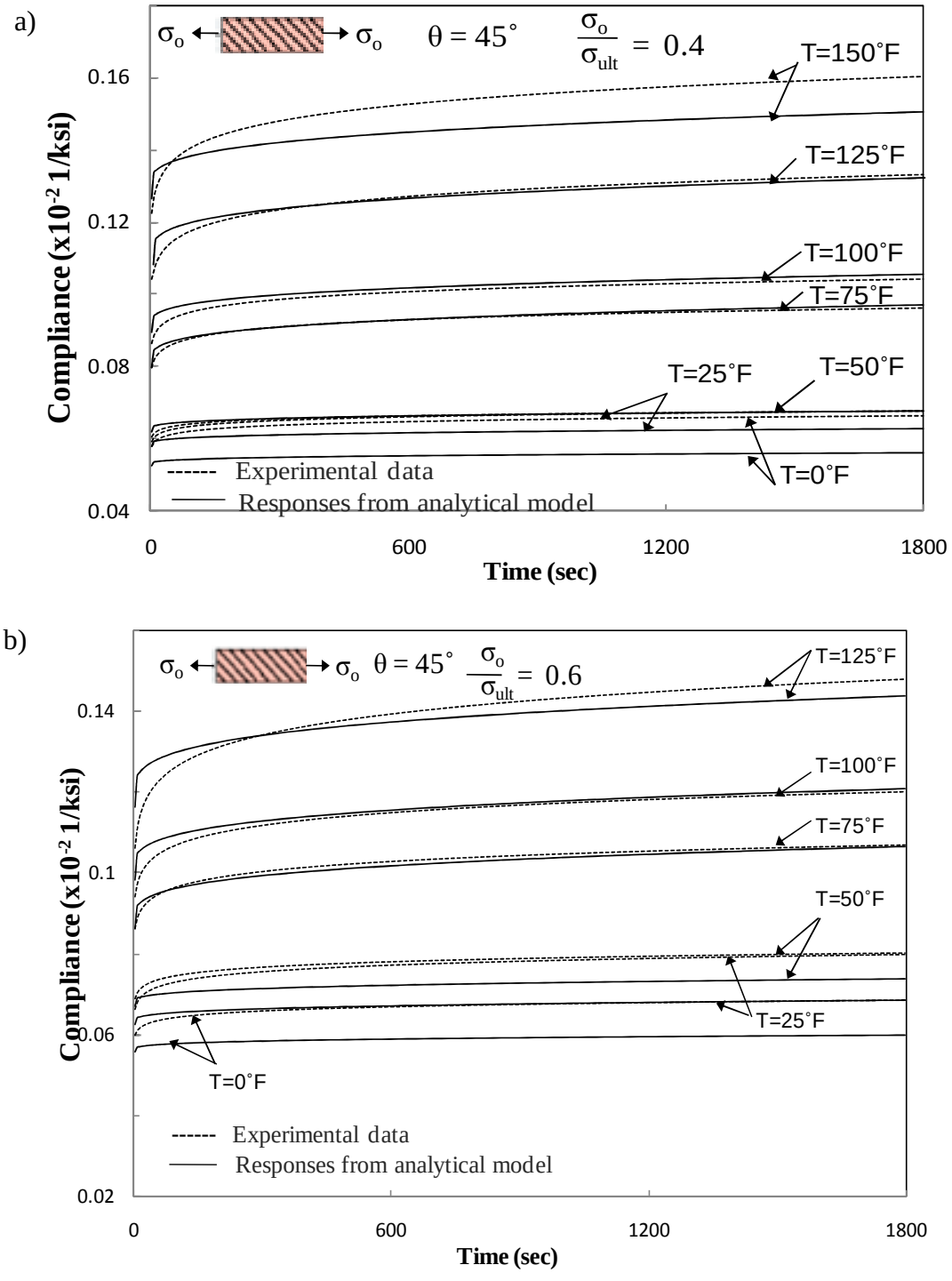

Figure 3.10 Prediction of the model for 45 off-axis specimens for load ratio a) 0.4 and b) 0.6

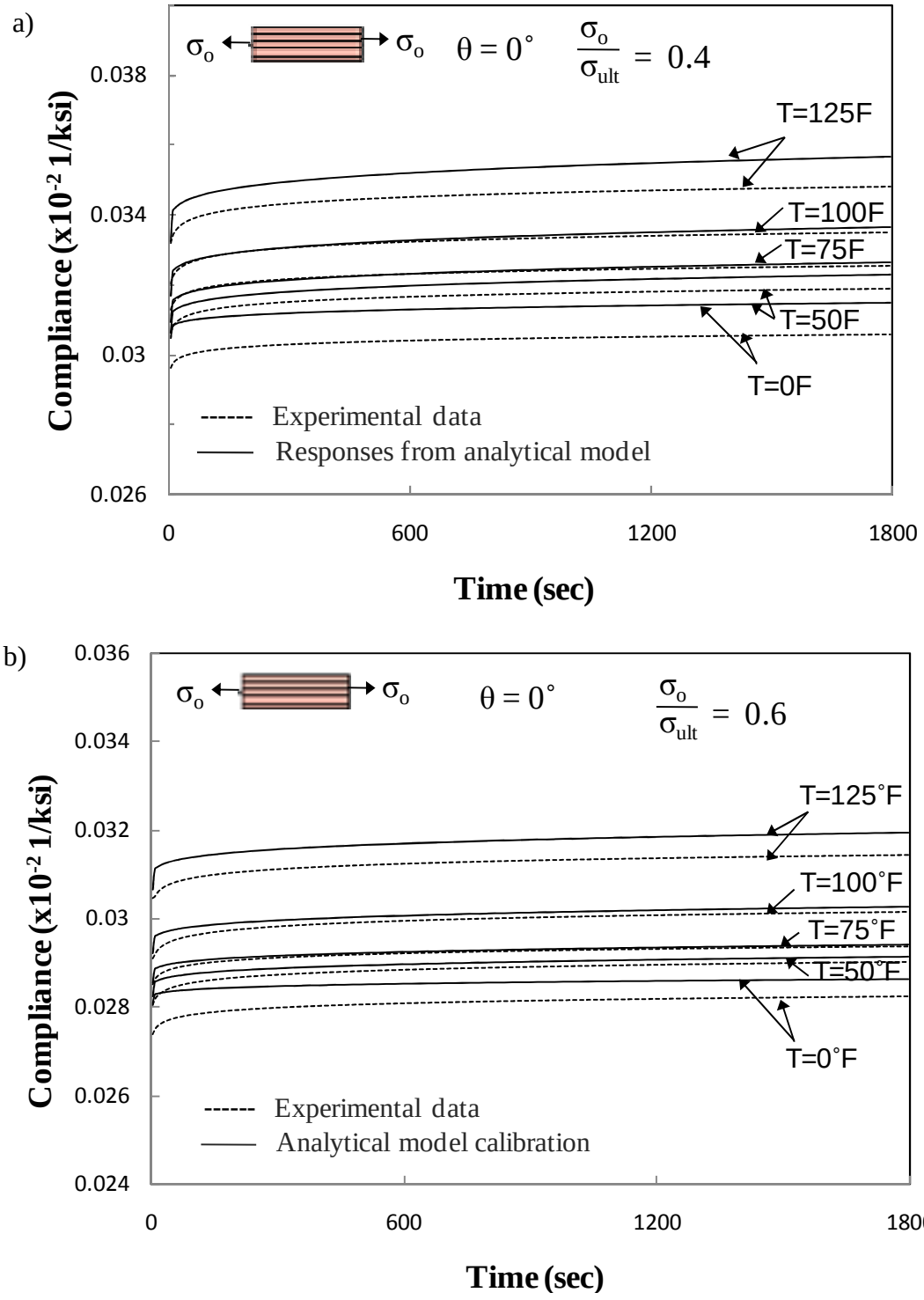

Figure 3.11 Prediction of the model for axial specimens for load ratio a) 0.4 and b) 0.6

CHAPTER IV

FINITE ELEMENT ANALYSIS: SENSITIVITY ANALYSIS OF CREEP TESTS AND THERMO-VISCOELASTIC RESPONSES OF PULTRUDED COMPOSITE SLABS

This chapter presents thermo-viscoelastic analysis of composite structures using finite element (FE). The numerical integration algorithm developed by Sawant and Muliana [28] was used to integrate the time-dependent constitutive material model for orthotropic materials to FE structural analyses. Sensitivity analysis is conducted to examine the effects of grip pressures and error margins in the off-axis angles. FE model of uniaxial tensile creep testing is generated to simulate the creep tests. It is found that the effect of these testing parameters on the recorded strain data is insignificant. Finally, the effect of through-thickness temperature variations on the bending of composite slabs subject to uniformly distributed load is studied.

4.1 IMPLEMENTATION OF THE CONSTITUTIVE MODEL IN FE ANALYSIS

The creep behaviors are simulated using the nonlinear viscoelastic model of orthotropic composite materials presented in Sawant and Muliana [28]. They modified the Schapery [29] nonlinear single integral equation to include the effects of stress and temperature on viscoelastic material responses. Material symmetry of the compliance matrix is imposed thus giving nine independent time integral equations. The integrated structural and material levels require performing linearized solutions of the nonlinear constitutive equations and iterative schemes simultaneously at those levels. Iterative

schemes are needed to minimize errors arising from the linearization. The numerical schemes are compatible with a displacement-based FE analysis. At each global iteration within the incremental time-step $\Delta t^{(m)}$, trial incremental component of strain tensor $\Delta\varepsilon ij^{t,(m)}$ and temperature $\Delta T^{t,(m)}$ are given and the component of strain tensor and temperature at the current time are defined by:

$$\varepsilon_{ij}^{t,(m)} = \varepsilon_{ij}^{t-\Delta t} + \Delta\varepsilon_{ij}^{t,(m)} \tag{4.1}$$

$$T^{t,(m)} = T^{t-\Delta t} + \Delta T^{t,(m)} \tag{4.2}$$

The superscript (m) denotes global iteration counter within the current incremental time step. The current total stresses $\sigma ij^{t,(m)}$ and material's consistent tangent stiffness $C_{ijkl}{}^{t,(m)}$ are calculated from given current variables and history variables stored at the previous converged solution at time (t-Δt). The converged $C_{ijkl}{}^{t,(m)}$ after M global iteration at the current time t is used to provide incremental trial strains for the next time step (t+Δt). The above procedure is performed at each material (Gaussian) integration point within elements at every structural iteration to achieve structural and material convergence simultaneously. Detailed numerical algorithm is given in Sawant and Muliana [28].

The transient compliance is expressed using Prony series given in Eq. 3.10. Thus, linear time-dependent characterization is once again performed from the 30 minute creep tests on the axial, transverse and 45 off-axis specimens at the reference conditions. The methods of characterization listed in chapter III (section 3.2) are repeated and the time-dependent parameters are obtained. Table 4.1 presents the Prony coefficients from 1800 second creep data in a second unit time. The orthotropic effective linear elastic properties

of the E-glass/polyester system are given in Table 4.2. The major Poisson's ratio ν_{12} is assumed to be constant and this assumption was proven to be valid for the experimental data as discussed in chapter II (section 2.3).

Table 4.1 Prony series coefficients for axial, tranverse and shear compliances from 30 minute calibration.

N	$\boldsymbol{\lambda_n}$ (1/sec)	$\mathbf{D_n}$ x 10^{-6} 1/ksi		
		D_{1212}	D_{2222}	D_{1111}
1	1	0.1	0.1	0.01
2	$5x10^{-1}$	0.18	0.1	0.018
3	10^{-1}	210.00	26.0	3.50
4	10^{-2}	170.00	18.0	2.10
5	10^{-3}	310.00	31.0	3.10
6	10^{-4}	500.00	31.0	5.10

Table 4.2 Elastic properties of the E-glass/polyester system

Modulus (ksi)				Poisson's ratio	
E_{11}	$E_{22}=E_{33}$	$G_{12}=G_{13}$	G_{23}	$\nu_{12}=\nu_{13}$	ν_{23}
3717.98	1455.91	445.711	356.569	0.33	0.35

The stress and temperature dependent nonlinear material properties (g,f) are expressed as polynomial functions as discussed in Chapter III (Table 3.2-3.3). In the case of the stress-dependent parameter, g , for the axial specimens being fit with polynomial function (see Fig 3.5 b), there were convergence issues in the FE analyses at stress levels of 0.6 ratio and higher. The equilibrium equations have not converged and the force equilibrium was not achieved within tolerance. Also, negative Eigen values were obtained. The polynomial approximation of f and g leads to negative slopes at higher stress levels and during the iteration process, there is a possibility of negative values in f and g. Hence piecewise linear functions are used to improve convergence during creep analyses for the axial specimens. The functions are expressed as:

$g(\sigma) = 0.02284(\sigma) + 0.8489$ for $0.2 < \sigma/\sigma_{ult} < 0.4$

$g(\sigma) = -0.0136(\sigma) + 1.33094$ $0.4 < \sigma/\sigma_{ult}$

4.2 SENSITIVITY ANALYSIS

Sensitivity analysis is carried out using FE simulation of creep testing. The purpose is to investigate the effects of geometric imperfection, misalignment of testing instruments, end-clamping conditions and manual error on the recorded strain data. During experimental tests, there is possibility of error in the recorded strain data due to several testing parameters. For example, when cutting the coupons from sheets of pultruded composite there may be an error in the dimensions of the specimens and its cross-section area and also the orientation of the fiber angles leading to a geometric and material imperfection. Also when the specimen is attached to the grips, it may not be

aligned perfectly vertical and thus the creep load may not be applied in a perfectly longitudinal direction to the specimen, again leading to an effective error margin in the fiber off-axis angles. Also, when tightening the grips to attach the specimen, the bottom and the top grips may not be perfectly in line with each other, thus inducing an effective torque on the specimen. The end-clamping conditions such as grip pressure may also have an impact on the data. Also there may be a manual error in attaching the gauges exactly at the center leading to results away from the center of the coupon. The effect of such parameters on the experimental data has to be studied in order to understand its significance. In this study, we examine the effects of grip pressures and error margins in the off-axis angles and investigate the variation in the recorded strains at points slightly away from the center of the specimen. This helps us in understanding the parameters that affect the measured response of pultruded off-axis coupons.

4.1.1 FE model of Uniaxial Creep Tests

In order to perform this sensitivity analysis, the testing procedure is simulated in Finite Element software. The specimen dimensions in the simulation are the same as those in real testing, i.e, 9.5x1.25x0.25. Figure 4.1 describes the FE model and the geometry of the coupons. The specimen has the E-glass/polyester material properties as given in Table 4.2. The grips are modeled as a material of high strength and stiffness: High Strength Steel. The grips are fixed on one side and pressure is applied on the other side in the 2 direction as shown in Figure 4.1. The FE model is generated using eight noded brick element (C3D8). The model is created such that the nodes of the grip and

the specimen are common so as to transfer the loads between them. The FE analysis consists of two successive steps. The first step is where the grip pressure is applied. The second step is where the uniaxial tensile load is applied along the 1 direction. The loads are not applied directly on the specimen but are applied on the top surface of the two top grips. The amount of load applied for all of the simulations in the study is the highest value of 0.6 ratio of the ultimate tensile strength of the specimen being tested. The bottom grips are fixed in the 1 direction. The specimen and the grips are also fixed in the 3 direction.

The numerical integration algorithm developed by Sawant and Muliana [28] is used to integrate the constitutive material model to FE structural analyses. A parametric study is conducted by performing the simulations for different end-clamping conditions and variations in fiber off-axis angles of the material so as to check for the effect of grip pressure, material imperfection, and misalignment of testing instruments on each off-axis specimen. The resulting axial strain field from each simulation is studied at the center of the specimen where the strain gauge would be attached. The strain field is also studied slightly away from the strain guage, i.e., at points offset from the center in the longitudinal and transverse direction by 2% of the specimen length. This is done in order to justify recording the strains at the center and also to account for manual error in attaching the strain gauge at the center.

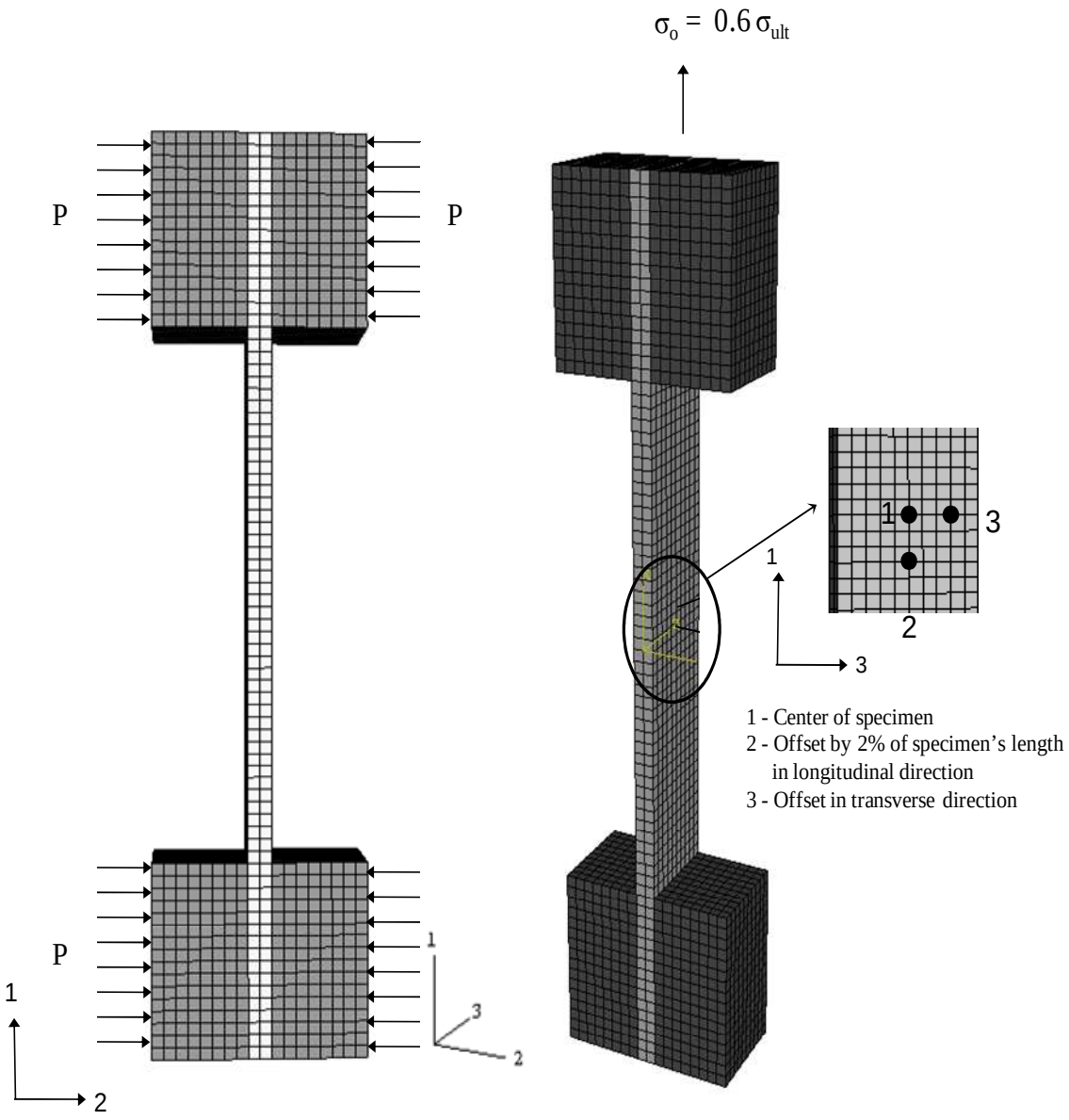

Figure 4.1 FE model for simulating uniaxial tensile creep tests on off-axis multilayered composite specimen

4.1.2 Effect of end-clamping conditions

Several studies have been performed to investigate the end-clamping effect of the specimen in off-axis tensile tests in layered composites. Haj-Ali and Kilic [7] found in their study that the added shear stress in tension due to misalignment of the material can be reduced by using longer coupons and also relatively larger section areas. It was also said that the data recorded at the center of the specimen was less affected by the end conditions than that away from the center. Rizzo [25] recommended to use specimens with length to weight ratio larger than 10 to reduce the end-clamping effect. In our testing process, the application of grip pressure was done manually as opposed to the application of hydraulic grip pressure. Thus the value grip pressure applied is not known and may vary for different tests conducted. A parametric study is performed to analyze the effect of grip pressure on the output strain data for each off-axis specimen.

In order to check for the effect of end-clamping conditions on the strains recorded the parametric study is conducted by varying the grip pressures from 0.5 to 4 ksi at an applied tensile load ratio of 0.6 on the specimen. The resulting axial strain field is studied at the center of the specimen where the strain gauge would be attached and also slightly away from the strain guage, i.e., at points offset from the center along the longitudinal and transverse direction by 2% of the specimen length.

For each off-axis specimen the effect of grip pressure is shown in figure 4.2 (a-c). For the axial specimens the change in the axial strains from 0.5 to 2 ksi pressure is very negligible (fig. 4.2 a). Even upon increasing the pressure to 4 ksi, the strains are affected

by only 0.03%. Similar is the case with 45^{o} off-axis coupons as there is difference of 0.03% between 2 ksi and 4 ksi grip pressure application and no difference between 0.5 and 2 ksi grip pressures (fig. 4.2 c). In case of the transverse specimens the strains recorded were almost same for all of the three grip pressures (fig. 4.2 b). Hence the effect of end-clamping conditions can be stated as negligible on the off-axis specimens. Also the difference between the recorded axial strains at center and 2% away from the center in both the longitudinal and transverse directions is a maximum of 0.01% for all the specimens, and thus negligible, as seen in figure 4.2 (a-c).

a)

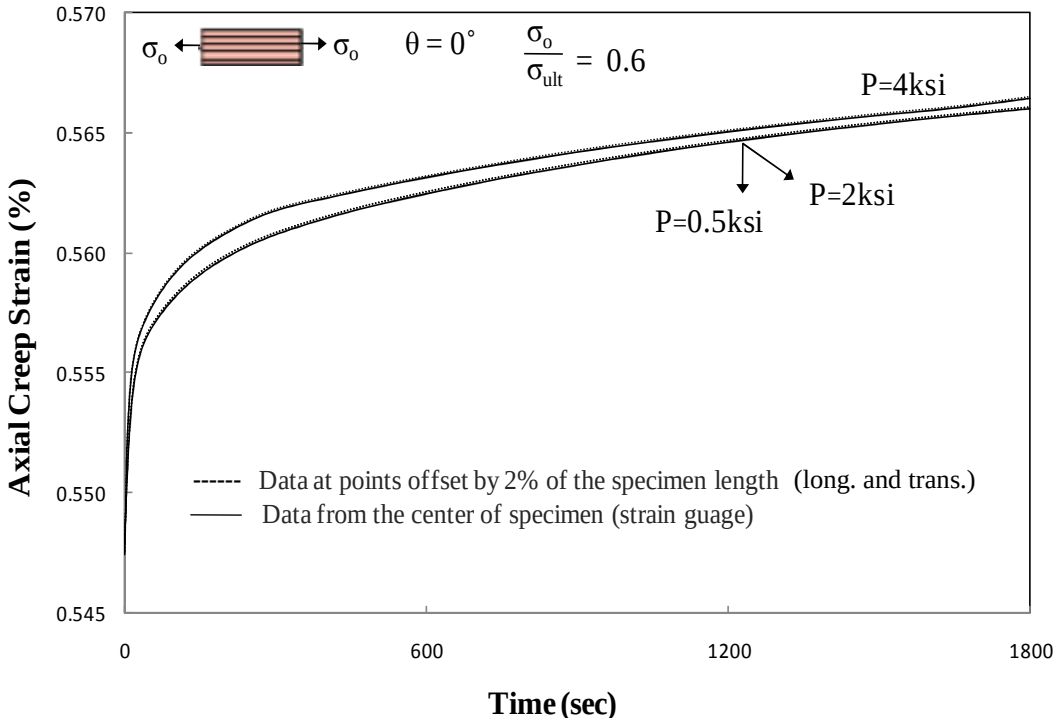

Figure 4.2 Parametric study of effect of grip pressure at P=0.5, 2, 4ksi for a) axial b) transverse and c) 45° off-axis specimens

b)

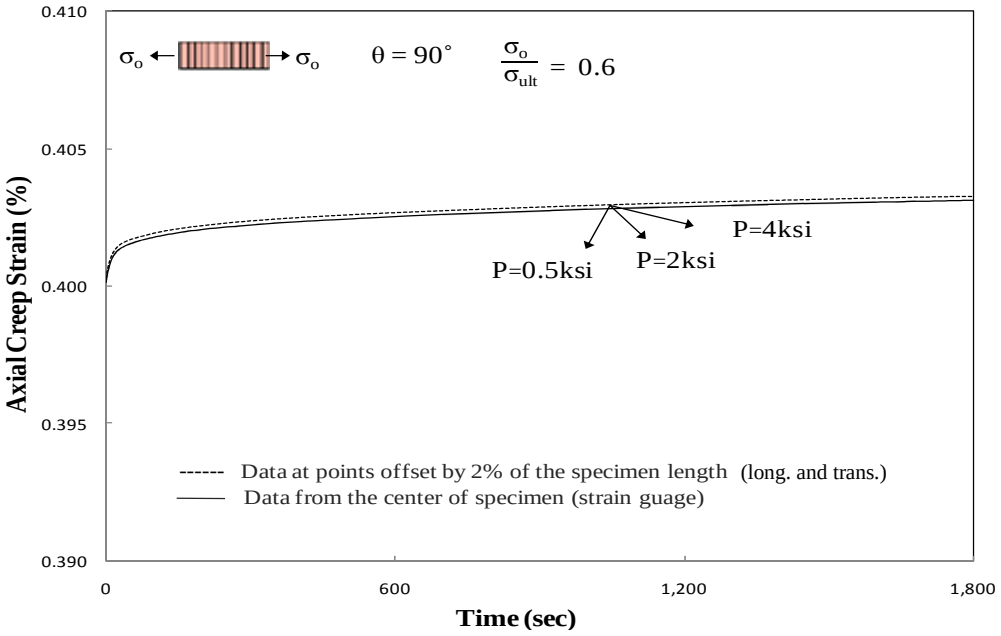

c)

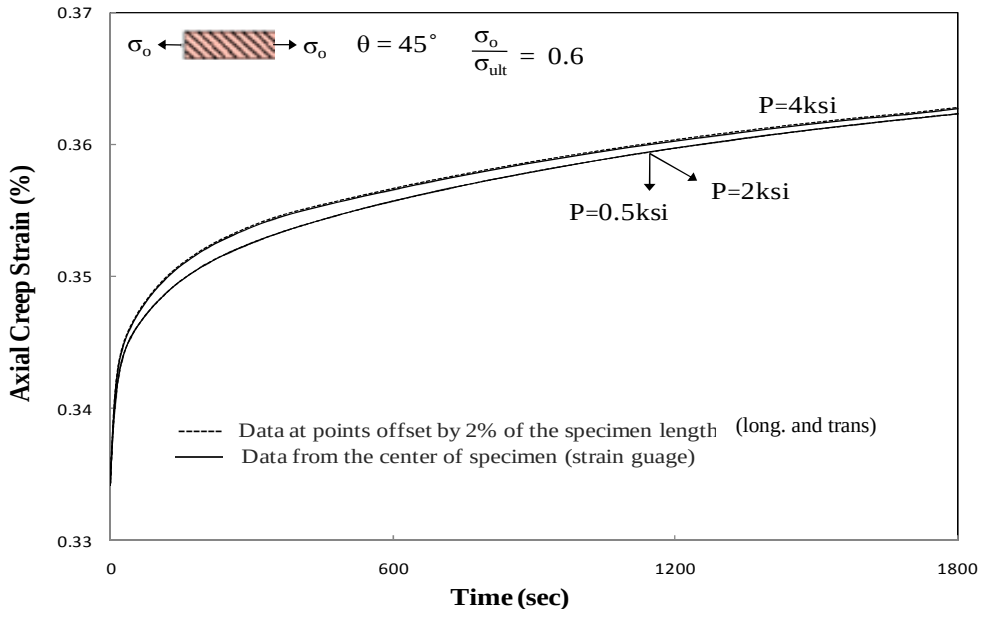

Figure 4.2 Continued

4.1.3 Effect of error margins in the off-axis angles

The specimens that are used for experimental tests are cut from 0.25 inch thick E-glass/Polyester sheets with rovings in axial direction such the orientation of the roving is controlled. Thus there may be an error while cutting leaving a change in the fiber angle of the specimen obtained. Also, while clamping the specimen for tensile testing there may be a misalignment of the specimen or the testing equipment thus leading to an effective change in fiber orientation of the specimen tested. Hence, a parametric analysis is conducted to study the effect of slight variations in the off-axis angle on the axial strains recorded.

In order to do this the off-axis tests are simulated for a change in the fiber angle by $\pm 5°$ and also $\pm 10°$ from the original fiber angle for each off-axis specimen at the reference temperature of 75°F. These simulations are carried out at 2ksi grip pressure and the tensile load applied is of 0.6 load ratio so as to easily note the effect. Figure 4.3 (a-c) shows the effect of material imperfection for axial, transverse and 45^{o} off axis specimens. Figure 4.3 (a) shows the effect on axial specimens. For this case a change in angle by +5° or -5° and +10° or -10° are same due to symmetry of fiber orientation with respect to the longitudinal axis of the specimen. The difference between $\pm 5°$ and 0° is negligible. The increase in strains from 0° to $\pm 10°$ is a considerable 14%. In case of the transverse specimen also there is symmetry involved in change of angle by +5° or -5°, and +10° or -10° leading to the same effect. The effect of change in angle from 0° to $\pm 5°$ is 3% and from 0° to $\pm 10°$ is 6% which is less than the other two off-axis specimens

(Figure 4.3 b). Also we can observe that the transient part has the most change than the instantaneous part. The 45^{o} off axis specimens has shown significant effect due to material imperfection. Here there is no symmetry in change of angle from +5° to -5° or +10° to -10° and each of this change has its own impact on the axial strains. The change in the recorded strains from 45^{o} to each of these values ranges from 3 to 20% and the error increased as the angle changed from +10° to -10°. Hence a slight material imperfection in the 45^{o} off-axis specimens could lead to major error. Again, the difference between the recorded axial strains at center and 2% away from the center in the longitudinal and transverse directions is negligible and the curves lie on top of each other for all the specimens.

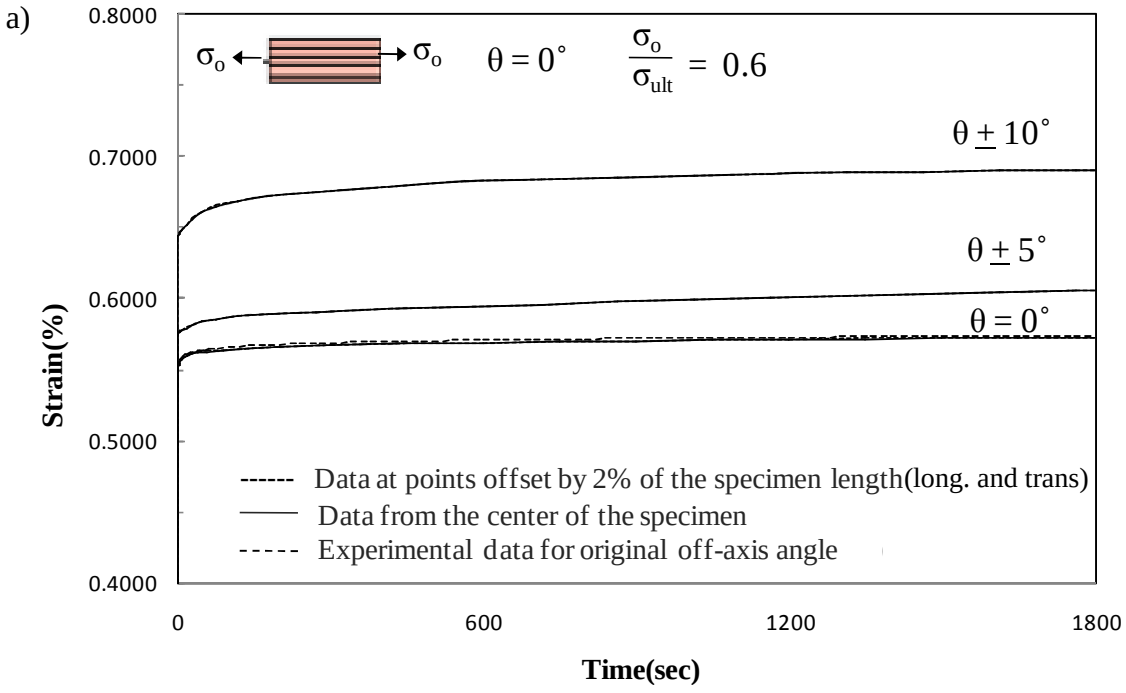

Figure 4.3 Parametric study of effect of material imperfection for θ = ±5°, 10° for a) axial b) transverse and c) 45° off-axis specimens

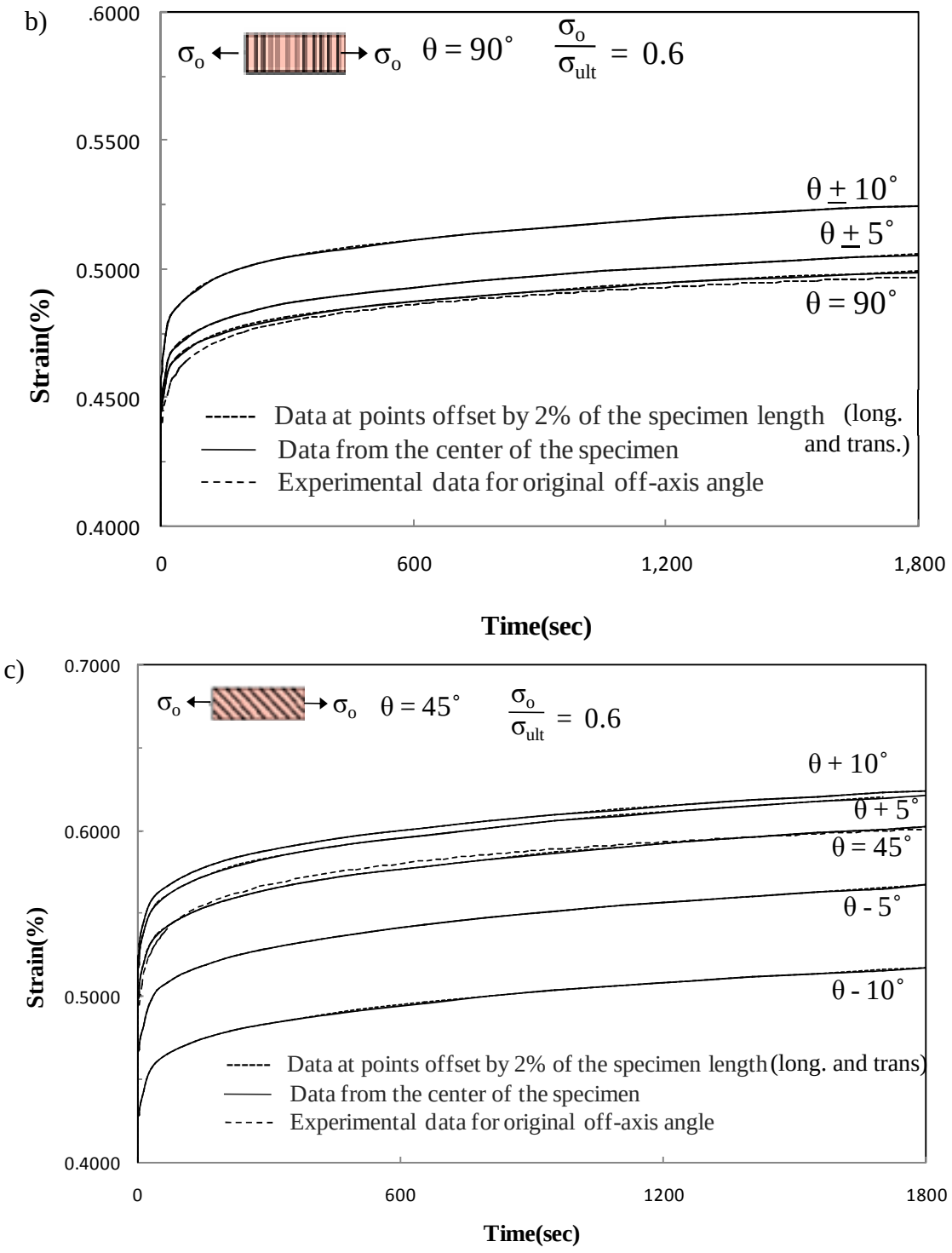

Figure 4.3 Continued

4.3 TIME-DEPENDENT ANALYSIS OF COMPOSITE SLABS SUBJECTED TO THERMO-MECHANICAL LOADING

A practical structural analysis is carried out using Finite Element software to predict the responses of composite slabs under practical environmental conditions of temperature and mechanical loading. The E-glass/polyester slabs manufactured by Creative Pultrusions Ltd. are used for flooring purposes in practicality and thus may be exposed to high loads and extreme environmental conditions. Hence a composite slab with fixed ends of dimensions shown in Figure 4.4 i.e., 60x48x1 in, is chosen to study the behavior under practical environmental conditions of 150°F temperature and 0.6 load ratio.

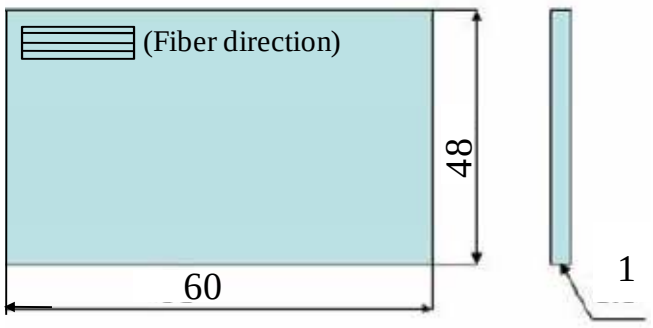

All dimensions are in inches

Figure 4.4 Geometry of the composite slab

In order to study the combined effect of mechanical and thermal loading on the slab a sequentially coupled analysis is performed in ABAQUS. The material model is shown in figure 4.5. Eight-noded brick elements are used for modeling the slab. Mesh convergence was studied for various sizes of the mesh and the results converged for a

mesh size of 1.5x1.5x0.25 in as shown in figure 4.6. For the thermal analysis a uniform field of 75°F is chosen as the initial condition. In the next step a temperature of 150°F is applied to the top surface. A sequentially coupled analysis is performed by first applying a uniformly distributed load to the top surface (figure 4.5) and then applying the temperature field to the top surface of the slab. The heat is conducted from the top surface through the entire thickness of the slab and the steady state condition is reached after 100 seconds. The viscoelastic analysis is then performed for 1 hour. The boundary conditions are also shown in the figure. The orientation of the axial roving is along the 1 direction and all the four end faces are chosen to be fixed. The amount of load applied (0.3 ksi) is such that the longitudinal stresses generated are about 60% of the axial composite ultimate tensile strength.

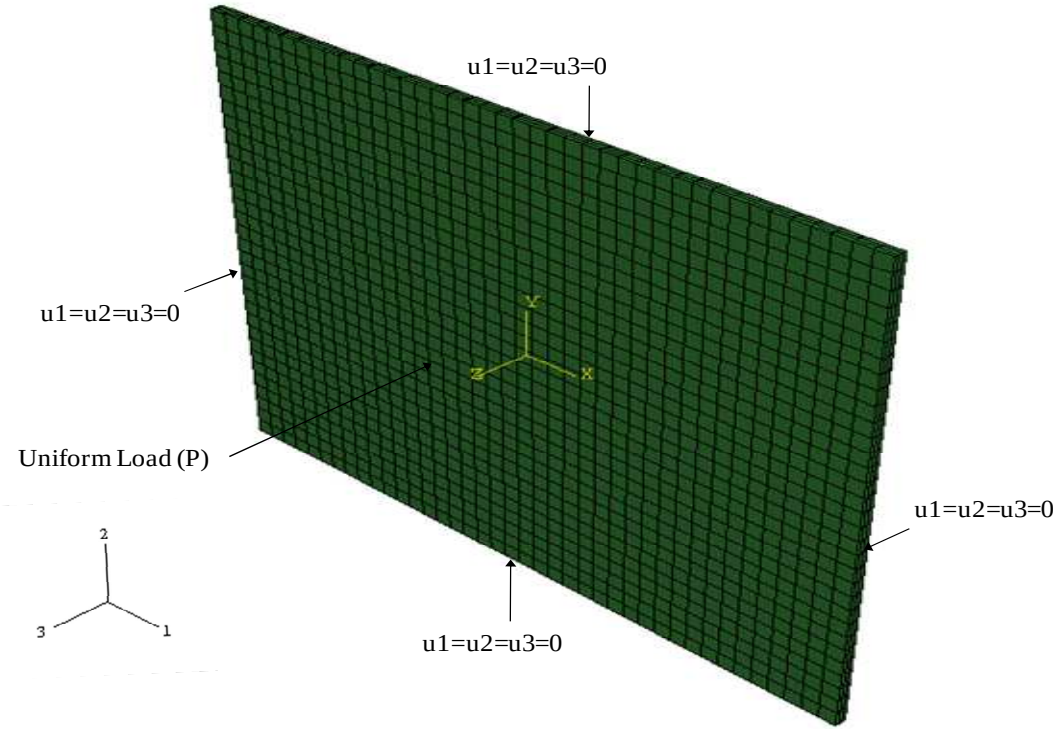

Figure 4.5 Finite Element Model of the slab

The displacement of the slab at the mid-span in 3 direction is plotted in figure 4.6 where the deflection would be a maximum. A considerable amount of creep can be observed. Convergence study was performed for two mesh sizes. The difference in result for different mesh sizes was 0.5% and thus it can be said that convergence is obtained for the mesh size of 1.5x1.5x0.25.

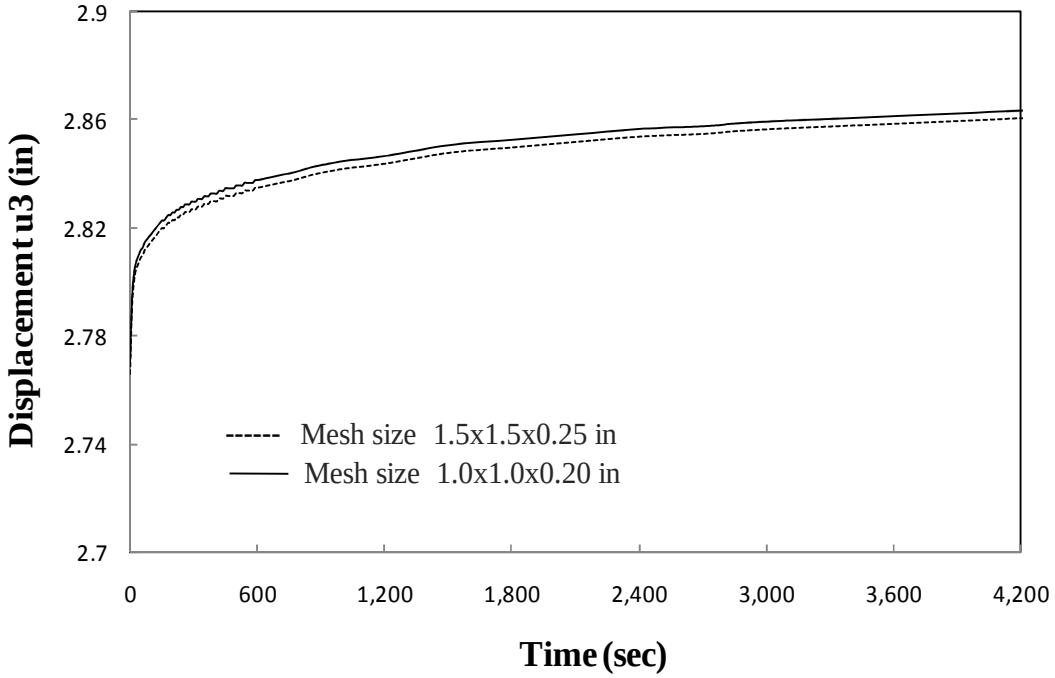

Figure 4.6 Displacement at the mid-node of the slab in the 3-direction for different meshes showing convergence and significant creep behavior

The effect of temperature is also analyzed. The axial and transverse creep strains in the slab are plotted (figures 4.7-4.8) at the mid-span on the bottom surface (tensile behaviors). The application of temperature on the top surface leads to a decrease in strains on the bottom surface due to the combined effect of temperature and load application. It is noted that during the transient heat transfer analyses, the temperature propagates from the top surface through to the bottom surface. This creates a non-uniform temperature distribution through the thickness. The existence of the coefficient of thermal expansion and also the fixed boundary conditions on all end faces result in compressive thermal stresses as illustrated later in figures on pages 92 and 93. These stresses lead to a decrease in the overall tensile stresses at the bottom surface, which are caused due to bending, and hence the decrease in strains.

When the analysis is performed at initial condition of 75°F throughout the slab, and with the temperature of 150°F being applied at the top surface, the decrease in the axial creep strains at the bottom surface is found to be a maximum of 1.5% (figure 4.7) and thus not very significant. For the transverse creep strains, it was about 3% (figure 4.8). This also relates to Table 2.3 and 2.4 in chapter II where the effect of temperature on creep strains was found to be negligible for the axial specimens and quite significant for transverse specimens.

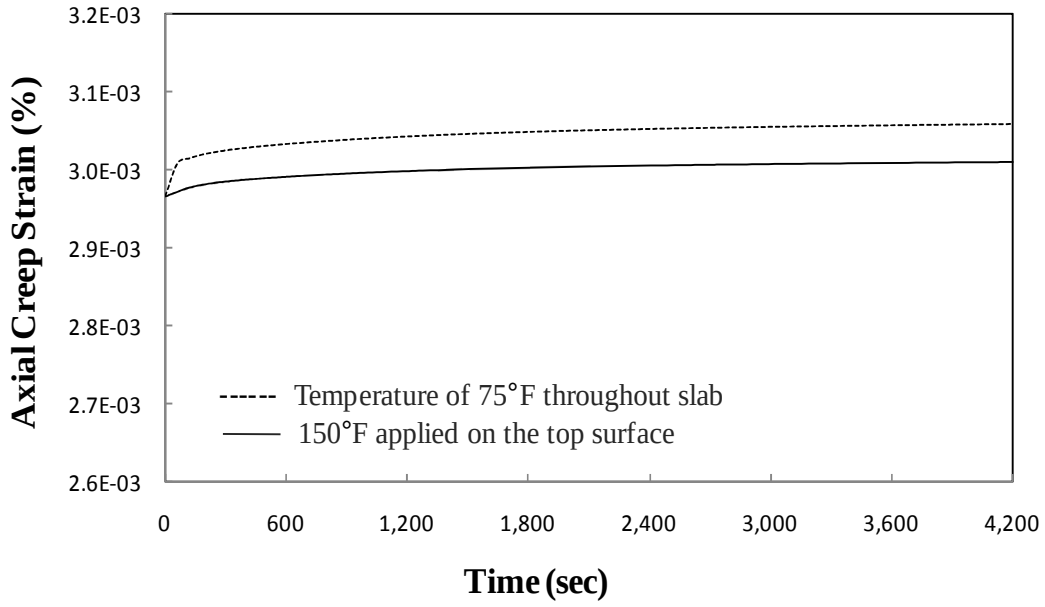

Figure 4.7 Comparison of axial strains at the center of the slab with and without temperature application

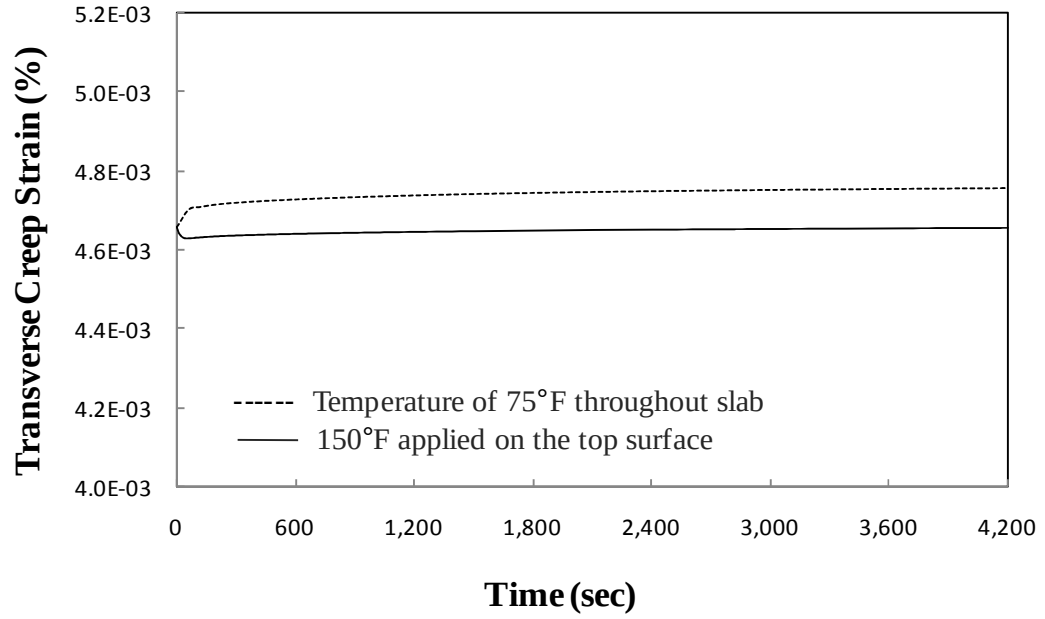

Figure 4.8 Comparison of transverse strains at the center of the slab with and without temperature application

The axial and transverse stresses are plotted through the thickness of the slab at the midpoint in figures 4.9-4.10. A comparison is made between the stresses in the slab at a uniform temperature of 75°F and with variation in through-thickness temperature due to application of 150°F on the top surface. The responses are measured at times t=10s, when steady state is not reached, and t=4200s, when steady state has been reached for sometime. It is noted that the steady state is reached after 100 seconds. At the top surface of the slab where bending leads to compression, the compressive stresses are further enhanced with temperature application. At the bottom surface, the tensile stresses are reduced with the application of temperature again due to the compressive thermal stresses being generated (see figures 4.11 and 4.12). The lack of symmetry of stresses throughout the thickness in the case with temperature being applied is due to the combined effect of temperature and mechanical loading. In case of S11 the stresses are offset at the center by about 2.5 ksi (figure 4.9) and for S22 by about 1.5 ksi (figure 4.10).

It should be noted that, the top surface is subjected to compression due to the bending action and this model is characterized based on tension responses. But the design will be on the safer side as the composite is two times stronger in compression than in tension, and designing based on the tension responses will only give a more sound design to the structure.

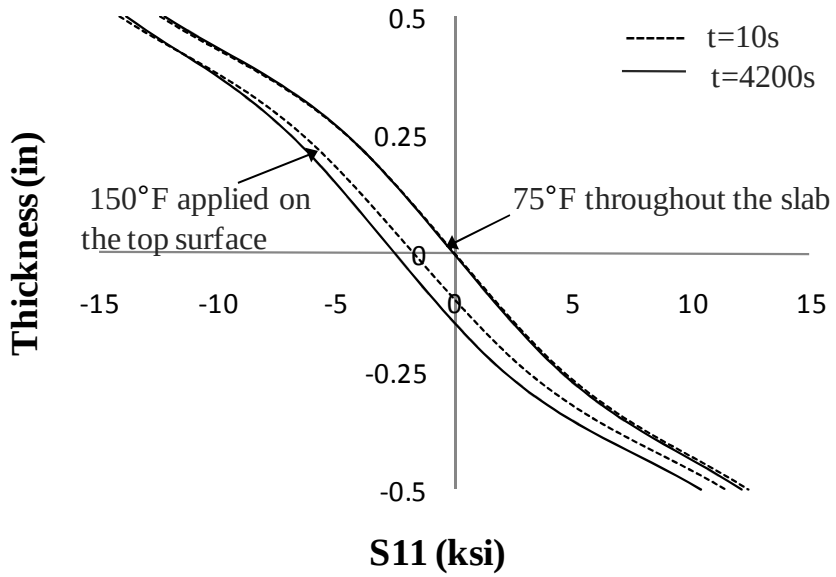

Figure 4.9 Comparison of stress, S11, through the thickness of the slab at the center with and without the application of temperature for t=10s (before steady state) and t=4200s (steady state)

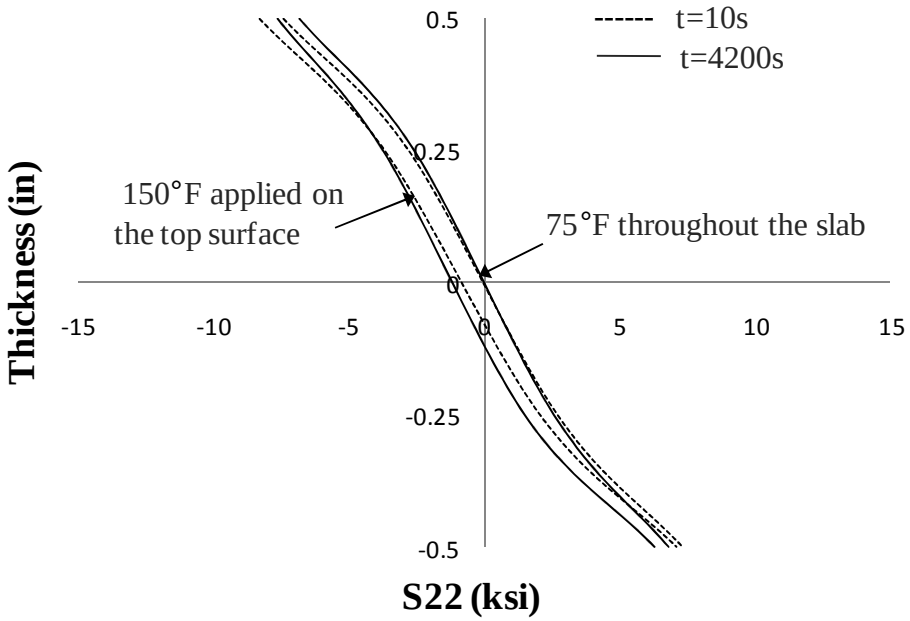

Figure 4.10 Comparison of stress, S22, through the thickness of the slab at the center with and without the application of temperature for t=10s (before steady state) and t=4200s (steady state)

In order to specifically understand the effect of temperature, the analysis is repeated without the application of mechanical loading i.e., with only temperature of 150°F being applied at the top surface thus eliminating the combined effect of thermal and mechanical stresses. The fixed boundary conditions remain on all the four end faces. It is seen that compressive thermal stresses are generated in both axial and transverse directions that are plotted in the figures 4.11 and 4.12. The distribution of the stresses is uneven before steady state is reached when temperature propagates from the top to the bottom surface. Once the steady state is reached, the compressive stresses are more evenly distributed throughout the thickness. These compressive stresses account for the reduction in tensile stresses and hence strains at the bottom surface of the slab in the previous case with mechanical loading.

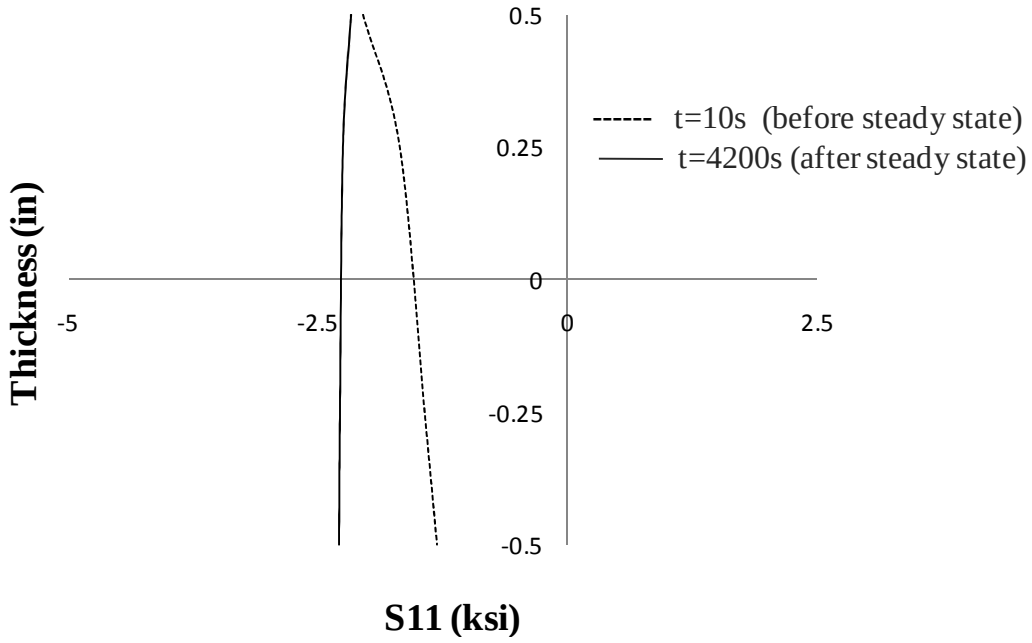

Figure 4.11 Comparison of stress, S11, through the thickness of the slab at the center in case of only thermal loading for t=10s (before steady state) and t=4200s (after steady state is reached)

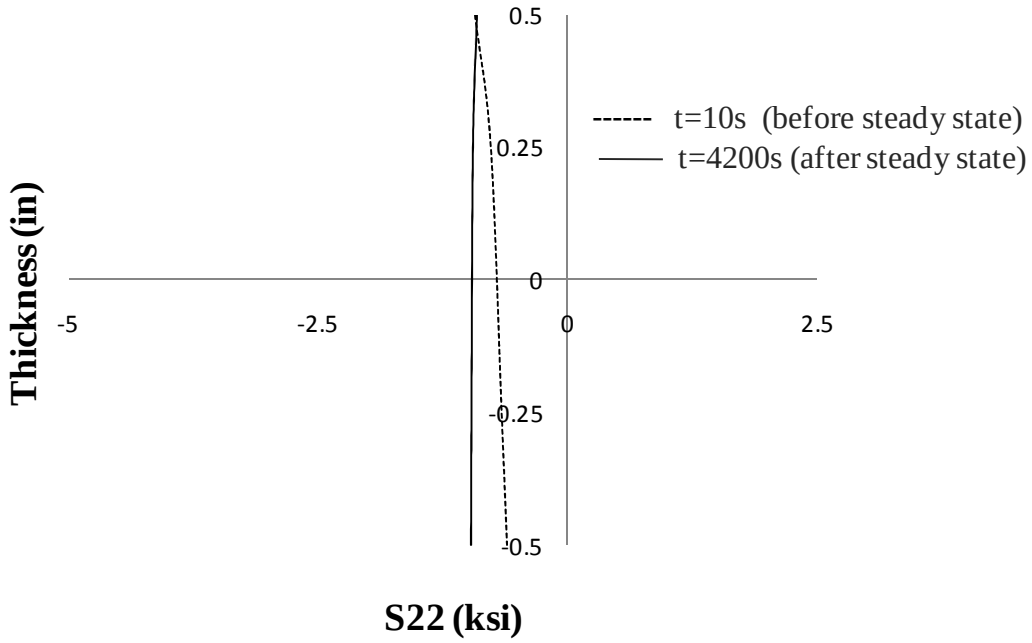

Figure 4.12 Comparison of stress, S22, through the thickness of the slab at the center in case of only thermal loading for t=10s (before steady state) and t=4200s (after steady state is reached)

CHAPTER V

CONCLUSIONS

This study presents experimental works and finite element analyses for understanding nonlinear thermo-viscoelastic behaviors of multilayered (pultruded) composites under tension. Uniaxial isothermal creep tests in tension are conducted on pultruded composites of 0^o, 45^o and 90^o off-axis fiber orientations subject to combined temperatures, ranging from 0°F to 125°F, and stress levels, ranging from 20% to 60% of the ultimate tensile strength of the composite specimen. It is seen that the axial specimens show negligible creep behavior and temperature dependence compared to the transverse and 45^o off-axis specimens. It is found that the creep behavior increases with increase in temperature from 75^oF onwards for each off-axis angle at all the load ratios. However, at the lower temperatures below 50^oF the creep responses do not systematically increase or decrease with increase in temperature but rather follow a random order. Also, the creep responses are very close to one another at these low temperatures. The effect of temperature on the creep responses was found to be significant, of about 10 to 45%, for the 45^o off-axis specimens, compared to the transverse (5-30%) or axial specimens (2-10%).

Isochronous curves of time-dependent material responses portray the nonlinear elastic and time-dependent behaviors of the material. It is found that that the nonlinearity increases with increase in temperature for higher temperatures while there is no

particular trend seen in the nonlinear responses with respect to temperature at lower temperatures (0^oF to 50^oF). Also, the axial specimens show negligible nonlinearity when compared to the transverse and 45 off-axis specimens. The increase in nonlinearity with temperature was studied as a function of time for each off-axis angle and it was concluded that the increase in nonlinearity with temperature is independent of time for t>0 s for all the temperatures except for at 125^oF.

The Poisson's effect is also analyzed by measuring the ratio of strains in the transverse direction to the ones in the axial direction during the creep tests and it is seen that the major and minor Poisson's ratio are independent of time for all the responses. The major Poisson's ratio υ_{12} remains almost constant with stress and temperature where as υ_{21} changes accordingly with change in temperature and stress levels. The material symmetry conditions for orthotropic material are also examined and found to be satisfied for the composite.

A nonlinear viscoelastic constitutive model based on convolution integral equation for orthotropic materials is used. The nonlinear stress-temperature-dependent material parameters, coupled in the product form in the integral equation, are calibrated using the uniaxial isothermal creep tests on off-axis specimens and modeled as a function of effective stress and temperature. Overall good predictions are shown excepting for a mismatch of about 6-10% in the prediction of the responses at temperatures below 50^oF. This owes to the random behavior of the creep responses at lower temperatures. The calibration procedure at reference conditions does not guarantee successful prediction of the responses at other conditions due to the lack of trend in the responses at these

temperatures. There was also a slight error in predicting the transient responses at 125 ^{o}F which could be accounted for by a previous conclusion that the temperature effect here is time-dependent. Thus the temperature-dependent parameters may be a function of time at this temperature.

The numerical integration algorithm for the nonlinear viscoelastic model of orthotropic composite materials developed by Sawant and Muliana [28] was used to integrate this constitutive material model to FE structural analyses. Sensitivity analysis is conducted to examine errors in experiments by numerically simulating the testing procedure and finding the effects of several testing error parameters such as material imperfection (error margins of fiber off-axis angle), misalignment of testing instruments, end-clamping conditions and manual error on the results obtained. It is found that the effect of end clamping conditions on the recorded strain data is negligible, of a maximum of 0.05%, whereas the effect of geometric imperfection was quite significant ranging from 6% to 15%. A practical structural analysis is carried out on composite slabs using ABAQUS and the constitutive model is used to predict the responses of slabs having axial roving, subject to 150 ^{o}F temperature and 0.3 ksi uniform load on the top surface for about 4200 sec. The initial condition is 75 ^{o}F. The temperature is allowed to conduct through the thickness and steady state condition is reached after 100 seconds. Significant creep behavior was observed in the slab. Also, the effect of temperature was studied and the strains were found to have increased by a negligible 2% with increase in temperature for the axial system matching with the study from experimental data.

REFERENCES

1. Al-Haik MS, Hussaini MY, Garmestani H. Prediction of nonlinear viscoelastic behavior of polymeric composites using an artificial neural network. Int J Plast 2006;22:1367–1392.
2. Bank LC, Mosallam AS. Creep and failure of a full-size fiber reinforced plastic pultruded frame. Compos Mater Technol 1990:49–56.
3. Bottoni M, Mazzotti C, Savoia MA. Finite element model for linear viscoelastic behavior of pultruded thin-walled beams under general loadings. Int. J. of Solids and Structures. 2008;45 (3):770-793.
4. Brinson HF, Dillard DA. The prediction of long term viscoelastic properties of fiber reinforced plastics. In: Hayashi T, Kawata K, Umekawa S, editiors. Proceedings of the Fourth International Conference on Composite Materials, Progress in Science and Engineering of Composites, vol. 1, 1982. p. 795.
5. Choi Y, Yuan RL. Time-dependent deformation of pultruded fiber reinforced polymer composite columns. J. Compos. for Constr. 2003;7:356-362
6. Findley WN, Lai JS, Onaran K. Creep and relaxation of nonlinear viscoelastic materials. New York: Dover Publication; 1976.
7. Haj-Ali RM, Kilic H. Nonlinear behavior of pultruded FRP composites. Composite Part B 2002;33:173–91.
8. Haj-Ali RM, Kilic H. Nonlinear constitutive models for FRP composites using artificial neural networks. Mechanics of Materials 2007;39:1035–1042.

9. Haj-Ali R, Muliana AH. Micromechanical models for the nonlinear viscoelastic behavior of pultruded composite materials. Int J Solids Struct 2003;40:1037–57.
10. Hiel CC, Brinson HF, Cardon AH. The nonlinear viscoelastic response of resin matrix composites. In: Marshall IH, editor. Composite structures, vol. 2. Applied science, 1983. p. 271–81.
11. Hilton H. Implications and constraints of time-independent Poisson ratios in linear isotropic and anisotropic viscoelasticity. J. Elasticity. 2001;63:221–251.
12. Katouzian M, Bruller OS, Horoschenkoff A. On the effect of temperature on the creep behavior of neat and carbon fiber-reinforced PEEK and epoxy resin. J Compos Mater 1995;29(3):372–87.
13. Knauss WG, Zhu W. Nonlinearly viscoelastic behavior of polycarbonate. I. Response under pure shear. Mechanics of Time-Dependent Materials **6:** 231–269, 2002.
14. Knauss WG, Zhu W. Nonlinearly viscoelastic behavior of polycarbonate. II. The role of volumetric strain. Mechanics of Time-Dependent Materials **6:** 301–322, 2002.
15. Lakes RS, Wineman A. On Poisson's ratio in linearly viscoelastic solids. J. Elasticity 2006; 85: 45–63
16. Lou YC, Schapery RA. Viscoelastic characterization of a nonlinear fiber-reinforced plastic. J Compos Mater 1971;5:208–34.
17. McClure G, Mohammadi Y. Compression creep of pultruded e-glass reinforced plastic angles. J Mater Civil Eng 1995;7(4):269–76.

18. Mohan M, Adams DF. Nonlinear creep-recovery response of polymer matrix and its composites. Exp Mech 1985:262–71.
19. Mottram JT. Short and long-term structural properties of pultruded beam assemblies fabricated using adhesive bonding. Compos Struct 1993;25:387–95.
20. Muliana AH, Haj-Ali RM. Nested nonlinear viscoelastic and micromechanical models for the analysis of pultruded composite structures. Mech Mater (MOM) J 2004;36:1087–110.
21. Muliana AH, Haj-Ali RM. Multi-scale modeling for the long-term behaviors of composite structures. AIAA J 2005;43(8):1815–22.
22. Muliana AH, Nair A, Khan KA, Wagner S. Characterization of thermo-mechanical and long-term behaviors of multilayered composite materials. Compos Sci Technol 2006;66:2907–2924.
23. Pasricha A, Tuttle ME, Emery AF. Time-dependent response of IM7/5260 composites subjected to cyclic thermo-mechanical loading. Compos Sci Technol 1995;55:49–56.
24. Rajagopal KR, Wineman AS. Mechanical response of polymers: An introduction. New York: Cambridge University Press; 2000.
25. Rizzo RR. More on the influence of end constraints on off-axis tensile tests. J. Compos Mater. 1969;3:202-19
26. Robert MJ. Mechanics of composite materials. Taylor & Francis, Inc; 1998

27. Roy, S. and Reddy, J. N. A finite element analysis of adhesively bonded composite joints with moisture diffusion and delayed failure. Computers and Structures 1988; 29(6): 1011-1031.

28. Sawant S, Muliana A. A thermo-mechanical viscoelastic analysis of orthotropic materials. Compos Struct 2008;83:61–72

29. Schapery RA. On the characterization of nonlinear viscoelastic materials. Polymer Engineering and Science 1969; 9(4):295–310.

30. Schapery RA. Stress analysis of viscoelastic composite materials. J Compos Mater 1967;1(3):228–67.

31. Scott DW, Zureick AH. Compression creep of a pultruded E-glass/vinylester composite. Compos Sci Technol 1998;58:1361–9.

32. ShaoY, Shanmugam J. Deflection creep of pultruded composite sheet piling. J. Compos. for Constr. 2004;8:471-479

33. Spence BR. Compressive viscoelastic effects (creep) of a unidirectional glass/epoxy composite material. In: 35th International SAMPE Symposium, 1990. p. 1490–3.

34. Sternstein SS, Srinivasan K, Liu SH, Yurgartis S. Viscoelastic characterization of neat resins and composites. Polym Preprints 1984;25(2):201–2.

35. Swanson SR. Introduction to design and analysis with advanced composite materials. Prentice-Hall; 1997.

36. Tuttle ME. Accelerated viscoelastic characterization of T300/5208 graphite-epoxy laminates, PhD dissertation, Virginia Polytechnic Institute and State University, 1984.

37. Tuttle ME, Brinson HF. Prediction of the long-term creep compliance of general composite laminates. Exp Mech 1986:89–102.

38. Tuttle ME, Pasricha A, Emery AF. The nonlinear viscoelastic–viscoplastic behavior of IM7/5260 composites subjected to cyclic loading. J Compos Mater 1995;29(15):2025–46.

39. Violette MG, Schapery RA. Time-dependent compressive strength of unidirectional viscoelastic composite materials. Mech Time-depend Mater 2002;6(2):133–45.

40. Yeow YT, Morris DH, Brinson HF. Time-temperature behavior of a unidirectional graphite/epoxy composite. In: Composite material: testing and design (Fifth Conference). In: Tsai, editor. ASTM STP 674. ASTM; 1979. p. 263–81.

41. Yi S, Hilton HH, Ahmad MF. Nonlinear thermo-viscoelastic analysis of interlaminar stresses in laminated composites. J Appl Mech 1996;63:218–24.

42. Yi S. Finite element analysis of free edge stresses in nonlinear viscoelastic composites under uniaxial extension, bending, and twisting loadings. Int J Numer Meth Eng 1997;40:4225–38.

43. Yi S, Ahmad MF, Hilton HH. Nonlinear viscoelastic stress singularities near free edges of unsymmetrically laminated composites. Int J Solids Struct 1998;35(24):3221–37.

VITA

Name: Maithri Muddasani

Address: Texas A&M University
Department of Mechanical Engineering
3123 TAMU
College Station TX 77843-3123

Email Address: maithri_m@tamu.edu

Education: B.E., Mechanical Engineering, Osmania University, 2006
M.S., Mechanical Engineering, Texas A&M University, 2008